論文 / 著書情報
Article / Book Information

題目(和文)	
Title(English)	The characterization and analysis of carrier behavior in organic solar cells by using Electric field induced optical second harmonic generation
著者(和文)	陳翔宇
Author(English)	Xiangyu Chen
出典(和文)	学位:博士(工学), 学位授与機関:東京工業大学, 報告番号:甲第9293号, 授与年月日:2013年9月25日, 学位の種別:課程博士, 審査員:岩本 光正,小長井 誠,山田 明,中川 茂樹,間中 孝彰,工藤 一浩
Citation(English)	Degree:Doctor (Engineering), Conferring organization: Tokyo Institute of Technology, Report number:甲第9293号, Conferred date:2013/9/25, Degree Type:Course doctor, Examiner:,,,,,
学位種別(和文)	博士論文
Type(English)	Doctoral Thesis

Tokyo Institute of Technology

The characterization and analysis of carrier behavior in organic solar cells by using Electric field induced optical second harmonic generation

Ph.D. thesis

Xiangyu Chen

Supervisor: Mitsumasa Iwamoto

Department of physical electronics

2013 年　　6 月　　12 日

ABSTRACT

My Ph. D research is related to analysis and characterization of the carrier behavior in organic solar cell (OSCs). The detailed researches can be divided into two directions, the fundamental characterization and the application of the analysis.

The first purpose of our researches is to study the carrier behavior inside the multilayer organic devices with taking into account the dielectric nature of the active organic layer. On the basis of the Maxwell-Wagner model we theoretically analyzed the carrier relaxation and accumulation inside the organic multilayer. The model showed the presence of the Maxwell-Wagner type interfacial charging at the donor-acceptor interface of the organic solar cell (OSCs), which was usually overlooked by other researchers. Moreover, both relaxation times and accumulated charges density can be also calculated form the equivalent model. In order to provide experimental support for our theoretical research, our group has been developing a technique of the electric field induced optical second harmonic generation (EFISHG) system. It is an optical laser system based on the theory of second harmonic generation. By coupling laser signal with the local electrical field, the generated second harmonic signal is proportional to the intensity of the local electric field. Hence, this technique is capable of directly probing electric field distribution inside the organic devices. Moreover, we applied high frequency laser signal to the sample and thus achieved real-time observation of electric field as well as carrier motion. With this technique, we proved the presence of the Maxwell-Wagner type interfacial charging. My contribution in this project is to apply this technique to the field of the OSCs. We shifted the sample into 45°position and thus we can observe the

average electric field in the thickness direction. By realizing the particularity of this technique, I have specially designed several experiments for its application in the OSCs field. We studied the carrier behaviors under various external conditions, such as external resistances, external biases and photo illumination, by using this technique and theoretical model. Hence, the photo induced carrier behavior inside the organic active layer was clearly probed by EFISHG measurement and the experimental data were in good agreement with the theoretical analysis. These results successfully demonstrate the influences of dielectric nature to the organic devices.

The second part of my research is related to the application of our theoretical model and technique to improve the performance of OSCs. In order to using our study to improve the performance of the OSCs, we have designed several further experiments with different OSCs samples. The results clarified the contribution of the Maxwell-Wagner type interfacial charging to I–V characteristic of OSCs. Firstly, the accumulated charges on the interfaces induce a recombination current and consequently the photo current is depleted by this recombination current at the interfaces. Meanwhile, the slow attenuation of this recombination current also leads to the deterioration of the fill-factor of OSCs. Moreover, accumulated charges require another external voltage V` to assist photo-generated charges from leaving the interface, which decreases the effective Voc. Hence, the existence of interfacial charging deteriorates the performance of OSCs. For solving this problem, we suggested two methods to suppress the interfacial charging inside the OSCs. By employing exciton blocking layer of BCP and charging blocking layer of CuPc, interfacial charge accumulation can be strongly decreased and the I-V performance of the OSCs was improved accordingly. These results not only proved that dielectric nature of organic active dominates the performance of OSCs, but also provided a possible way to further improve the performance of OSCs. Modeling the prepared OSCs as a Maxwell-Wagner effect element accounted for our experimental results.

Contents

Chapter 1 Introduction of background

Overview

Much effort has been expended during the past two decades in the research field of organic solar cell since it was proved to be a promising alternative to the traditional silicon solar cells. Most of the researches focused on developing photovoltaic materials and related device architectures since the donor–acceptor heterojunction interface was demonstrated to be an effective exciton-dissociation structure [1-8]. Quit recently, a German company, Heliatek, has achieved the power conversion efficiency of 12%. This value is close to the level of real application. However, it is still a long way to go for ultimate applications of a large number of these devices in industrial field due to lots of formidable obstacles such as operating instability, short lifetime even sealed with compliant plastic films, and so on. The power-conversion efficiencies of organic photovoltaic devices are dependent on three key processes: light absorption, exciton dissociation, and charge collection. Among them, the interfacial carrier behaviors, such as charge accumulation, carrier relaxation, also make great contribution to output performance. Moreover, due to the low carrier mobility, insulating performance of organic thin film is very significant. Hence, sometimes

the organic thin film in the solar cell sample can be considered as dielectric materials. Up to now, understanding of interfacial carrier processes based on dielectric physics is still not sufficient. This motivated us to study the contribution of the dielectric nature in OSCs to the interfacial carrier processes.

In this chapter, the brief history and knowledge about organic electronics as well as organic solar cell will be introduced. Meanwhile the detailed characteristic of organic solar cell`s operation, including the short-circuit current, open-circuit voltage and fill factors will be analyzed. In addition, the current problems and critical feature of the organic solar cell were also discussed and finally the scope of this thesis is summarized.

1.1 Organic electronics

1.1.1 Emergence of organic electronics

In today`s industry field, the mainstream of electronics application is dominated by inorganic materials, such as single-crystal, polycrystalline, or amorphous silicon. These materials are the fundamental composition for integrated circuits in all kinds of electronics products as well as the power generation device for the solar cell industry. However, the fast development of the silicon technologies was gradually slowed down due to the high cost of fabrication and depleted innovation possibility. For solving the cost problem, amorphous silicon, which has low cost for fabrication, is developed as a

candidate material for electronics and solar cell industry. One particular advantage of amorphous silicon is that it can be deposited at very low temperatures (as low as 75 degrees Celsius). The deposition can be conducted not only on glass, but also many kinds of plastics, which makes it to be a candidate for a roll-to-roll processing technique. Amorphous silicon is also possible for large areas fabrication by using plasma-enhanced chemical vapor deposition, which can leads to lower manufacturing cost [1-3]. Amorphous silicon has been successfully applied for many electronic devices such as tin film transistors or solar cell. However, for the application in the solar cell`s field, the low power conversion efficiency and time degradation is the strong limitation of the amorphous silicon solar cell. Besides, the developments of the entire silicon device are commonly restricted by the limited type of the materials, which resulted in limited improvements methods and innovation possibility.

Under such circumstance, a new type of electronics is drawing more and more attentions – organic electronics, which is considered as a possible alternative for inorganic materials for its light-weight, flexible and low-cost. Organic electronics uses conductive polymers, plastics, or small molecules to build electronic components and devices that are conventionally made from inorganic semiconductors such as silicon, gallium arsenide, etc. The important historical events of the development of organic electronics are shown in the Fig. 1.1 [4-9]. The research of the organic electronics started form a long time ago. But the intensive development happened within recent decades and the progress

of this field is getting more and more exciting. In recent twenty years, Organic electronic devices have been studied tremendously and the application of such devices concerned with many important technology field. Generally, organic electronic devices can be divided into three categories: organic light-emitting diodes (OLEDs), organic solar cells (OSCs), and organic thin film transistors (OTFTs). The development of organic semiconductors was strong promoted in the 1980s by a demonstration of efficient photovoltaic cell with bulk heterojunction structure [10] Then fabrication of thin film transistors from conjugated polymers and oligomers were also met significant success [4-6]. Another driving force is from the success of high-performance electroluminescent diodes, which were fabricated through vacuum evaporation [11] and conjugated polymers [12]. These recent advances in all these categories was related to the many promising commercial applications such as inexpensive photovoltaic cells, outstanding flat panel displays, and cheap yet high quality large-area circuits and sensors. In fact, some fashionable consumer products can already be seen on the market nowadays, such as cell phones, digital cameras, and display panels.

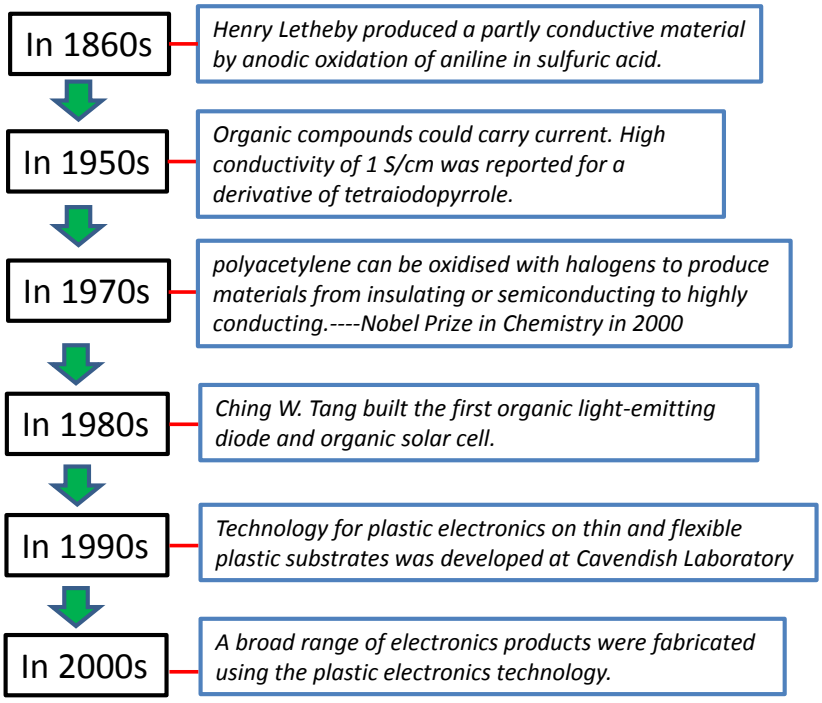

Figure 1.1: A brief history of organic electronics

One of the most important advantages of the organic electronics is the cheap cost for fabrication. Production will be possible to be fabricated trough roll-to-roll wet deposition processes, which deposit organic materials (mostly in solution state) onto a sheet of flexible substrate, similar to how newspapers are printed today. This allows for many devices to be fabricated at a much lower cost than traditional methods for silicon device. Of course, the stability of organic devices so far cannot compare with inorganic ones, but the low cost of fabrication can make up to this defect. Secondly, the study and improvement of the organic devices has a lot of potential due to the diversity of the organic materials. Various physical properties such as the band gap and surface affinity of organic devices can be controlled with the synthesis of new organic

semiconductors. In the past, such controllability has been used to modify the emitted colors of light from OLEDs by synthesizing different organic semiconductors. People also make different semiconductors that respond selectively to chemicals for sensing chemicals. In addition, the study of organic electrons is on the basis of the inorganic electronics and therefore many improvements methods for the inorganic devices can also applied to the organic electronics and thus. For example, people have tried to a useful stack multiple photoactive layers with complementary absorption spectra in series to make a tandem OSCs and the same method was used for amorphous silicon solar cell for using the radiation more effectively [13-15]. Because organic materials had several key advantages compared to silicon materials, the research of organic electronics draws great interest in both academia and industry fields.

Nowadays, we know that the most commercial applications for the organic electronics are belong to the application of OLEDs and many famous Japanese companies, such as IDEMITSU, TOSHIBA and so on, have already achieved a series of completed products and OLEDs possessed a substantial marketing share in the field of illumination. Meanwhile, other applications using OFETs and OSCs are expected to follow in the near future. For the study of OEFTs, it has been found that pentacene based OFET has reached the level of mobility similar to amorphous silicon, which is widely used to drive display technologies. Meanwhile, the power conversion efficiency of OSCs has been increased every year and it will sooner approach the level for the real application. In general, the

performance of small molecule organic materials is better than that of polymer, and both of them have achieved impressive progress in the last two decades. Many future uses of organic electronics have been presented by various companies. In Japan, a series of world famous companies also consider organic electronics devices as their next generation`s main product and put a tremendous effort in this field. Both Toshiba and Sumitomo Chemical Corp have their own research center specially target at the development of next generation flexible OLED or OSCSs. The Mitsubishi Chemical Company had kept the world record of the highest power conversion efficiency of the OSCs for over one year. We can expect that in the very recent future, organic electronics device can be the strongest competitor of the traditional silicon device in every industry field.

1.1.2 Carrier transport in organic materials

To better explain the carrier behavior in organic materials, we can start with the carrier behavior happened in the more common case, namely inorganic materials. In inorganic semiconductor, such as silicon or germanium, the strong coupling between the constituting atoms and the long-range order leads to the delocalization of the electronic states and the formation of allowed valence (VB) and conduction bands (CB), separated by a forbidden gap. As shown in the Fig 1.2, the key difference between semiconductors and conductors (like metal) is that conductors have a natural overlap between their valence electrons and the conduction band, while semiconductors have a noticeable gap between the two.

In this case, the electrons inside conductors can produce a current under any condition. On the other hand, the semiconductors require energy to excite the electron from VB, in order to generate conductive ability. As the energy was put into the semiconductor, electrons are promoted into the conduction band, increasing the number of available conducting electrons. This energy can come in the form of heat or illumination. By thermal activation or photo-excitation, free carriers are promoted into conduction band, leaving behind positively charged holes in the valence band. The transport of these free carriers is described in quantum mechanical terms by Bloch functions, wave vector-space and dispersion relations.

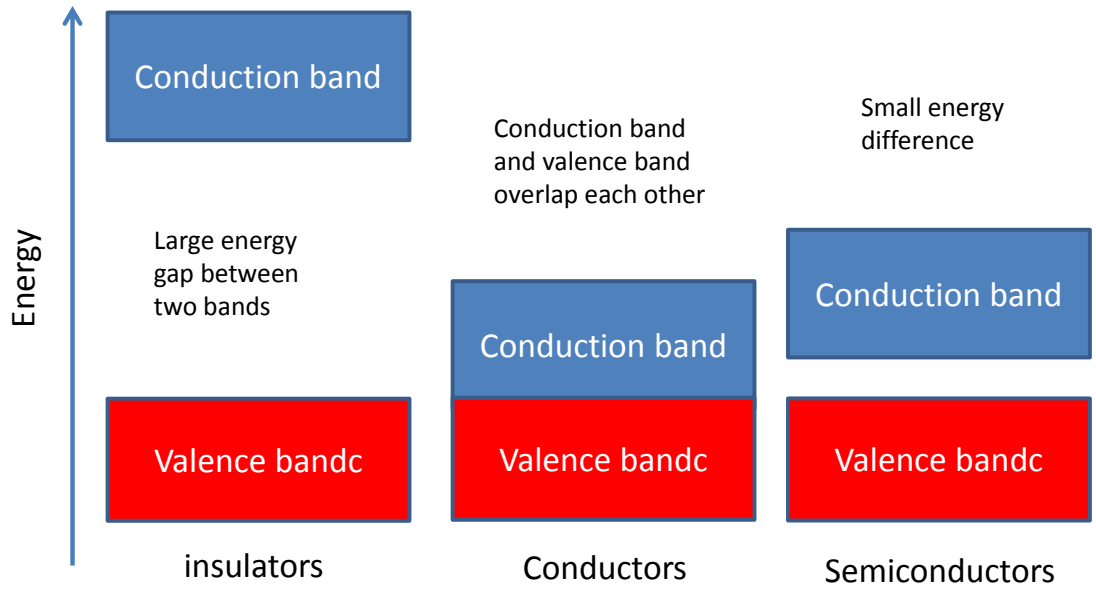

Figure 1.2: Energy band structure of different materials

On the other hand, band theories are not absolutely suitable for organic materials, even for some single-crystalline organic materials. The electrical properties of organic semiconductors are based on the unusual properties of the carbon-carbon double bonds. The carbon atoms comprising the double bonds can form the so-called sp^2-hybridizations where the sp^2-orbitals form a triangle within a plane and the p_z-orbitals are in the plane perpendicular to it. A s -bond between two carbons can then be formed by formation of an orbital overlap of two sp^2-orbitals [16, 17]. The energy between the occupied binding orbitals and the unoccupied anti-binding orbitals is quite large and well beyond the visible spectral range. Correspondingly, longer chains of bound carbon atoms would have a large gap between the highest occupied molecular orbital (HOMO) and the lowest unoccupied molecular orbital (LUMO), leading to insulating properties. Meanwhile, in organic materials, the intermolecular interactions in the force of molecular bond (the so-called van der Waals forces) are too weak to form 3D crystal lattices. The van der Waal bonds that hold organic molecules together are on the order of 0.1 eV in contrast to 1 eV of covalent bonds resulting in weak interactions of electron wave functions from adjacent molecules. Besides, the molecular structure of the organic material is only ordered in short-term, and disordered in long-term. Consequently the molecular LUMOs and HOMOs do not interact strongly enough to form a CB and VB. Thus there is no regular energy band in organic semiconductor for electrons to move smoothly. In the sp^2-hybridization, the p_z-orbitals form additionally π-bonds. These bonds

have much smaller energetic between the HOMO and LUMO, leading to strong absorption in or near the visible spectral range and to semiconducting properties. In most case, the motion of carriers in organic semiconductor is described by hopping transport between localized states, which is a phonon-assisted tunnelling mechanism from site to site [18]. The hopping rate can be increased by external electric field and temperature. The charge transport sites have a Gaussian distribution of energies and are localized [19]. The shape of the density of states (DOS) is suggested to be Gaussian based on the observed Gaussian shape of the optical spectra [20]. Hopping transition can be generally illustrated as Fig 1.3 [21] where the solid and dashed lines depict the carrier wave functions on sites i and j, respectively; α is the localization radius. Accordingly, hoping transport of the carrier means that charge carrier mobility in organic and polymeric semiconductors are generally low compared to inorganic semiconductors.

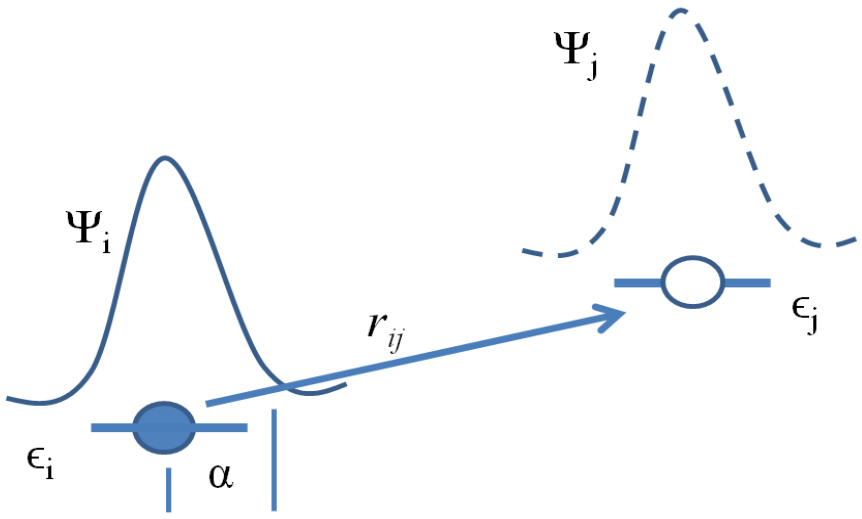

Figure 1.3: Illustration of hopping transition between two localized states.[21]

On the other hand, charge separation is more difficult in organic semiconductors due to the low dielectric constant. We know that the dielectric constant of the silicon is around 12. Meanwhile, the dielectric constants of organic materials are usually around 2 or 3. The Coulomb force between photo-generated electrons and hole are rather strong and make them hard to separate automatically. In many inorganic semiconductors photon absorption produces a free electron and a hole (sometimes called charge carriers), whereas the excited electron is bound to the hole (at room temperature) in organic semiconductors. This bounding condition is so-called exciton. Conjugated polymers lie somewhere between the inorganic semiconductors and organic dyes. In general, excitons are considered to be localised on specific chain segments. However, there are cases where excitons seem to be delocalised. In these cases, the excitons are referred to as polarons [22]. In simple OSCs devices and diodes based on organic semiconductors the primary exciton dissociation site is at the electrode interface (other sites include defects in the crystal lattice, absorbed oxygen or impurities) [23]. This limits the effective light-harvesting thickness of the device, since excitons formed in the middle of the organic layer never reaches the electrode interface if the layer is too thick. Rather they recombine as described above. Typical exciton diffusion distances are on the order of 10~20 nm.

1.1.3 Organic solar cell

Recently, organic solar cells have received significant attention all over the world, and many types of OSC have been proposed. The diversity and flexibility of organic materials lead to many exciting and advanced new applications for the further development of OSCs. The solar cell group currently on the market or being developed can be briefly divided into two classes, inorganic solar cell and organic solar cell, as can be seen in the Fig. 1.4. For the inorganic solar cell, the mainstream is the silicon materials, which can provide rather high efficiency and longtime stability. There are thin film and crystalline silicon solar cells, and crystalline ones include single crystal and polycrystal types. Usually, silicon with high purity is used as the basic material for crystalline solar cells, and therefore high temperature fabrications are necessary for producing the raw silicon and ingots. Thin-film silicon solar cells can be manufactured by plasma CVD using silane gas, but they have lower efficiency than crystalline solar cells. Practical applications of thin film solar cells that make use of compound semiconductors such as copper indium gallium selenide (CIGS) and CdTe have come about to eliminate these deficiencies. However, little progress has been made to reduce energy and money cost for these inorganic solar cells because high temperature and vacuum processes are inevitable. Moreover, the materials used for manufacturing these devices are still limited resources, which means the improvement methods for these devices are almost exhausted.

As the development of the inorganic solar cell getting more and more difficult, people try to explore some new field for the cheap and clean energy generation. Accordingly, organic solar cell draws a lot of attention, since these devices allow rather low cost for fabrication and full of improving possibility. Of course, strictly speaking, organic solar cell has two kinds, one is the thin film organic solar cell and another one is dye-sensitized solar cell. However, dye-sensitized solar cell is a special kind. Dye-sensitized solar cells are devices where a dye is absorbed into porous titanium oxide. Its working principle is based on electrochemical reactions and the current is generated through photo-induced ionization of electrolyte. There have been reports of efficiency exceeding 10%. However, there are problems with liquids leaking since an iodine solution is used, so they have still not become practical. For organic solar cell`s study, the most of researchers are focusing on the thin film organic solar cell and it is also our research topic. In this thesis, the organic solar cell (OSCs) is referring to thin film organic solar cell.

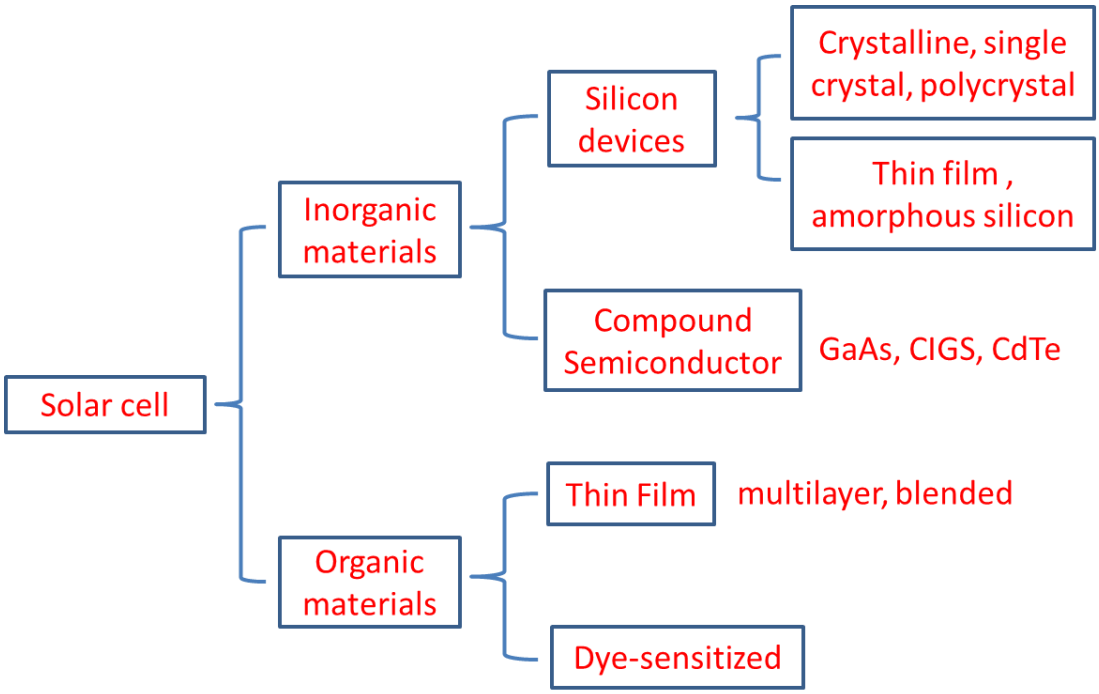

Figure 1.4: The solar cell group currently being developed

OSCs are a new generation of solar cells, which can be a possible alternative to inorganic solar cells for new energy generation. These devices have for the last 2 decades received considerable attention as a possible choice for photonic based electronics. The scientific and financial benefit for using flexible, lightweight and cheap plastics as the solar cell (photovoltaic) material of choice offers significant advantages to more traditional inorganic based ones. As shown in Fig. 1.5, working principle of OSCs is similar to the organic light-emitting diodes (OLEDs), but the direction of the energy transfer is reversed. OLEDs generate light from electricity, but OSCs are devices that extract electricity with exposure to the sun. The materials for these devices are usually selected as conjugated polymers, for the fabrication can be conducted with low cost.

Meanwhile, the small molecule materials require high temperature manufacturing processes are also good candidates for OSCs fabrication but usually for the academic field only. Classically, the optical properties of plastics have huge potential, they can convert almost all light into energy (charge carrier generation). The future target of the OSCs is high and stable power conversion efficiency with low cost for fabrication. Meanwhile, plastic substrates can be used for deposition and a common feature is the ease of making them flexible.

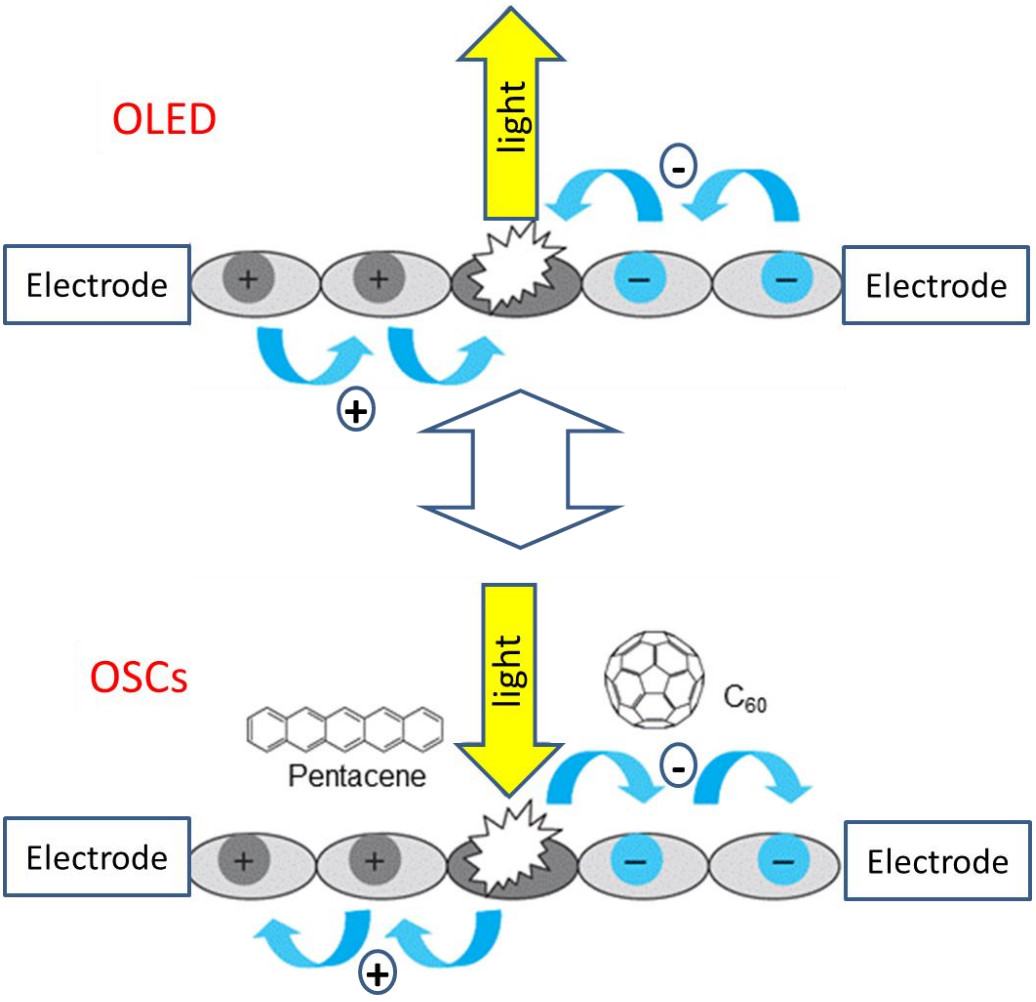

Figure 1.5: A simple explanation of working principle of OSCs

The standard form of an organic photovoltaic cell is based upon sandwiching several thin semiconducting organic layers between two conducting layers having different work functions. The higher work function conductors typically used are gold or ITO, whereas the lower work function conductors are typically aluminum or calcium. The detailed structure of the organic solar cell can be briefly divided into three kinds, single layer, double active layers and bulk heterojunction.

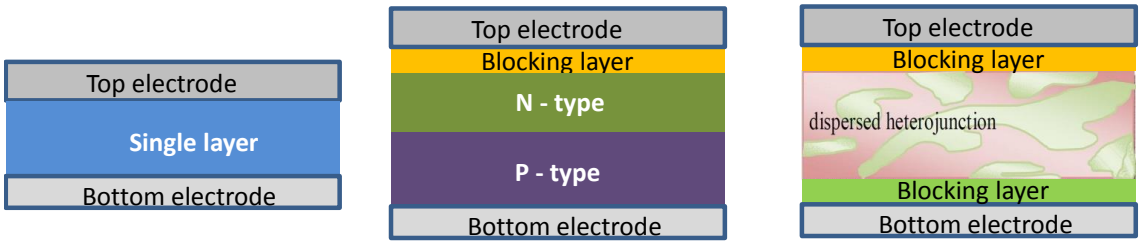

(a) (b) (c)

Figure 1.6: (a) single layer OSCs (b)double-layer OSCs (c) OSCs with blended active layer

Single layer organic photovoltaic cells have the simplest of all the organic photovoltaic cells. These cells are made by sandwiching a layer of organic electronic materials between two metallic conductors, as can be seen in Fig. 1.6 (a). The difference of work function between the two electrodes leads to a potential drop in the organic layer. When the organic layer absorbs light, electrons and hole will be excited to the LUMO and HOMO, respectively and excitons are generated. The potential created by the different work functions

helps to separate the exciton pairs, pulling electrons and hole to the opposite electrodes. The current and voltage generated through this process can be used to provide output. As early as 1958, Kearns et al. reported the photovoltaic effect or the creation of voltage of a cell based on magnesium phthalocyanine a macrocyclic compound having an alternating nitrogen atom-carbon atom ring structure (MgPh), which had a photovoltage of 200 mV. [25] Ghosh et al. investigated the Al/MgPh/Ag cell, and obtained photovoltaic efficiency of 0.01% under illumination at 690 nm. [26] However, using electric fields to separate the exciton is not the best way. Therefore, single layer organic photovoltaic cells usually have low power conversion efficiencies (<0.1%). Lacking of sufficient force to break up the excitons, the electrons often recombine with the holes rather than move to the electrodes. In order to solve this problem, the multilayer organic photovoltaic cells were developed.

The second type of the organic solar cell is the double active layer OSCs. This type of OSCs contains two different organic active layers as the main part of the structure (see Fig. 1.6(b)). These two layers of materials have differences in electron affinity and ionization energy. Therefore electrostatic forces, which are generated at the interface between the two active layers, can be used to assist exciton separation. In this case, the layer with higher electron affinity and ionization potential is the electron acceptor, and the other layer is the electron donor. A lot of work has been done to develop this type OSCs. C60 has high electron affinity, which makes it to be a good electron acceptor for this type

OSCs. Sariciftci et al. fabricated a C60/MEH-PPV double layer cell, which had a relatively high fill factor of 0.48 and a power conversion efficiency of 0.04% under monochromatic illumination.[27] For PPV/C60 cells, Halls et al. reported a monochromatic external quantum efficiency of 9%, a power conversion efficiency of 1% and a fill factor of 0.48.[28] While a critical step in inorganic solar cells is to collect minority carriers before they recombine by having them migrate to the opposite side of the junction, the challenge in organic cells is to dissociate the excitons before they decay to the ground state; this requires that they rapidly diffuse to the D/A heterojunctions, which is the only location where dissociation is efficient in pure materials. Hence, the thickness of the organic layers has to be comparable to the exciton diffusion length L ($L = (D\tau)^{1/2}$ where D is the diffusion coefficient and τ the lifetime of the exciton) [29, 30]. However, usually an organic active layer needs a thickness of around 100 nm to absorb enough light. At such thickness, only a small part of the photo-generated excitons can reach the donor-acceptor interface and the rest parts are just contribute to decrease of the conductance of the whole devices. To address this problem, the third type of bulk heterojunction OSCs is designed.

For the OSCs with bulk heterojunction structure, the electron donor and acceptor materials are mixed with each other, forming a blended organic active layer (Fig 1.6(c)). If the length scale of the blend is similar to the exciton diffusion length, most of the excitons generated in either material may reach the interface, where they can be separated efficiently. Electrons move to the acceptor

domains then were carried through the device and collected by one electrode, and holes were pulled in the opposite direction and collected at the other side. Bulk heterojunctions are fabricated via blending or codeposition methods. The interpenetrating networks have proven to be very efficient exciton-dissociation systems, especially for recently reported highefficiency polymer-based devices. The exciton- and charge transport properties are altered after the formation of bulk heterojunctions, since phase separation and film morphology play more important roles compared to in the respective pure materials, so that the mixtures might be considered as whole systems and their properties must be determined after fabrication. This bulk heterojunction OSCs usually can offer us better power conversion efficiency and higher output. However, the current path inside these devices is indistinct and no clear existed in the devices, which means that the interfacial carrier study is difficult to be conducted with this type of OSCs. On the other hand, the second type of OSCs with double active layer is relatively simple systems and the transport properties, crystalline order, and film morphology can be preserved relatively well. Therefore, materials can be characterized independently before device fabrication and the different components can be substituted conveniently. Many valuable parameters can be determined experimentally in these multilayer systems, since it possesses clear interfaces and straightforward physical process. In this case, OSCs with double active layer are well suited to the investigation of new materials and theoretical

approaches for photovoltaic devices. Hence, in our study, we mainly focused on the OSCs with multilayer structure.

1.2 Characteristic of organic solar cell

In this part, we will briefly introduce the characteristic and operation of OSCs based on several important parameters of OSCs. Power conversion process of OSCs is to convert light energy into electrical energy. The photo illumination applied to OSCs leads to a generation of exciton and charge carriers, which ultimately gives rise to photocurrent that can be used to drive an external load. Current density–voltage (J–V) characteristics for a typical PV cell in the dark and under incident illumination are shown in Figure 1.7 [31]. From the figure, we can distinguish two important parameters, the short-circuit current density (J_{SC}) and open-circuit voltage (V_{OC}), under illumination. In addition, the points of current and voltage (J_m and V_m, respectively) that correspond to maximum power output. The operating range of the solar cell is therefore $0 < V < V_{OC}$, where the device generates power. The fill factor (FF) can be calculated as

$$FF = \frac{J_m V_m}{J_{SC} V_{OC}} \tag{1.1}$$

Then, the power conversion efficiency, η_P, is

$$\eta_P = \frac{J_m V_m}{P_0} = \frac{J_{SC} V_{OC} FF}{P_0} \tag{1.2}$$

here P_0 is the power from illumination source. The detailed analysis of all these parameters will be explained one by one in following part.

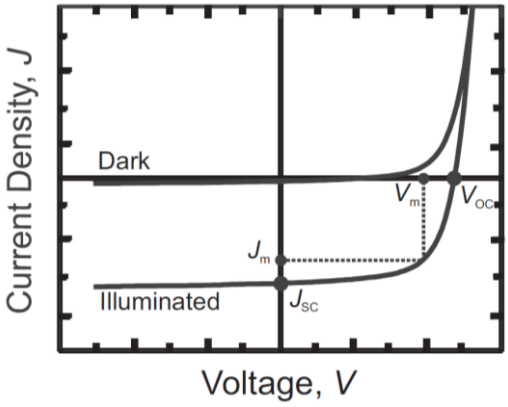

Figure 1.7. Typical current density vs. voltage (J–V) curves of a solar cell in the dark and under illumination. The various device parameters are also shown, including open-circuit voltage (V_{OC}), short-circuit current density (J_{SC}). The rectangular region in the fourth quadrant indicates maximum power output. [31]

1.2.1 Short-circuit current J_{SC}

The photocurrent generated by an organic solar cell with photo-illumination under short-circuit condition is J_{SC}. J_{SC} is dependent on the incident light intensity and many other parameters. Basically, there are two factors that can decide the performance of J_{SC}. One is the quantum efficiency of the organic materials and another is the interfacial properties of OSCs. A solar cell's quantum efficiency value indicates the amount of current that the cell will produce when irradiated by photons of a particular wavelength. We can use the cell's quantum efficiency (QE) to relate the photocurrent density to the incident spectrum. QE

(E) illustrates probability that an incident photon with energy E will deliver one electron to the external circuit. Then we can get the follow equation:

$$J_{SC} = q\int b_S(E)QE(E)dE \qquad (1.3)$$

where b_s(E) is the incident spectral photon flux density, the number of photons of energy in the range E to E+dE which are incident on unit area in unit time and *q* is the electronic charge [32] . *QE* depends upon the absorption coefficient of the solar cell material, the efficiency of charge separation and the efficiency of charge collection in the device but does not depend on the incident spectrum. QE and spectrum can be given as functions of either photon energy or wavelength, λ. The relationship between *E* and λ is defined by:

$$E = \frac{hc}{\lambda} \qquad (1.4)$$

where *h* is Planck's constant and c the speed of light in vacuum. A convenient rule for converting between photon energies, in electron-Volts, and wavelengths, in nm, is *E*/e*V* = 1240/(λ=nm). [32] It is therefore a key quantity in describing solar cell performance under different conditions.

The interfacial properties of the OSCs also make great contribution to the performance of J_{SC}. The interface of the electrodes decides the extraction of the carrier from inside of the OSCs to the external circuit and certain surface treatment can improve this extraction process. It has been reported that a monolayer can induce some surface dipole moment, which can enhance the

transport of the charge to the electrode. Meanwhile, smooth extraction of the charges can also be achieved by reducing the barrier between the electrode and organic active layer. The author's group also proved that the interface between organic active layers can also influence the J_{SC}. The charge accumulation would happen on each interface inside the OSCs. This charge accumulation leads to the consumption of the photo-generated carriers, which can also decrease the J_{SC}. (See section 5.1) Therefore, how to establish a smooth internal environment for charge transport is also a key point for OSCs study and a clear physical picture of the carrier behavior may be helpful.

1.2.2 Photovoltaic effect and V_{OC}

When excitons are created, electrons and holes must be separated from each other so that they do not recombine and return their energy to heat or light. As described in the previous section 1.1.2, photo-generated charge is very difficult to be separated in organic materials due to the low dielectric constant. In order to separate the exciton, we need to apply another electrostatic force to overcome the Coulomb force between photo-generated electrons and hole. This electrostatic force can be induced by the external electric field or the point defects inside organic active layer. The most efficient method for exciton separation is to employ the donor-acceptor interface to separate the exciton. The donor-acceptor interface is formed by combining a p-type organic material and a n-type organic materials together. These two layers of materials have differences in electron

affinity and ionization energy. Therefore electrostatic forces, which are generated at the interface between the two active layers, can be used to assist exciton separation. Thus, excitons generated by photo-illumination diffuse to the interfaces, such as donor-acceptor molecular-interface and double layer interface, to separate into electron and holes. After that, electrons and holes are conveyed to the opposite electrodes to generate photo-voltage. This is a basic carrier process of photovoltaic effect.

Since the separation of exciton happening on the donor-acceptor interface, the generated open circuit voltage is related to energy band structure of the adjacent donor and acceptor materials. It has been report by several researchers that the energy difference ΔE_{HL} between the HOMO of the donor and the LUMO of the acceptor can decide the effective value of V_{oc}. [33, 34] Based on the current equation derived from the Shockley equivalent circuit of solar cells, an analytical expression of the V_{oc} can be proposed here.

Under an applied voltage, or bias in the dark, a reverse current is presented inside the OSCs. This reverse current is called the dark current ($I_{dark}(V)$) which flows across the device in the direction opposite with *Jsc*. Under such circumstance, OSCs behave like a diode in the dark, admitting a much larger current under forward bias ($V > 0$) than under reverse bias ($V < 0$). This rectifying behavior is a feature of OSCs, since an asymmetric hetrojunction is needed for exciton separation. For an ideal diode the dark current density $J_{dark}(V)$ varies like:

$$J_{dark}(V) = J_o(e^{qV/k_BT} - 1) \qquad (1.5)$$

where J_o is a constant, k_B is Boltzmann's constant and T is temperature in degrees Kelvin.

The overall current voltage response of OSC, can be approximated as the sum of the short circuit photocurrent and the dark current. With this consideration the net current density in the OSCs is expressed as:

$$J(V) = J_{SC} - J_{dark}(V) = J_{SC} - J_o(e^{qV/k_BT} - 1) \qquad (1.6)$$

When the contacts are isolated, the potential difference has its maximum value, the open circuit voltage V_{oc}. The same condition can be achieved when the dark current and short circuit photocurrent are exactly equal to each other.

$$V_{OC} = \frac{kT}{q}\ln(\frac{J_{SC}}{J_0} + 1) \qquad (1.7)$$

The detailed description about the constant J_0 can be obtained through fitting technique coupled with experimental data of the temperature dependence of the he reverse saturation current. Figure 1.8(a) shows one example of the electrical characteristic of a pentacene/C_{60} device in the dark within the temperature range studied (275–336 K) [35] . Analysis of the data showed that it could be best fitted with a thermally activated injection expression of the form:

$$J_o = J_{00}\exp(\frac{-\phi_B}{kT}) = J_{00}\exp(\frac{-\Delta E_{HL}}{n`kT}) \qquad (1.8)$$

where ϕ_B is the activation energy and J_{00} is a prefactor for the current. The effective barrier ϕ_B can also be written as ΔE_{HL} adjusted by an ideality factor n`. This ideality factor is induced by the effects such as energy level bending at the heterojunction and interface dipoles and so on. As shown by the solid lines in Fig. 1.8(b), the reverse saturation current density of the dark characteristics can be well fitted within the temperature range studied (275–336 K) with this model using J00=3090 A/cm2 and with ψ_B =0.55 eV. Combining the previous simple expression of V_{OC} (see Eq. (1.7)) with the expression of the reverse saturation current density given by Eq. (1.9), the following equation can be derived:

$$eV_{OC} = \frac{\Delta E_{HL}}{n`} - nkT\ln\left\{\frac{J_{00}}{J_{SC}}\right\} \qquad (1.9)$$

If we consider the Coulomb force between photo-generated electrons and holes, the equation can be write in the further form:

$$eV_{OC} = \frac{\Delta E_{HL}}{n`} - nkT\ln\left\{\frac{J_{00}}{J_{SC}}\right\} - \frac{q^2}{4\pi\varepsilon_0\varepsilon_r r_{DA}} \qquad (1.10)$$

Therefore, we know that the V_{OC} is decided by the energy difference ΔE_{HL} between the HOMO of the donor and the LUMO of the acceptor. However, if we realize the dielectric nature of the organic active layer, the charge accumulation happened on the interfaces would induce an electrostatic energy inside OSCs. Accordingly, in order to transport charges from interface to top and bottom electrodes, this electrostatic energy should be neutralized firstly, which lead to the consumption of photo-generated energy. Thus, the V_{OC} would be further

suppressed by this energy consumption and this part will be described in the section 5.2.

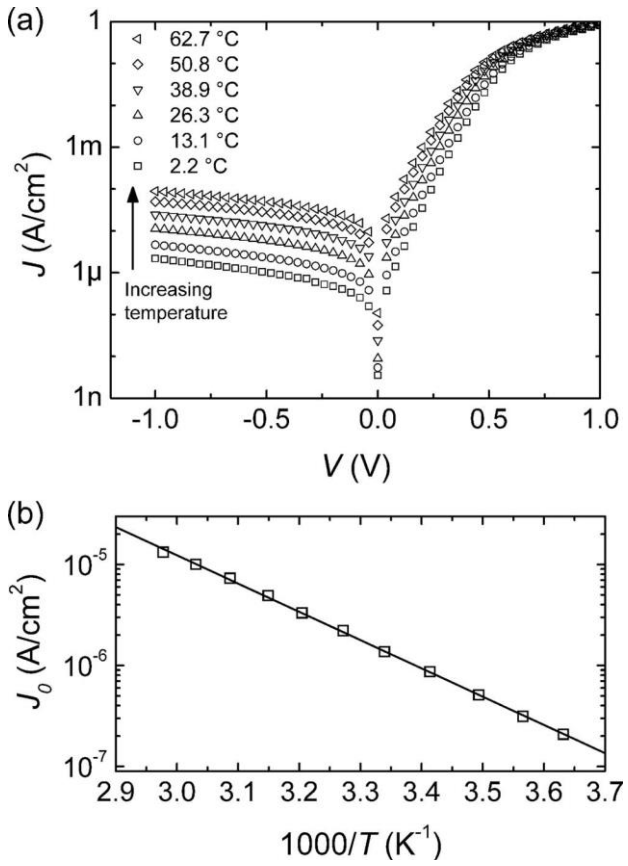

Figure. 1.8: (a) Experimental J-V characteristics of pentacene/C_{60} devices in the dark. Current density can be seen to increase with temperature. (b) J_0 calculated at different temperatures by fitting the equivalent circuit model to the experimental data plotted as a function of 1000/T and fit to the data [35].

1.2.3 Fill-factor

The fill factor is defined as the ratio of the actual maximum obtainable power to the product of the Voc and Jsc. This is a key parameter in evaluating the

performance and efficiency of solar cells. Typical commercial silicon solar cells have a fill factor > 0.70, whereas OSCs usually have a fill factor (FF) < 0.6. The analysis of the FF can depend on the common equivalent circuit of the solar cell. The equivalent circuit can be seen in the Figure. 1.9. The J-V characteristic of an illuminated solar cell can be described by this simple equivalent circuit, in which a diode and a current source are connected in parallel. The solar cells power is dissipated through the resistance of the contacts and through current loss happened inside the device. In the equivalent circuit, these effects are equivalent electrically by two parasitic resistances in series (R_s) and in parallel (R_p) with the cell and the FF is influenced by these resistances of a solar cell. The influence of these parameters on the J-V characteristic of the solar cell can be studied using the equivalent circuit presented in Figure 1.9. The J-V characteristic of the one-diode equivalent circuit with the series resistance and the shunt resistance is described by (A is the area of the solar cell, V is the output voltage):

$$J = J_0\left[\exp\left(\frac{q(V - AJR_s)}{kT}\right) - 1\right] + \frac{V - AJR_s}{R_p} - J_{ph} \quad (1.11)$$

The series resistance (R_s) arises is related to the resistance in the path for the current to flow across the cell, particularly focusing on contacts between the front surface to organic active layer, and from electrodes resistance. Under concentrated light or other conditions with high current densities, the problem of Rs is more significant. The parallel resistance (R_p) arises from leakage of current through the cell, around the edges of the device and between contacts of different

layers. It is a problem in poorly rectifying devices. The effect of R_s and R_p on the J-V characteristic is illustrated in Figure 1.10(a) and 1.10(b), respectively. In our study, by realizing the dielectric nature of OSCs, we applied a different model to the study, Maxwell-Wagner model. We are also proved the charge accumulation on the interfaces of OSCs can bring significant influence to the FF and other parameters. Maxwell-Wagner model can be briefly considered as more specific illustration of the R_p but it also reveal some special understanding about carrier behavior of OSCs. The detailed explanation can be found in section 2.2. Moreover, the charge accumulation happened inside OSCs would also alter the output of OSCs, which results in the decrease of fill-factor. Especially, the charging process happened on the electron donor-acceptor interface and its contributions to the fill-factor of OSCs were usually overlooked by other researchers. We offered detailed characterization about this point in section 5.3.

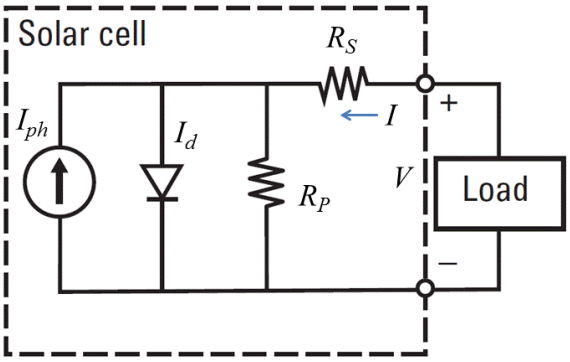

Figure 1.9: Equivalent circuit

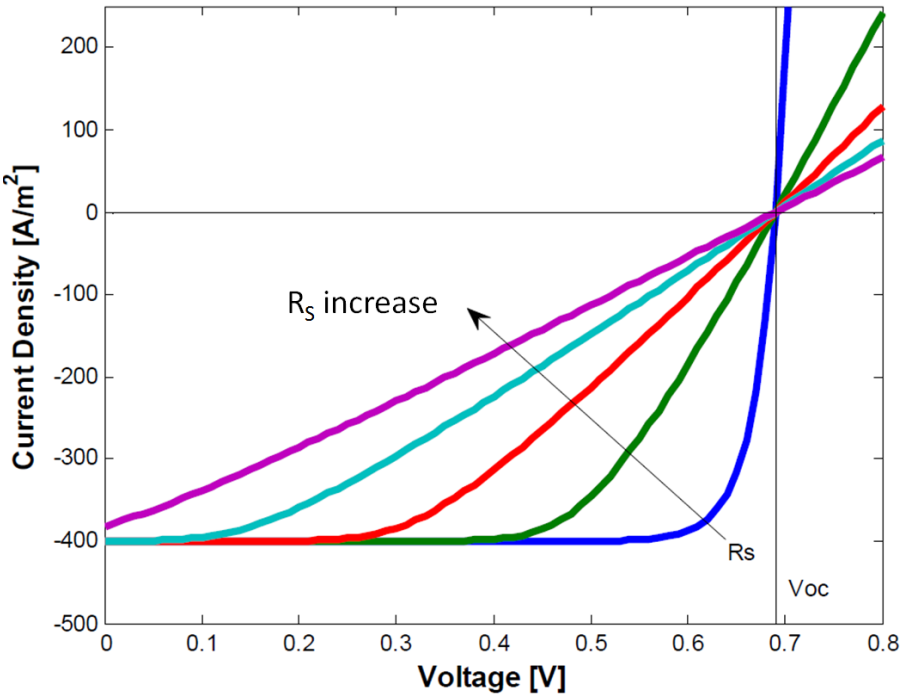
Current Density [A/m^2]
Voltage [V]
R_S increase
Rs
Voc
200
100
0
-100
-200
-300
-400
-500
0
0.1
0.2
0.3
0.4
0.5
0.6
0.7
0.8

(a)

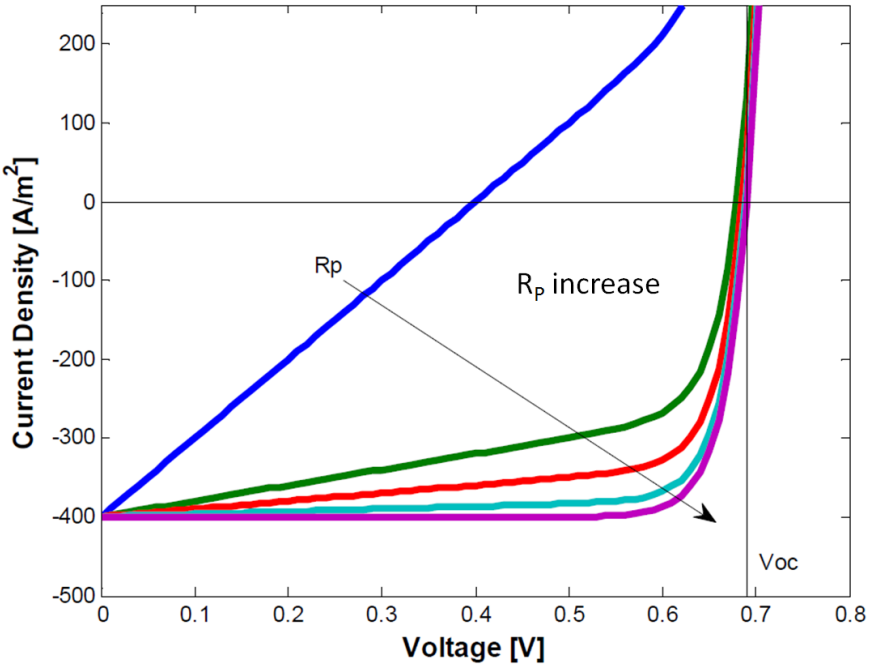
Current Density [A/m^2]
Voltage [V]
Rp
R_P increase
Voc
200
100
0
-100
-200
-300
-400
-500
0
0.1
0.2
0.3
0.4
0.5
0.6
0.7
0.8

(b)

Figure 1.10: (a) The effect of R_s on the J-V characteristic (R_p keep unchanged) (b) The effect of R_p on the J-V characteristic (R_s keep unchanged) [36]

1.2.4 Challenge for OSCs

Organic semiconductors are a less expensive alternative to inorganic semiconductors like Si. Also, organic molecules can be processed by techniques not available to crystalline inorganic semiconductors. The superior material properties of organic materials combined with a series of cheap fabrication methods have made OSCs draw a lot of expectation in both academic and industrial fields. Meanwhile, the development of the OSCs also meets with several challenges. The current Challenges for organic solar cells are described as follow:

1. Carrier behavior: The optical properties of organic materials have huge potential for they can convert almost all light into energy (charge carrier or exciton). However, the generated exciton can only travel very short distances (typically 10-20 nm) and the mobility of the organic materials remains rather low. All these carrier behaviors of OSCs, such as carrier generation, carrier transport and carrier extraction, strongly influence the efficiency of photovoltaic (PV) possess. The design for organic devices is consequently to build sufficiently thin films with optimized structure to get the carriers out. For further improvement, a clear physical picture of carrier behaviors in actual devices is needed in terms of PV effect. This is also our group’s research target.

2. Transparency: In order to increase the conductance of the OSCs, the organic films inside OSCs are usually very thin. Thus light lost is very significant due to transparency. One of the practical solutions to this problem can be the use of antireflection coatings. Another possible way is to make a tandem OSCs consisted of multiple photoactive layers with complementary absorption spectra. Yang yang group in UCLA has reported a solution processed tandem solar cell with certified 10.6% power conversion efficiency last year, which is the first certified polymer solar cell efficiency over 10% [37] (sample structure can be seen Fig. 1.11). However, both two methods are not perfect and some other better ways to effectively reduce illumination loss is still being expected. On the other hand, the structure optimization for a better utilization of the illumination also results in more complicated device structure. In the meantime, the detailed study related to the carrier behavior as well as the electrical phenomena induced by these more complicated structures is still not sufficient. Therefore, a clear physical picture of the carrier behavior in OSCs will be of help to further improve the device performance.

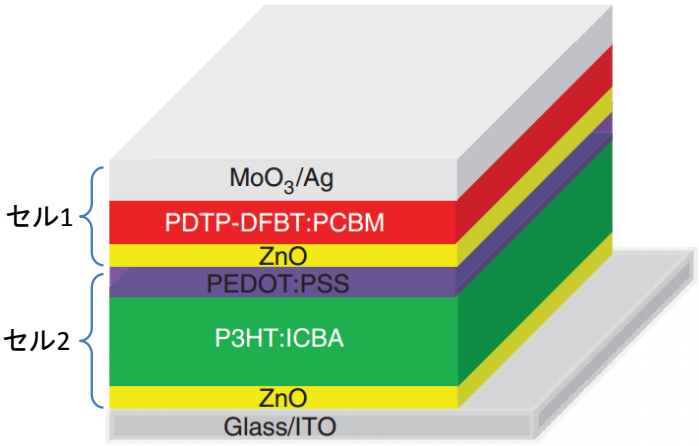

Figure 1.11: Sample structure of tandem solar cell with certified 10.6% power conversion efficiency [37]

3. Degradation with air: OSCs based electronics require stringently controlled lab conditions to minimize oxygen contamination in the polymers and composites. Nowadays, for OSCs, the highest power conversion efficiency of 12% is achieved by a German company Heliatek this year, as shown in Fig. 1.12. Before that, the world record was kept by a Japanese company Mitsubishi Kagaku, which is about 11.5%. The development of the efficiency is fast enough and it is quite possible that efficiency will soon reach the commercialized level. However, the stability of OSCs, especially the stability in the open air, is still a serious problem. This can be addressed by use encapsulation which is a necessary additional fabrication technique in current devices. So the reliable encapsulation technique is also an urgent problem for the development of OSCs

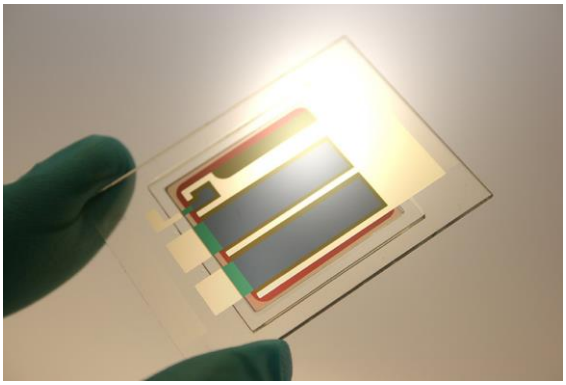

Figure 1.12: New world record achieved by Heliatek (http://www.heliatek.com)

1.3 Motivation of the present study

As we can see in the above introductions, recently organic solar cells (OSCs) have received significant attention all over the world, and many kinds of OSCs have been proposed. Among them, there are several mainstreams: Among them are bulk hetero-junction type OSCs, double-layer OSCs, single layer OSCs and so forth [38, 39]. However, the real industrial application of these devices still needs many further efforts. To accelerate the technology development of OSCs, various aspects about these devices are under investigation. Basically, the research of OSCs improvements can be divided into two groups. One group researchers are focusing on the development of new materials and news processes for OSCs. They hope to overcome the problems of OSCs, such as low efficiency or short life time, by exploring some new technique or more efficient materials. The other researchers pay more attention to the mechanism of OSCs and photovoltaic effect. They are trying to clarify the operation principle of

OSCs and thus conclude some optimization method for OSCs with only existing materials and techniques. Our group is belonging to second part.

It is well-known that carrier processes, such as separation of excitons into electron and hole pairs, life-time of carriers, and so forth, play a dominant role in OSCs devices [40, 41]. However, the detailed understanding is somehow insufficient in terms of interfacial carrier behaviors. In OSCs, excitons generated by photo-illumination diffuse to the interfaces, such as donor-acceptor molecular-interface and double layer interface, to separate into electron and holes. After that, electrons and holes are conveyed to the opposite electrodes to generate photo-voltage. This is a basic carrier process of OSCs, but in actual devices the carrier process is very complex, owing to the ambiguity of interfaces, the presence of carrier traps, the complexity of the carrier path, etc. In order to improve the efficiency of OSCs, many ideas have been presented. Among them are the development of new organic molecules with appropriate HOMO and LUMO states, the use of blocking layers between electrodes and active layers of OSCs, and so forth [31-33]. These efforts have made a contribution to increase open voltage as well as short-circuit current of OSCs, and thus to improve the efficiency of OSCs. However, the detailed study related to the carrier behavior as well as the electrical phenomena induced by the introduction of different organic layer is still not sufficient. Owing to the dielectric nature of organic materials, accumulated charges at the interface due to the Maxwell-Wagner effect significantly changes the potential distribution in OSCs, and results in the

modification of the energetic. Therefore, direct probing of the electric field and potential profiles in OSCs will be of help to understand carrier behaviors in OSCs, and thus to improve the device performance.

We have been developing a technique of the electric field induced optical second harmonic generation (EFISHG) measurement that is capable of directly probing carrier motions and electric field distribution in organic devices, e.g., organic field effect transistors, organic electroluminescence devices, and organic solar cells [42, 43], and could show the presence of the Maxwell-Wagner effect interface charges at various interfaces. EFISHG technique can be a power tools for the study of OSCs.

This motivated us to study the contribution of the dielectric nature in OSCs to the interfacial carrier processes by means of the EFISHG measurement. In this thesis, we prepared OSCs with both double and triple layer structures, and studied the dielectric nature of OSCs by using the EFISHG measurement. Firstly, we will demonstrate the capability of EFISHG for the application in the field of OSCs. After that, we will prove the presence of charge accumulation at the each interface of OSCs and the detailed variation principle of these charge accumulations will also be characterized by using EFISHG coupled with Maxwell-Wagner model. Finally, we will show that these accumulated charges can significantly influence the performance of OSCs and offer several methods to solve this problem. Modeling the prepared OSCs as Maxwell-Wagner effect

elements accounted for our experimental results, and the possible methods for improving the performance of OSCs has been concluded.

1.4 Objective and framework of this thesis

Organic solar cells have been considered as promising candidates for the next generation power device, where low-cost and printable methods are available in device fabrication. Accordingly, many kinds of OSCs have been proposed and power conversion efficiency of OSCs has been improved year-after-year [31-40]. However, the detailed study related to the carrier behavior as well as the electrical phenomena induced by the dielectric nature of organic active layer are still not sufficient. Therefore, it is important to do some fundamental study of carrier behaviors at the interface is needed in terms of photovoltaic effect, because it typically dominates the behavior of organic solar cell as we have showed in previous sections.

This thesis is organized in the following manner. For the convenience of the readers, the detailed framework of the thesis is also presented in a flowchart as in Figure 1.13.

In Chapter 1, a brief background and overview of organic electronics and organic solar cell was given, including a brief historical of organic electronics and mechanism of carrier transport in organic materials. After that, introduction on detailed characteristic of OSCs was also included as they were the essential part of the thesis and will be carefully discussed in later chapters. The challenges

of the OSCs study as well as the motivation of the research are also introduced in this chapter.

Chapter 2 presents physical models and experimental techniques employed in this thesis. The Maxwell-Wagner (MW) model based on dielectric physics has been selected as the fundamental element for the OSCs study. The MW model can be applied to both double-layer and triple-layer OSCs sample. The MW model is based on charge accumulation on the interface as a result of the difference in the relaxation times of the materials, while both accumulated charge density and time constant can be deduced by the model. This chapter we also describes the techniques used in our experiments, many of which include original concepts and improvements. First, the current-voltage (I-V) characteristics of an OSCs are explained. Then the impedance spectroscopy (IS), electric field induced optical second harmonic generation (EFISHG) techniques for characterization of carrier behavior of OSCs are introduced in detail.

Having explained about the techniques and model, we then focus on using them to investigate the carrier behaviors in OSCs devices in Chapter 3 and Chapter 3. If you want to apply a new technique (EFISHG) to the study of OSCs, you need to compare it with some well-accepted ones. Hence, we first implemented the IS technique on the OSCs structure and observed the dielectric performance of OSCs. Because this technique is based on carrier propagation, contact resistance effects can be neglected. The equivalent circuit analysis using Maxwell-Wagner effect model well accounted for the interfacial carrier

relaxation observed by IS measurement. Later on, the EFISHG measurements directly probed the interfacial carrier behaviors caused from the photovoltaic effect. The results showed the suppression of the Maxwell-Wagner type carrier relaxation in OSCs by applying a voltage corresponding to the open circuit voltage V_{oc}. EFISHG measurement coupled with IS measurement provides a clear physics picture of interfacial phenomena related to the photovoltaic effect in OSCs.

Chapter 4 takes a look at two charging processes happened inside OSCs, interfacial charging and electrode charging. It can be found that OSCs establish its internal electric field through these two charging processes. By connecting external resistance and external voltage biases to the OSCs, we showed that EFISHG measurements effectively characterize transient carrier behavior in the OSCs, in terms of photovoltaic effect. Thus, we can obtain a whole physical picture about carrier behavior of OSCs under various working conditions. These results well explained by the Maxwell-Wagner model based on dielectric physics with taking into account the photovoltaic effect.

In order to using our study to improve the performance of the OSCs, we designed several further experiments with different OSCs samples. In Chapter 5, EFISHG results clarified the contribution of the Maxwell-Wagner type interfacial charging to I–V characteristic of OSCs. The existence of interfacial charging deteriorates the performance of OSCs. For solving this problem, we suggested two methods to suppress the interfacial charging inside the OSCs. By

employing exciton blocking layer of BCP and charging blocking layer of CuPc, interfacial charge accumulation can be strongly decreased and the I-V performance of the OSCs was improved accordingly. Modeling the prepared OSCs as a Maxwell-Wagner effect element accounted for our experimental results

Lastly, Chapter 6 summarizes the thesis and proposes future prospects of this work.

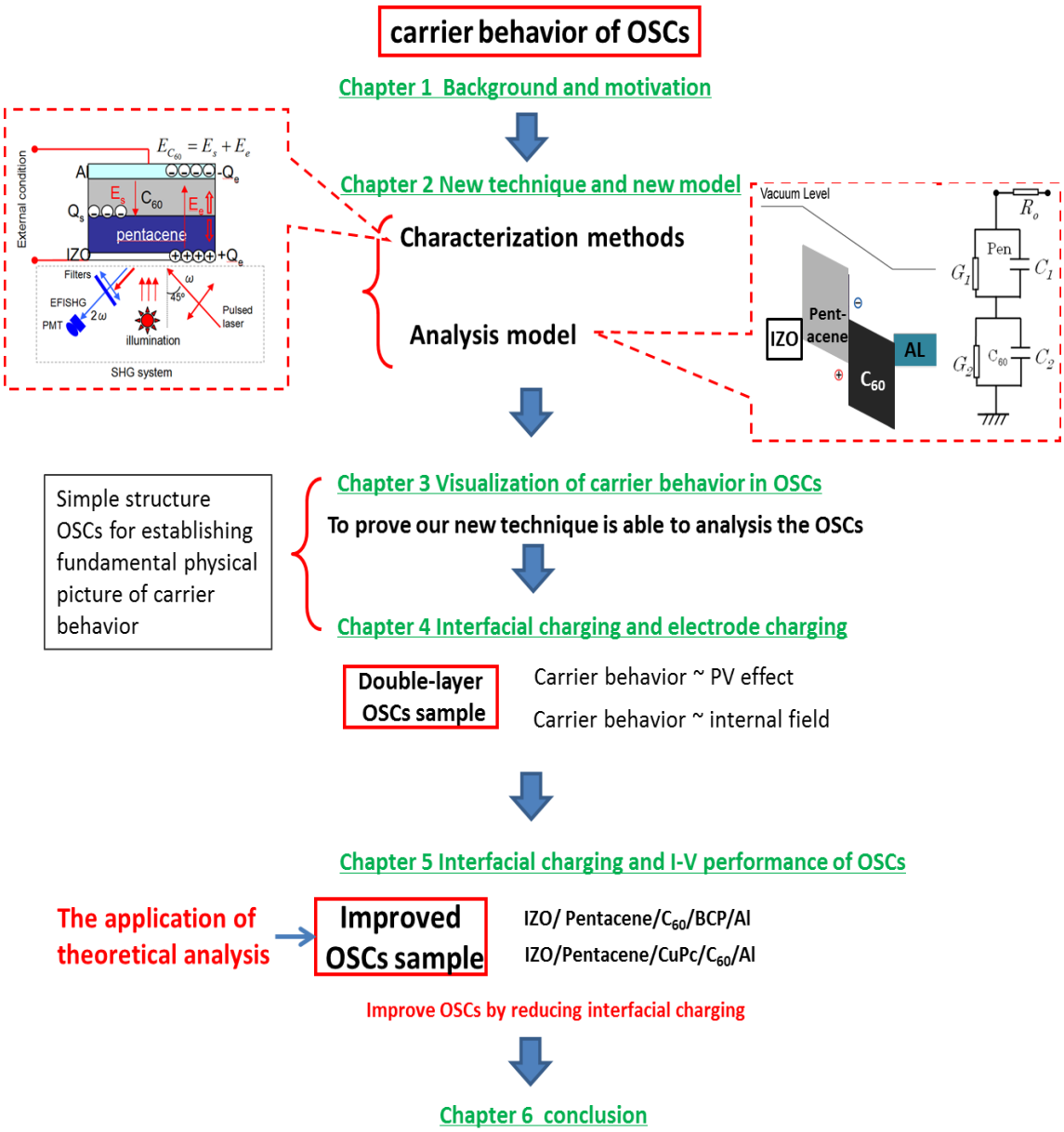

Figure 1.13: Structure of this thesis

Bibliography of Chapter 1

[1] S. Reineke, F. Lindner, G. Schwartz, N. Seidler, K. Walzer, B. Lu¨ssem, K. Leo, Nature (London) 459 (2009) 234.

[2] P. Peumans and S. R. Forrest, Appl. Phys. Lett. 79 (2001) 126.

[3] J. Xu, S. Uchida, B. P. Rand, and S. R. Forrest, Appl. Phys. Lett. 84 (2004) 3013.

[4] Herbert Naarmann, “Polymers, Electrically Conducting” in Ullmann's Encyclopedia of Industrial Chemistry 2002 Wiley-VCH, Weinheim.

[5] R. McNeill, R. J. Siudak, H. Wardlaw, D. E. Weiss, Aust. J. Chem. 16 (1963) 1056.

[6] B. A. Baracus, D. E. Weiss, Aust. J. Chem. 16 (1963) 1076.

[7] B. A. Bolto, R. McNeill, D. E Weiss, (1963). Aust. J. Chem. 16 (1963) 1090.

[8] M. R. Cutkosky, R. D. Howe, and W. Provancher,"Force and Tactile Sensors," in Springer Handbook of Robotics", B. Siciliano and K. Oussama, Eds. Heidelberg: Springer, Berlin, 2008

[9] C. D. Dimitrakopoulos and D. J. Mascaro, *IBM Journal of Research and Development*, vol. 45, (2001) 11.

[10] C. W. Tang, *Applied Physics Letters*, vol. 48, (1986) 183,.

[11] C. W. Tang and S. A. Vanslyke, Applied Physics Letters, 51, (1987) 913.

[12] J. H. Burroughes, D. D. C. Bradley, A. R. Brown, R. N. Marks, K. Mackay, R. H. Friend, P. L. Burns, and A. B. Holmes, Nature, 347, (1990) 539.

[13] T. Ameri , G. Dennler , C. Lungenschmied, C. J. Brabec, Energy Environ. Sci. 2, (2009) 347.

[14] S. Sista, Z. R. Hong, L. M. Chen, Y. Yang, Energy Environ. Sci. 4, (2011) 1606.

[15] A. Hadipour, B. Boer, J. Wildeman, F. B. Kooistra, J. C. Hummelen, M. G. R. Turbiez, M. M. Wienk, R. A. J. Janssen, P. W. M. Blom, Adv. Funct. Mater. 16, (2006) 1897.

[16] J. M. Shaw, P. F. Seidler, IBM Journal of Research and Development, 45, (2001) 3.

[17] C. C. Mattheus, A. B. Dros, J. Baas, A. Meetsma, J. L. De Boer, and T. T. M. Palstra, Acta Crystallographica Section C: Crystal Structure Communications, 57, (2001) 939.

[18] A. Miller and E. Abrahams, Phys. Rev., 120, (1960) 745.

[19] M. Pope, Electronic processes in organic crystals and polymers, Oxford University Press, 1999.

[20] H. Bassler, Phys. Stat. Sol.(b), 175, (1993) 15.

[21] S. Baranovski, Charge transport in disordered solids with applications in

electronics. Chichester, England ; Hoboken, NJ: Wiley, 2006.

[22] R.H. Friend, G.J. Denton, J.J.M. Halls, N.T. Harrison, A.B. Holmes, A. Köhler, A. Lux, S.C. Moratti, K. Pichler, N. Tessler, K. Towns, Synth. Met. 84 (1997) 463.

[23] U. Rauscher, H. Bässler, D.D.C. Bradley, M. Hennecke, Phys. Rev. B 42 (1990) 9830;

[24] E.L. Frankevich, A.A. Lymarev, I. Sokolik, F.E. Karasz, S. Blumstengel, R.H. Baughman, H.H. Horhöld Phys. Rev. B, 46 (1992), p. 9320

[25] D. Kearns, M. J. Calvin, Chem. Phys. 29, (1958) 950.

[26] A.K. Ghosh, L. Morel, T. Feng, R. F. Shaw, C. A. Rowe, J. Appl. Phys. 45, (1974) 230.

[27] N.S. Sariciftci, D. Braun, C. Zhang, V.I. Srdanov, A.J. Heeger, G. Stucky, F. Wudl, Appl. Phys. Lett. 62, (1993) 585.

[28] J.J.M. Halls, K. Pichler, R.H. Friend, S.C. Moratti, A.B. Holmes, Appl. Phys. Lett. 68, (1996) 3120.

[29] G. Yu, J.C. Hummelen, F. Wudl, A. J. Heeger, Science 270, (1995) 1789.

[30] G. Yu, J. Wang, J. McElvain, A. J. Heeger, Adv. Mat. 10, (1998) 1431.

[31] Barry P. Rand , J. Genoe, P. Heremans, J. P. Prog, Photovolt: Res. Appl. 15, (2007) 659.

[32] J. Nelson, The Physics of Solar Cells, Imperial College, UK, 2003.

[33] S. Yoo, B. Domercq, B. Kippelen, Appl. Phys. Lett. 85, (2004) 5427.

[34] A. C. Mayer, M. T. Lloyd, D. J. Herman, T. G. Kasen, G. G. Malliaras, Appl. Phys. Lett. 85, (2004) 6272 .

[35] W. J. Potscavage, S. Yoo, B. Kippelen, Appl. Phys. Lett. 93, (2004) 193308.

[36] M. Zeman, G.B. Delft, J. Krc, J. Mater. Res., 23, (2008) 4.

[37] J. You, L. Dou, K. Yoshimura, T. Kato, K. Ohya, T. Moriarty, K. Emery, C. Chen, J. Gao, G. Li and Y. Yang. Nature Communications, 4, (2013) 1446.

[38] S. Günes, H. Neugebauer, N. S. Sariciftc, Chem. Rev. 107, (2007) 1324.

[39] B. P. Land, S. Schols, D. Cheyns, H. Gommans, C. Girotto, J., Genoe, P. Heremans, J. Poortmans, Org. Electron. 10, (2009) 1015.

[40] S. Yoo, B. Domercq, B. Kippelen, Appl. Phys. Lett. 85, (2004) 22.

[41] P. Peumans, S. R. Forrest, Appl. Phys. Lett. 79, (2001) 126.

[42] D. Taguchi, T. Shino, L. Zhang, J. Li, M. Weis, T. Manaka, M. Iwamoto, Appl. Phys. Express. 4, (2011) 021602.

[43] X. Chen, D. Taguchi, T. Shino, T. Manaka, M. Iwamoto, J. Appl. Phys. 110, (2011) 074509.

[44] D. Taguchi, T. Shino, X. Chen, L. Zhang, J. Li, M. Weis, T. Manaka, M. Iwamoto, Appl. Phys. Lett. 98, (2011) 133507.

[45] X. Chen, D. Taguchi, K. Lee, T. Manaka, M. Iwamoto, Chem. Phys. Lett. 511, 491 (2011).

Chapter 2 Theoretical models and experimental technique

This chapter is intended to give the reader a more detailed introduction of our researches, from a wider scope of general knowledge of device physics to more specific information such as the application of the theoretical model and the build-up of the experimental system. Two physical models for explaining the charge carrier transport and relaxation are presented and discussed, the Maxwell–Wagner (MW) model with both double layer and triple layer system. The MW model is well-known for physical explanation of charge accumulation on the interface and organic thin film inside OSCs will be considered as dielectric materials according to this model. Hence, at the beginning of this chapter, we discussed dielectric performance happened in OSCs sample and clarified the difference between organic materials and inorganic materials. In our experiments, MW models are used to explain the charge propagation in multilayer systems represented with taking into account of photovoltaic effect and the photo-induced carrier behavior can be analyzed by using dielectric physics. The charge carrier propagation is a challenge in order to understand device physics in organic electronics. This study is important for basic understanding to interface charge propagation, i.e. dielectric physics of surfaces and interfaces. In other words, modification of the effective dielectric properties we can design interface charge and device behavior. In order to investigate the electrical properties, two conventional techniques were applied such as current-voltage (I-V) measurement and impedance spectroscopy (IS) and another novel technique which can directly observe the carrier

propagation which is second harmonic generation technique (SHG). All the details of these techniques are also explained in this chapter

2.1 Dielectric nature of OSCs

The photovoltaic process of the OSCs is started with the absorption of a photon, which generates an exciton due to the high Coulomb force induced by the low dielectric constant of organic materials. Exciton is staying at excited state. This quasi-particle can move inside the organic layer through diffusion as long as recombination processes do not take place. If the diffusion length is sufficiently long to allow the exciton to meet an internal field, hole and electron separation occurs and the charges are transported at their respective electrodes. This is the basic processes happened inside OSCs. However, in real devices the photovoltaic process is very complex, owing to the ambiguity of interfaces, the presence of carrier traps, the complexity of the recombination process, etc. In order to further analyze the physical processes of OSCs, a clear physical picture about OSCs and photovoltaic process happened inside organic active layer is necessary.

In order establish clear physical model for analyzing the operation of an OSC, it is useful to compare OSCs with conventional inorganic solar cells based on p–n junction and to highlight their fundamental differences. When an p–n junction is formed from two doped inorganic semiconductors, the carrier distributions and concentrations in the materials under equilibrium conditions can be modeled and derived from the semiconductors parameters and the properties of their interfaces with the electrodes .[1, 2] The condition of invariance of the equilibrium Fermi level leads to

the conventional band energy diagram used to describe a p–n junction in which the energies of the valence band and conduction band are position dependent near the junction (see Fig. 2.1(a)) [3] . The charge redistribution happens in the depletion region and results in a built-in potential, which is confined to the vicinity of the junction. For constant doping case, the electric field outside the depletion region vanishes and energy band shows flat structure in the middle part of semiconductor, as can be seen in Fig. 2.1(a).

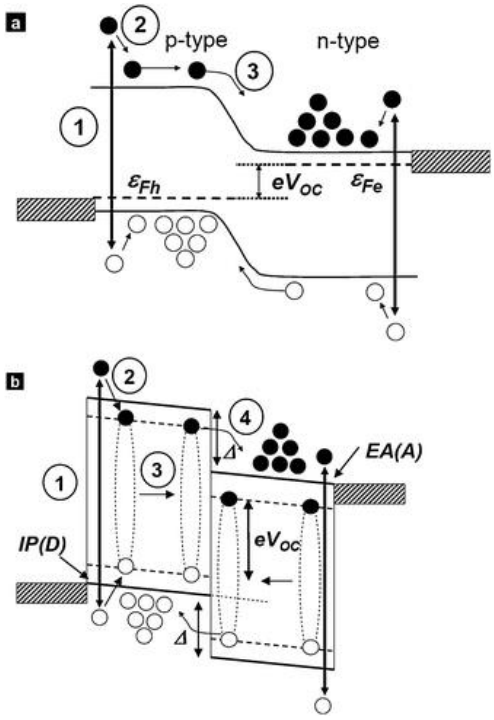

Figure 2.1: (a) energy band structure of semiconductor (b) energy band structure of organic materials [3]

Illumination applied to the materials induces electron/hole pairs. The excess of photogenerated electrons in the n-doped semiconductor and holes in the p-doped side of the junction are negligible compared to the densities of majority carriers on both sides at thermal equilibrium. In contrast, electrons and holes densities created in the

p-doped and n-doped semiconductors, respectively, are significant relative to the densities of minority carriers at equilibrium in the dark. At the junction region, the minority carriers are moving away through a drift process due to the junction potential. In the flat band region away from the junction, the moving of the minority carriers is mainly decided by diffusion. In such conditions, the photocurrent density of a conventional inorganic solar cell can be derived from the minority carrier diffusion equations obtained by combining the continuity and current equations with the consideration of the boundary conditions and surface recombination velocities. For the OSCs case, due to very low charge carrier mobility in organic materials, the insulating performances of these materials were very significant (therefore they were commonly used as insulating wires and so on since decades ago). Hence, unlike their inorganic counterparts, charge redistribution and built-in potential do not only concentrate in the depletion region and the electric field may cross the whole organic layer, as can be seen in Figure 2.1(b). The Fig. 2.1(b) showed energy level diagram of an organic heterojunction under illumination. IP(D) and EA(A) are related to the ionization potential (HOMO level energy) of the donor molecular layer and the electron affinity (LUMO level energy) of the acceptor molecular layer, respectively. The difference between IP(D) and EA(A) determines the maximum open circuit voltage (V_{OC}) under illumination. The Δ arrows denote the energy offsets between the ionization potential values (HOMO energies) and electron affinities (LUMO energies). The interface between the donor and acceptor layers plays a role for excitons similar to that played by the junction for minority carriers in inorganic cells. Since the organic layers are sandwiched between electrodes with different work functions, a built-in potential appears and results in an electric field that assists the transport of charges.[4]

Thus, the electron and hole currents in the device under illumination after exciton dissociation are governed by an interplay of drift and diffusion.[5]

On the other hand, a dielectric material is referring to an electrical insulator that can be polarized by an applied electric field. When a dielectric is placed in an electric field, electric charges do not flow through the material as they do in a conductor, but only slightly shift from their average equilibrium positions causing dielectric polarization [6]. Because of dielectric polarization, positive charges are displaced toward the field and negative charges shift in the opposite direction. This creates an internal electric field which reduces the overall field within the dielectric itself.[6] The energy level diagram in Fig. 2.1(b) is a typical display of the potential distribution of a dielectric materials, which means electric field travers the whole materials rather than focuses only on the depletion region. The distribution of the built-in potential inside the OSCs is studied many researchers, [7, 8, 9, 10], including our group. The results all showed that the energy level diagram of OSCs corresponds to the banding shape like Fig. 2.1(b) rather than Fig. 2.1(a), which indicates that the built-in potential traverse the whole organic active layer. Here is one example of observed cross-sectional potential distributions in the OSCs using Kelvin probe force microscopy [7], as shown in Fig. 2.2(a) and (b). For the thick film`s case, the total energy level diagram is similar to the inorganic materials performance, suggesting that potential drop mostly focuses on the depletion region and the middle part of the materials shows almost flat energy bang banding. However, we also noticed that thickness of the depletion region in that research is larger than 50 nm, which is close to the usual thickness of a single organic active layer. Hence, this result provided a

guideline for understanding the macroscopic device operation of OSCs and also proved the dielectric performance of the OSCs.

In fact, it is well accepted that the OSCs cannot be treated using common semiconductor model, but, at the same time, people also questioned if the dielectric model is absolutely correct for the analysis of OSCs. The main reason may be attributing to the insufficient evaluating technique. However, considering the low carrier mobility and small thickness of the organic film in OSCs, it is necessary to consider the dielectric performance of the devices. In our group, by realizing the dielectric nature of the organic thin films, we applied a simple equivalent circuit based on Maxwell-Wagner effect to the study of OSCs. Meanwhile, our self-designed laser system can also provide some direct observation about the potential distribution and carrier motion, which can support the analysis from theoretical model. The Maxwell-Wagner model coupled with experimental measurements can offer some clear understanding about device physics of OSCs.

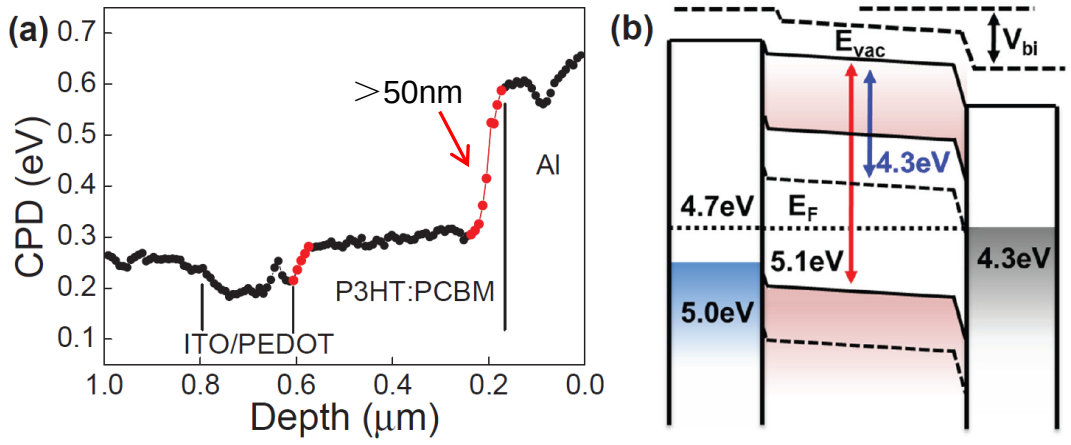

Figure 2.2: (a) The mean-field potential line-profile of the cross-sectional image and (b) the corresponding energy band diagram after contacting of all layers. [7]

2.2 Maxwell-Wagner model

2.2.1 Double-layer OSCs

The MW model is well-known for physical explanation of charge accumulation on the interface [11, 12], and relies on the microscopic electrical properties of materials. According to Maxwell's electromagnetic field theory [1, 2], charge Qs is accumulated at the interface between two dielectric materials with different relaxation times given by ($\tau=\varepsilon/\sigma$, where$\varepsilon$is the dielectric constant and$\sigma$is the conductivity) when current I(t) flows across the two-material interface[13]. More precisely, $\nabla \bullet j = 0$ with $j=E\sigma \neq 0$ is satisfied when steady state current density j flows across the interface. Under this condition, the following relation concerning electric flux density D is derived naturally at the interface:

$$\nabla \bullet D = \nabla \bullet (\varepsilon E) = \nabla \bullet \frac{\varepsilon}{\sigma} j = Q_s \qquad (2.1)$$

This is the Maxwell-Wagner effect, indicating that Q_s is accumulated at the interface when adjacent two materials have different relaxation times [14]. This simple theory illustrates the possibility that charge Q_s is accumulated at the pentacene-SiO_2 interface when a charge is injected from source electrode.

In order to understand the charge accumulation and carrier transport in double-layer OSCs, we used an equivalent circuit portrayed in Fig. 2.3, which well accounts for the interfacial charging and discharging processes due to the Maxwell-Wagner effect. Each layer is modeled using a paralleled circuit comprised of conductor (G_1, G_2) and capacitor (C_1, C_2). Two macroscopic physical parameters characterize organic thin

film existed in OSCs. These are dielectric constant $\varepsilon_{1,2}$ and conductivity $\sigma_{1,2}$, respectively. The ratio ε/σ gives a relaxation time and stands for spreading time of excess charge carriers in the materials. That is a steady-state charge distribution is established after an elapsed time around $\tau = \varepsilon/\sigma$. Note that conductivity is in proportion to carrier density n0, and give by $\sigma = \varepsilon n_0 \mu$. The carrier density n_0 is generally intrinsic carrier density of materials at thermodynamic equilibrium. According to the electro-magnetic field theory, total current flowing across organic materials is sum of the conduction current and the displacement current. The current density j of conduction current and displacement current is given by σE and dD/dt with $D = \varepsilon E$, respectively. Here E is electric field and D is electric flux density. The charge transport in each organic film can be simply described by the drift of carriers in the average electric field, on satisfying the square root of time dependence along the direction of the electric field.

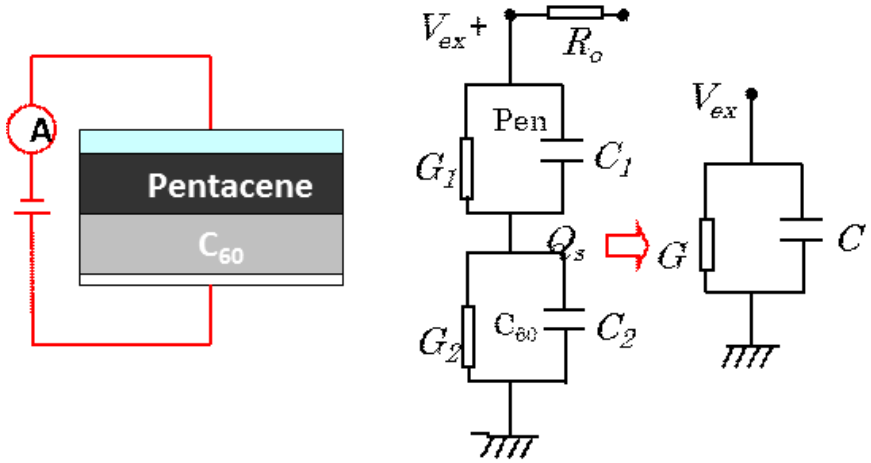

Figure 2.3: Model of OFET for Maxwell-Wagner effect

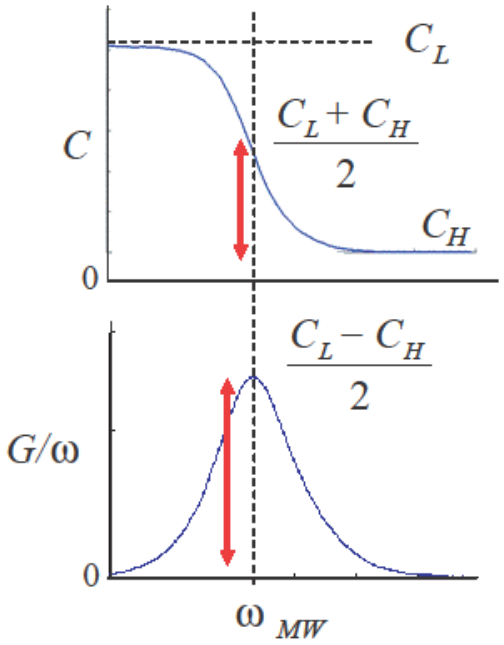

Figure 2.4: $C(\omega)$ and $G(\omega)/\omega$ plots in frequency domain.

Due the relaxation time difference between two different organic layers, the access charges would accumulate on the middle interface of the two layers according to the Maxwell-Wagner effect. Based on the simplified model of the OSCs, we can calculate the charges density on the top and bottom electrodes (Q_1 and Q_2) as follow:

$$Q_1 = -\frac{C_1 C_2}{C_2 + C_1} V - \frac{C_1}{C_2 + C_1} Q_s \qquad (2.2)$$

$$Q_2 = \frac{C_1 C_2}{C_2 + C_1} V + \frac{C_1}{C_2 + C_1} Q_s \qquad (2.3)$$

In the equation 1.2 and1.3, the V_{ex} is the external voltage applied on the two electrodes and the Q_s is the charge density accumulated on the interface between the organic and insulator layer. We can also define the value of the charge density on the interface Q_s using the equivalent circuits. As can be seen in the figure 2.3, the G_1, C_2, G_2 and C_2 are the unit conductance and capacitance of the organic and insulator layer.

$$Q_s = \frac{G_2}{G_2+G_1}VC_1 - \frac{G_1}{G_2+G_1}VC_2 = -\frac{G_2G_1}{G_2+G_1}(\tau_2-\tau_1)V \qquad (2.4)$$

On the other hand, the admittance Y of the double layer system is represented as

$$Y = G + j\omega C = \frac{1}{\mathrm{Z}} = \frac{1}{\frac{1}{G_1+j\omega C_1}+\frac{1}{G_2+j\omega C_2}} \quad ,$$

with $$G = \frac{G_1G_2}{G_1+G_2} + \frac{(G_1C_2-C_1G_2)^2}{(G_1+G_2)^3}\cdot\frac{\omega^2}{1+\tau_{MW}^2\omega^2} \qquad (2.5)$$

and $$C = \frac{C_1C_2}{C_1+C_2} + \frac{(G_1C_2-C_1G_2)^2}{(C_1+C_2)^3}\cdot\frac{\tau_{MW}^2}{1+\tau_{MW}^2\omega^2} \qquad (2.6)$$

where a response time $\tau_{WM} = \frac{1}{\omega_{WM}} = \frac{C_1+C_2}{G_1+G_2}$.

According to the Maxwell-Wagner effect, charge Q_s is accumulated with a response time τ_{MW} at the interface between layers 1 and 2 [15]. Using the equivalent circuit of Fig. 2(a), $Q_s(t)$ is derived as

$$Q_s(t) = Q_s(\infty)[1-\exp(-\frac{t}{\tau_{MW}})], \qquad (2.7)$$

when a step external voltage V_{ex} is applied. Here $Q_s(\infty) = I_c(\frac{C_2}{G_2}-\frac{C_1}{G_1})$ with $I_c = V_{ex}\frac{G_1G_2}{G_1+G_2}$. I_c is the conduction current flowing across the double-layer system. Eq. (2) indicates that $Q_s(t) = 0$ when $\frac{C_1}{G_1} = \frac{C_2}{G_2}$ $(\tau_1 = \tau_2)$, whereas $Q_s(t) \neq 0$ when $\frac{C_1}{G_1} \neq \frac{C_2}{G_2}$ $(\tau_1 \neq \tau_2)$. Accordingly the 2nd terms of G and C in Eq. (1) are zero when

$\tau_1 = \tau_2$, whereas they are non-zero when $\tau_1 \neq \tau_2$. That is, the Maxwell-Wagner type relaxation appears at the angular frequency $\omega_{MW} = \tau_{WM}^{-1}$ in the IS spectrum, but it disappears when $\tau_1 = \tau_2$. Figure 2.4 plots the $C(\omega)$ and $G(\omega)/\omega$ near the frequency of ω_{MW}, where C_L and C_H are the capacitance in the limit $f \to 0$ and $f \to \infty$, respectively. Noteworthy that in actual devices there is a dielectric relaxation due to charging onto electrode with a response time $\tau_{RC} = R_o C_t$, where C_t is the total series capacitance of the device, $C_t = \frac{C_1 C_2}{C_1 + C_2}$ (see Fig. 2.3). Therefore capacitance changes from C_H (=C_t) to zero in the high frequency limit ($f \to \infty$).

In our previous study, we successfully employed this Maxwell–Wagner (MW) model analysis for studying interfacial phenomena in double-layer organic devices, e.g., double layer organic light-emitting diode (OLED), and showed the potentiality of this analysis based on a dielectrics physics approach [15-17]. These results motivated us to apply the MW model to analyze carrier injection and transport processes in OSCs.

2.2.2 Triple-layer OSCs

In order to improve the power conversion efficiency, many ideas have been proposed to optimize the structure and the composition of the OSCs. Among them are the use of an exciton-blocking buffer layer, insertion of a hole-collection layer for the increase of open voltage, insertion of a buffer layer to shift the effective work function of the electrode, and so forth [18-20]. Noteworthy, all of these ideas suggest that the use of a multi-layer structure system with a plenty of layer-layer interfaces is key. The

carrier behaviors of OSCs will be more complex with the increase of the number of layers, though the improvement of the performance of OSCs can be anticipated. It is known that the charge accumulation on the interface of blocking layer leads to the deterioration of the I-V characteristics [21], while the insertion of a thin layer such as a copper phthalocyanine layer is an effective way to improve the power conversion efficiency [22]. Further study on carrier transport in multi-layer structure device will be helpful to improve the performance of OSCs. Hence, all of these mentioned above motivated us to study carrier motion in the multi-layer structure OSC devices by using the Maxwell-Wagner model analysis and the experiment of the EFISHG measurements.

In a manner as described in our previous paper [23], the OSC device with a BCP blocking layer is modeled using a parallel conductor-capacitor (*G*-*C*) circuit, as shown in Fig. 2.5.

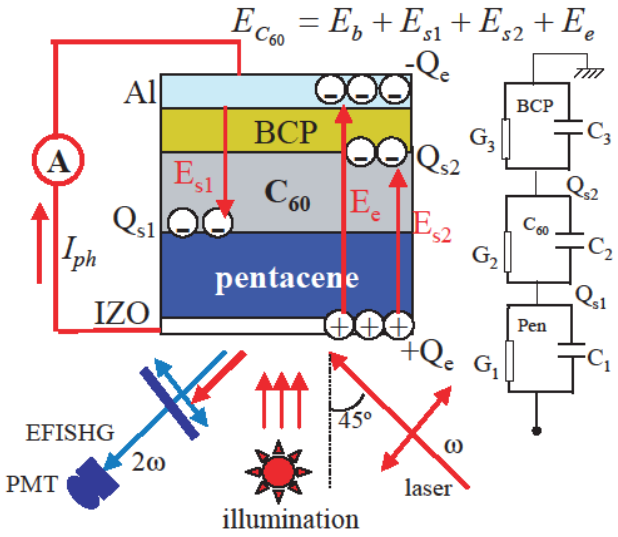

Figure 2.5: Triple-layer sample and its equivalent model.

With a DC voltage applied to the OSC in dark, charge $\pm Q_e(t)$ are induced on the top and bottom electrodes with a response time $\tau_{RC} = R_e \frac{C_1 C_3 C_2}{C_1 C_2 + C_1 C_3 + C_2 C_3} \approx 2 \times 10^{-7} \mathrm{s}$, where R_e= 160Ω is the resistance of the electrodes [23]. This is the electrode charging process. After that, the charges on the IZO electrode inject into the pentacene, and charge Q_{s1} (Q_{s2}) accumulates at the pentacene/C_{60} (C_{60}/BCP) interface. Here we assume that the BCP layer is working as a blocking layer. Using the equivalent circuit of Fig. 2.5, we get the relationship between the V_1, V_2 and V_3, under assumption that a constant d.c. current flows across the OSC. Here V_1, V_2 and V_3 are the voltage across the pentacene, C_{60} and BCP layer, respectively. That is,

$$C_1 \frac{dV_1}{dt} + G_1 V_1 = C_2 \frac{dV_2}{dt} + G_2 V_2 \quad (2.7)$$

$$C_1 \frac{dV_1}{dt} + G_1 V_1 = C_3 \frac{dV_3}{dt} + G_3 V_3 \quad (2.8)$$

with $V_3 = V - V_1 - V_2$.

After Laplace transform, eqs. (2.7) and (2.8) are rewritten as:

$$(sC_1 + G_1)V_1 + (-sC_2 - G_2)V_2 = 0$$

$$(sC_1 + sC_3 + G_1 + G_3)V_1 + (sC_3 + G_3)V_2 = (C_1 + C_3)V_1^0 + C_3 V_2^0 + \frac{G_3 V}{s}$$

Here, V_1^0 and V_2^0 are the initial voltage value across the pentacene and C_{60} layer. After a lengthy calculation, we get the V_2 as

$$V_2 = \frac{V}{C_1 C_2 + C_2 C_3 + C_3 C_1} \left(\frac{A}{s} + \frac{B}{s + \alpha} + \frac{C}{s + \beta} \right) \quad (2.9)$$

$$A = \frac{G_1 G_3}{G_1 G_2 + G_2 G_3 + G_3 G_1}(C_1 C_2 + C_2 C_3 + C_3 C_1)$$

$$B = \frac{-\alpha C_1 C_3 - A\beta + C_1 G_3 + C_3 G_1}{-\alpha + \beta}, \quad C = \frac{\beta C_1 C_3 + A\alpha - (C_1 G_3 + C_3 G_1)}{-\alpha + \beta}$$

$$\alpha = \frac{P + \sqrt{Q}}{2(C_1 C_2 + C_2 C_3 + C_3 C_1)} \quad (2.10) \text{ and } \beta = \frac{P - \sqrt{Q}}{2(C_1 C_2 + C_2 C_3 + C_3 C_1)} \quad (2.11),$$

where $P = G_1 G_2(\tau_1 + \tau_2) + G_2 G_3(\tau_2 + \tau_3) + G_1 G_3(\tau_1 + \tau_3)$ and

$$Q = G_1^2 G_2^2(\tau_2 - \tau_1)^2 + G_2^2 G_3^2(\tau_3 - \tau_2)^2 + G_1^2 G_3^2(\tau_1 - \tau_3)^2 - 2G_1^2 G_2 G_3(\tau_3 - \tau_1)(\tau_1 - \tau_2) - 2G_3^2 G_2 G_1(\tau_3 - \tau_1)(\tau_2 - \tau_3) - 2G_2^2 G_1 G_3(\tau_2 - \tau_3)(\tau_1 - \tau_2),$$

where $\tau_i = C_i / G_i$ is the relaxation time for the each layer of the OSCs. Here, 1/α and 1/β are time constants of the two relaxation processes and the interaction between two relaxation processes dominate the whole transient process of the OSCs.

Finally, the accumulated charge density of the pentacene/C_{60} (Q_{s1}) and C_{60}/BCP (Q_{s2}) interface is derived as:

$$Q_{s1} = C_2 V_2 - C_1 V_1 = \frac{G_1 G_2 G_3(\tau_2 - \tau_1)}{C_1 C_2 + C_3 C_2 + C_1 C_3}\left(\frac{1}{\alpha\beta} + \frac{\frac{1}{\alpha} - \tau_3}{\alpha - \beta} e^{-\alpha t} - \frac{\frac{1}{\beta} - \tau_3}{\alpha - \beta} e^{-\beta t}\right). \quad (2.12)$$

$$Q_{s2} = C_3 V_3 - C_2 V_2 = \frac{G_1 G_2 G_3(\tau_3 - \tau_2)}{C_1 C_2 + C_3 C_2 + C_1 C_3}\left(\frac{1}{\alpha\beta} + \frac{\frac{1}{\alpha} - \tau_1}{\alpha - \beta} e^{-\alpha t} - \frac{\frac{1}{\beta} - \tau_1}{\alpha - \beta} e^{-\beta t}\right) \quad (2.13)$$

Here 1/α and 1/β stand for the time constants. In the limit $t \to \infty$, $Q_{si}(\infty) = I_c \Delta\tau_i$, where I_c is the steady-state current flowing across the OSCs [21], and $\Delta\tau_i$ (i = 1, 2) is the relaxation time difference between the adjacent materials, i.e., pentacene and C_{60} (i=1), and C_{60} and BCP (i=2). From eqs. (2.12) and (2.13), we know that two relaxation processes happen during the transient process and the

interaction between them dominates two interfacial charging processes. Meanwhile, both interfacial charging processes proceed with the same two time constants (1/α and 1/β) and thus depend on each other. Under the actual experimental conditions, we can simplify eqs. 2.12 and 2.13. Due to the insulating performance of the BCP blocking layer, τ_3 should be much longer than τ_1 and τ_2. Hence, if the two interfacial charging processes can be totally separated and the relaxation of the pentacene/C_{60} interface is much faster than that of C_{60}/BCP interface ($\frac{1}{\alpha} << \frac{1}{\beta} \approx \tau_3$), the third part of eq. (2.12) and the second part of eq. (2.13) are neglected. In this situation, two interfacial charging processes are approximately considered as two independent single relaxation processes. Consequently, the accumulated charges on the two interfaces are given as:

$$Q_{si}(t) = Q_{si}(\infty)[1 - \exp(-\frac{t}{\tau_{MWi}})] \quad (i = 1, 2), \qquad (2.14)$$

with the Maxwell-Wagner type relaxation times $\tau_{MWi} \approx 1/\alpha$ for the petacene/C_{60} interface and $\tau_{MWi} \approx 1/\beta$ for C_{60}/BCP interface. From the calculation of 1/α and 1/β, we know that both *P* and *Q* in α and β are proportional to the conductance value of the organic layer. Hence, with the increase of the conductance $G_{i,}$ both 1/α and 1/β decrease and the two interfacial charging processes become faster. Meanwhile, the difference between the two relaxation times is expressed as $\Delta\tau_{MW} = 1/\alpha - 1/\beta = \frac{4\sqrt{Q}(C_1C_2 + C_2C_3 + C_3C_1)}{P^2 - Q}$ and $\Delta\tau_{MW}$ should also decrease with the increase of the conductance G_i. Therefore, if the conductivity of the organic active layer is very high, the two interfacial charging processes will proceed in the same

way, where $\frac{1}{\alpha} \approx \frac{1}{\beta}$. In that case, the second and third parts of both eq. (2.12) and (2.13) are equal to each other, which results in the suppression of the charging accumulation on the two interfaces. In that situation, the charging of the two interfaces may not be detectable individually using the second harmonics generation measurement.

2.3 Measurement techniques

2.3.1 Evaluating technique for OSCs

Various experimental techniques have been employed to observe the carrier transport and relaxation in OSCs, including time-of-flight, transient photovoltage, and photoinduced charged carrier extraction by linearly increased voltage methods. [24–26] Generally speaking, the evaluating technique of carrier behavior in OSCs can be briefly divided into two kinds, electrical measurement and optical measurement, as can be seen in Figure. 2.6. For the electrical measurement, the sample is triggered by electrical signal, such as voltage pulse, DC biases or continuous wave signal. The electrical measurements are rather easy to perform and thus they are commonly used by many researchers. However, some of the experimental techniques require intentionally thick devices, are applicable to only blend thin films (not devices), or focus on injected dark current. Moreover, for the electrical measurement, the probing signal is usually applied from outside of the sample, while the response signal is also collected from the external part of the device. Hence, the electrical measurements also have been considered as the black-box measurement, which means that there is no

direct observation form the inside the OSCs. The external attachments for the measurement not only increase the possibility of the experimental error but also restrict the experimental conditions. For example, the exact open-circuit and short-circuit conditions cannot be easily achieved by electrical methods. Thus, direct comparison of carrier behaviors under the different cell operating conditions is more possible with non-contact measurements, like optical measurements.

In most of reported optical techniques, the focusing points are always related to the carrier dynamics and lifetime inside OSCs. While the dynamics of the charge separation reaction in such organic thin film directly decide the generation of photovoltaic effect, the reverse charge recombination reaction also receives significant attention. The kinetic competition between this recombination reaction and charge collection by device electrodes is a key factor which may limit device performance. In the optical measurements, a transient response to an intense pulsed photo excitation is measured and analyzed for clarifying the carrier behavior, while the relaxation time of the carrier can be deduced from both equilibrium state and transient conditions. Among these optical techniques, there are Light-induced Electron Spin Resonance, Photo-induced Reflection/Absorption, Transient Absorption and more recently, Continuous-Wave Photoinduced Absorption Spectroscopy [27-30]. It is no doubt that these techniques will give us a deeper understanding of separation and recombination of carriers in a working OSCs at various time scales and temperatures, which are the key factors for the further improvement of OSCs. However, in our research, we try to study the dielectric nature of OSCs and to improve the performance of OSCs by clarifying the physical process in it. We need a strong technique can provide us some direct observation of the electric field

distribution inside OSCs and thus we can confirm the dielectric performance of OSCs. Of course, the dynamics of carrier behavior is very important, but only by studying the lifetime of the photo-generated carriers cannot establish a whole picture about the operation of OSCs. Thus, the above techniques cannot fulfill our requirements. Consequently we are paying attention to electric-field-induced second-harmonic generation (EFISHG) measurement, which is available for directly probing the electric field distribution in organic devices in terms of carrier behaviors. This EFISHG technique has been developed by our group. It is a technique of the electric field excited optical laser system that is capable of directly probing carrier motions and electric field distribution in organic devices, e.g., organic field effect transistors, organic electroluminescence devices [16, 22], and simple metal-insulator-metal structure [17, 23], and could show the presence of the Maxwell-Wagner effect interface charges at various interfaces. These previous studies motivated us to study the dielectric performance and interfacial carrier processes of OSCs by means of the EFISHG measurement.

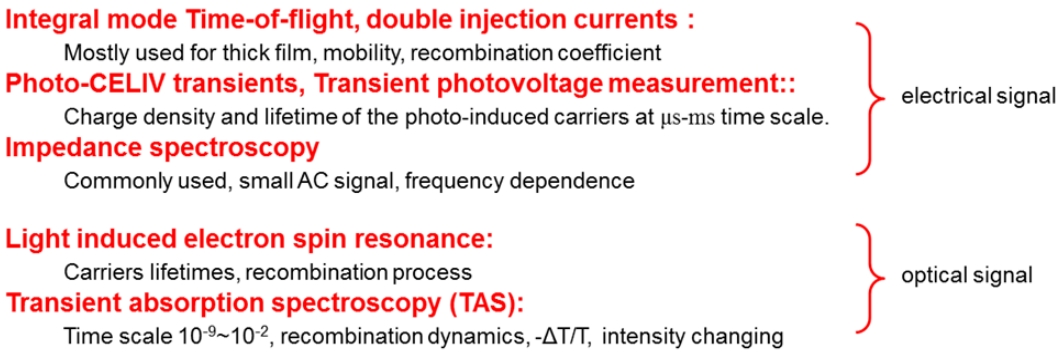

Figure 2.6: Classification of measurement technique for OSCs

2.3.2 I-V measurements

Current-voltage (I-V) measurement is a very common and straightforward method to characterize electrical property of a material or a device. In the case of organic materials, there is only one-carrier injection current, thus a considerable understanding of the one-carrier injection property is quite important. The theory of one-carrier currents must deal with free and trapped charge density, free-carrier drift velocity (namely, the problem of mobility), and electric field intensity. For simplicity we can only pay attention to its average values and the relations connecting them, which is already a good representative property of the material and the intrinsic physics. Since we employ Maxwell-Wagner model to analyze OSCs, the discussion of the I-V characteristic should also correspond to the situation of dielectrics, (free of traps and negligible density of free carriers in thermal equilibrium). All injected charge carriers remain free and contribute to the space charge. At low electric field region, the carrier drift velocity is proportional to the applied field, namely

$$\upsilon = \mu E = \mu \frac{V}{L}$$

where μ is the carrier drift mobility and E is the average electric field intensity. If the current is limited by the drift component of inject carriers, the space-charge-limited conduction current density can be written as:

$$J = \frac{9\mu\varepsilon V_{ex}^2}{8L^3} \qquad (2.15)$$

where V_{ex} is the applied voltage, and L is the length of the plane-parallel sample. This expression is known as the Mott-Gurney law.

As described previously, many important parameters of OSCs can be directly determined from current-voltage (I-V) measurements of the solar cell. The I-V characteristics are measured using one of the source meters, namely Keithley 2400, which can source and measure both current and voltage. Note that the Keithley 2400 electrometer was used to measure precise current down to 10^{-12} A. At the low current level, a significant correction due to the grid current of the Keithley became necessary. From the most general point of view, grid current and amplifier zero drift are also background noise. The full scale input for each voltage and current measurement range is 105.5% of the selected range. Once the scale has been set the saturation occurs above 1.05. When the input levels exceed the maximum levels, the `OVERFLOW' message to be displayed on the front panel of the Keithley and constant reading. Use the lowest possible range without causing an overflow to ensure best accuracy and resolution. On the other hand, the voltage was applied with the Keithley 2400 instrument. The voltage sweeping rate is rather slow (in the order of mHz) to ensure that the OSCs work in the steady state. All measurements were conducted in air at room temperature. A red light from a light-emitting diode (wavelength 630 nm, intensity 10 mW/cm^2) was used as a light source to provide illumination pulse (repetition rate 10 Hz, duration 50 ms, switching on and off times within 50 ns) to the OSCs devices. The samples were tested with two conditions, both with and without illumination.

2.3.3 Impedance spectroscopy measurement

Impedance spectroscopy (IS) is a small signal analysis and widely used for characterizing device parameters [31]. By applying a small AC signal to devices

under various DC biasing conditions, components of the equivalent circuit of devices are evaluated. I.H. Campbell et al were considered the first to apply impedance measurement on MEH-PPV in 1995 [32]. They found that, for thin transparent gold as the positive contact and calcium as the negative contact (Au/MEH-PPV/Ca), in reverse bias, because the polymer layer is fully depleted, capacitance is independent of bias. A capacitance increase due to the charging of the traps was observed under a small forward bias, while a capacitance decrease due to the neutralization of the traps was observed under a larger forward bias. From the capacitance increase, trap density was also estimated.

One advantage of impedance spectroscopy's ability is that it can separately observe the behaviors of interactions with various time constants. G. Yu et al have measured complex admittance of polymer LECs [33]. They applied a pulsed driving scheme that takes advantage of the slow ionic response and rapid electronic response to independently control the carrier injection. Thus, they proposed an operating scheme to separately control the distribution of ionic charges and the flow of electronic current. Impedance spectroscopy also has an advantage in that it can distinguish contributions of the interface from the bulk, when the equivalent circuit of device is well-known on the basis of device physics. Consequently it has been used as a tool for characterizing devices over the past several ten years [34, 35].

In our research, the IS measurements were performed with a Solartron 1260 impedance/gain-phase analyzer in the frequency range of 10 Hz -1 MHz in dark and under photo-illumination. The OSCs were short-circuited, and an AC voltage with amplitude of 10 mV was applied in the measurements. In the IS measurement, the

equivalent circuit model and fitting method are commonly used to evaluate the experimental results. The equivalent circuit model should precisely describe and model the electrical properties of the device. It usually consists of basic components such as resistors and capacitors, which mirror the behavior of various layers in the structure. The understanding of the AC characteristics of such model can also decide the explanation of the data. In our case, the obtained spectra were curve-fitted using the equivalent circuit of Maxwell-Wagner model. For the situation of analyzing organic device, organic device physics is still not clear and thus the equivalent circuit for IS measurement is not able to precisely present all the physical phenomenon happened inside the devices. On the other hand, photovoltaic effect is essential in OSCs. Accordingly we are searching for a method capable of finding the contribution of photovoltaic effect. However this is not so easy to evaluate the organic photovoltaic effect only by using IS measurement, without knowing the variation of the electric field in the organic layer. Consequently we are paying attention to electric-field-induced second-harmonic generation (EFISHG) measurement, which is available for directly probing the electric field distribution in organic devices in terms of carrier behaviors [16, 22, 23]. The EFISHG measurement coupled with IS measurement provides a clear physics picture of interfacial phenomena related to the photovoltaic effect in OSCs.

2.3.4 Electric-Field-Induced Second Harmonic Generation

Optical second harmonic generation (SHG) method is a well-known technique. During the measurement, the amount of second-harmonic signal is produced when an intense laser beam with the fundamental wavelength is applied to the sample.

According to dielectric physics, material with insulating performance under electric field will generate some polarization, since any material can be thought of as a collection of charged particles - electrons and positively charged cores. The polarization can be expanded in a Taylor series in terms of the total applied electric field (including external electric field, inner electric field such as generated by accumulated charge, electromagnetic wave electric field, etc.) as the following form:

$$P = P^{(1)} + P^{(2)} + P^{(3)} + ... = \chi^{(1)} : E + \chi^{(2)} : EE + \chi^{(3)} : EEE + ... \quad (2.16)$$

where $P^{(1)}$, $P^{(2)}$ and $P^{(3)}$ are linear, quadratic, and cubic polarization in the electric field (E), $\chi^{(1)}$, $\chi^{(2)}$ and $\chi^{(3)}$ are the first-, second-, and third-order electric susceptibilities (or linear, first-, and second-nonlinear electric susceptibilities), and the operation ":" represents the scalar product between matrices. Note that the higher order polarization contributes less and less since the higher susceptibility becomes more and more negligible. Thus the higher order of polarization, namely the nonlinear polarization could not be observed only until 1960s while the powerful laser was developed and used to study the non-linear optics, since the laser has a very high electric field, typically 1 MV/cm.

In this study we pay attention on $P^{(2)}$, which contributes to the second-order nonlinear optical phenomena. Since the electric susceptibility connects the product of the two electric field vectors with the polarization vector, it is a tensor of rank 3. In other words, it contains 27 components and can be treated as a 3×3×3 matrix. Simply, for a material with inversion symmetry illuminated under a laser light (with frequency of ω), all 27 components of the susceptibility are vanished, namely become zero, thus there should be no second order polarization phenomena; namely no second harmonic

generation (SHG) with frequency of 2ω can be observed. On the contrary, the SHG is possible to be detected for the material with non-inversion symmetry. Does this mean that we could not detect SHG signal from a material with inversion symmetry? Not absolutely. Recently our lab has developed some unique method, the electric field induced second-harmonic generation (EFISHG) for the material, since the external electric field applied on the sample will disturb the electronic distribution of the material and thus change the symmetry, as illustrated in Fig. 2.7. In details, by laser irradiation, EFISHG signal is generated from organic layers due to the coupling of electrons in molecules and electro-magnetic waves E (ω) in the presence of electrostatic local electric field E (0). The EFISHG intensity is given as:[11, 14]

$$I(2\omega) \propto \left|\vec{P}(2\omega)\right|^2 \qquad \vec{P}(2\omega) = \chi^{(3)}(-2\omega;0,\omega,\omega)\vdots E(0)E(\omega)E(\omega) \qquad (2.17)$$

where $\vec{P}(2\omega)$ is the nonlinear polarization induced in the organic layers and $\chi^{(3)}$ is the third order nonlinear susceptibility tensor. E (0) is the electrostatic local field in the organic layers (we define as that positive electric field E (0) points from the IZO electrode to the Al electrode), and E (ω) is the electric field of incident laser beam. Equation indicates that the square-root of the SHG intensity is in proportion to the electric field E (0) in the organic layers. Here, E (0) is given by E_0+E_s, where E_0 (=$Q_m/\varepsilon_r\varepsilon_0$) is the electric field originated from charges $\pm Q_m$ on top and bottom electrodes of the OSCs and E_s is the electric field originated from charges in organic devices, e.g., charges Q_s accumulated at the double-layer interface. Consequently, the EFISHG measurement probes the charges $\pm Q_m$ on electrodes as well as charges Q_s at the interface.

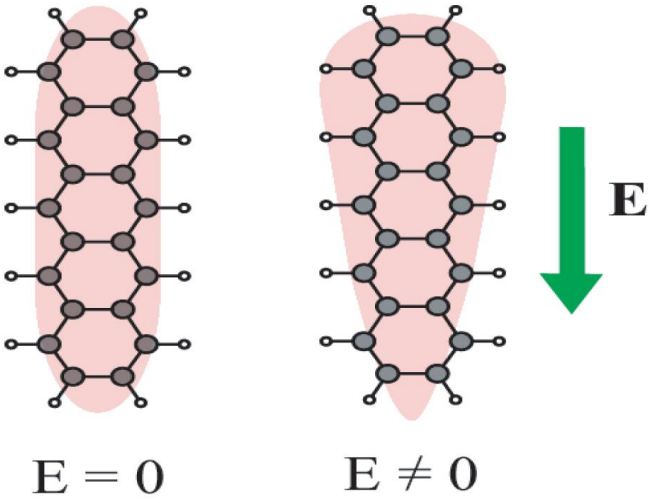

Figure 2.7: Sketch of distortion of electronic cloud for a pentacene molecule under external electric field.

Figure 2.8 portrays an experimental arrangement for the EFISHG measurement. We used a pulsed laser as a probing light (repetition rate 10 Hz, average power 1mW, duration 4 ns), which was generated using an optical parametric oscillator pumped with the third-harmonic light of Qswitched Nd:YAG laser. p-polarized pulsed laser beam focused onto the sample surface at an incident angle of 45^{o}, where the spot size was smaller than the device area. The reflected fundamental laser beam was eliminated using optical filters and a monochromator. The SHG light generated from the sample was detected using the photomultiplier tube (PMT), and the intensity $I(2\omega)$ was measured using a digital multimeter. The susceptibility tensor $\chi^{(3)}$ in eq. (2.17) is a material dependent parameter and is a function of the optical frequency ω. The difference in $\chi^{(3)}$ among materials allows us the electric field in each layer of a

double-layer OSCs to be selectively probed by the use of an appropriate laser beam wavelength.15) In the most of researches, we used the laser beam at a wavelength of λ_{ω}=1000 nm and recorded the generated SHG at a wavelength of $\lambda_{2\omega}$=500 nm to selectively measure the electric field in C_{60} layer. In the time-resolved SHG measurements, we illuminated the OSCs under various external conditions. Photocurrent was generated under a red illumination (50 ms illumination at the intensity 10 mW/cm^2 followed by 50 ms break) from the LED synchronized with the incidence laser beam. Under the short-circuit condition, excess charges Q_s is expected to be accumulated at each interface of OSCs due to the Maxwell–Wagner effect, while exciton separation is provoked at the interface. The presence of charge Q_s changes the electric field in OSCs, and the EFISHG probes the electric field change.

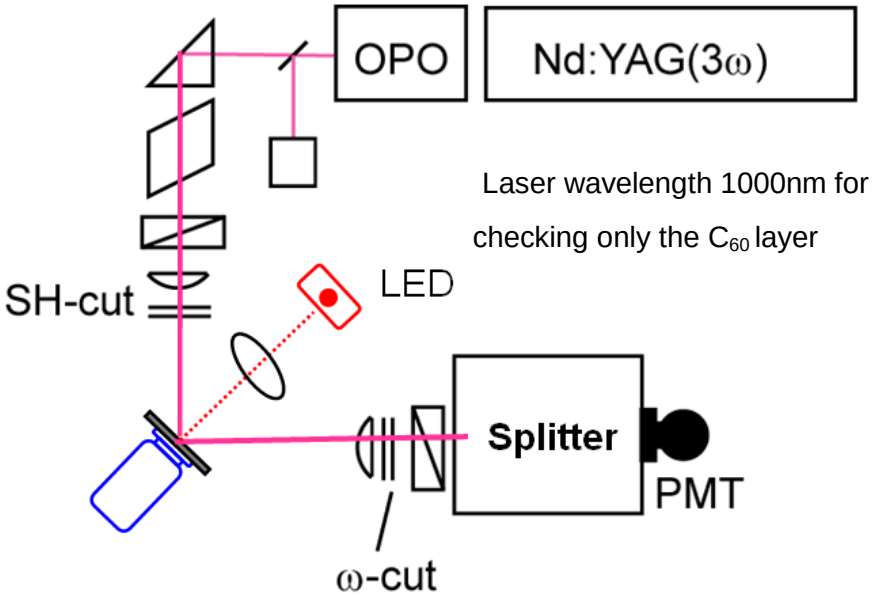

Figure 2.8: The arrangement of the EFISHG measurement on the OSCs sample.

2.4 Summary

The theoretical model and experimental methods are illustrated in this chapter, in order to bring out some fundamental materials for our research. In the first part, we focused on the explanation of dielectric nature of OSCs. By realizing dielectric nature of the organic layer, we established our theoretical model based on Maxwell–Wagner effect and thus the interfacial carrier relaxations of OSCs with both double-layer and triple-layer have been analyzed by using this model. The results revealed that charge relaxation processes happened on each interface of OSCs and the interaction between these charging processes dominated the carrier behavior inside the OSCs. Moreover, for triple-layer sample, two interfacial charging processes can be clearly observed for the sample with low conductivity, while two interfacial charging processes merged each other for the sample with high conductivity. By using the Maxwell-Wagner model, we proved that dielectric nature of the OSCs governs the working mechanism of photovoltaic effect.

On the other hand, we have also elaborated the evaluation technique of OSCs. We mentioned how to obtain the important parameters of OSCs through simple I-V measurement, IS method and EFISHG measurement. The importance of each measuring methods to study the OSCs on carrier generation and transport on bias of photovoltaic effect were well explained. The IS method can investigate the carrier trapping and relaxation inside OSCs by using Maxwell-Wagner equivalent circuit fitting. However, they are not sufficient for analyzing the carrier behavior well as they resemble a black box. Thus, optical EFISHG measurement, which enables us directly probe electric field generated in the semiconductor layer, will be coupled with the

conventional I-V measurements to study the carrier behavior in the OSCs due to photovoltaic effect. Finally, a combination of these techniques may bring us further insights in device operation and charge relaxation and transport mechanisms. A comparison is made in Table. (2.1) for these techniques. Here TAS related to Transient Absorption Spectroscopy. We didn't employ this technique, but it is commonly used as an optical method for deciding the carrier life time inside OSCs. We put it here to show the difference between EFISHG and other common optical method.

Table 2.1: The comparison between different measurements

	I-V	IS	TAS	SHG
Measurement	Electrical		Optical	
Applied signal	External bias	Small AC @ bias	Laser signal @excitation	Laser signal @ excitation
Obtained signal	current	Conductance capacitance	-ΔT/T	Harmonics signal
Type	Steady State	Transient		
Isolated sample	✘	✘	✓	✓
Relaxation time	✘	✓	✓	✓
E-field distribution	✘	✘	✘	✓
Difficulty ($$$)	*	**	***	****
Precision	**	*	****	****

Bibliography of Chapter 2

[1] R. F. Pierret, Semiconductor Device Fundamentals, Addison Wesley, Reading, Massachusetts, 1996 .

[2] S. M. Sze, K. K. Ng, Physics of Semiconductor Devices, Wiley Interscience, Hoboken, New Jersey, 2007.

[3] B. Kippelen and J.L. Brédas, Energy & Environ. Science 2, (2009) 241.

[4] I. H. Campbell, T. W. Hagler, D. L. Smith, J. P. Ferraris, Phys. Rev. Lett., 76, (1996) 1900

[5] P. W. M. Blom, V. D. Mihailetchi, L. J. A. Koster, D. E. Markov, Adv. Mater., 19, (2007) 1551

[6] R. Hippel, Dielectric Materials and Applications, Technology Press of MIT and John Wiley, NY, 1954

[7] J. Lee, J. Kong, H. Kim, S. Kang, K. Lee, Appl. Phys. Lett. 99, (2011) 243301.

[8] M. Zeman, Thin Film Solar Cells Fabrication, Chapter 5, John Wiley & Sons, New York, 2006

[9] T. Kobayashi, Y. Terada, T. Nagase, H. Naito, Appl. Phys. Express 4, (2011) 126602.

[10] H. Hoppe, N. Arnold, N.S. Sariciftci, D. Meissner, Solar Energy Materials & Solar Cells 80 (2003) 105

[11] J. C. Maxwell, A treatise on electricity and magnetism, New York,: Dover, 1954.

[12] K. W. Wagner, Electrical Engineering (Archiv fur Elektrotechnik), 2, (1914) 371.

[13] T. Manaka, E. Lim, R. Tamura, D. Yamada, and M. Iwamoto Appl. Phys. Lett. 89, (2006) 072113.

[14] T. Manaka, E. Lim, R. Tamura, and M. Iwamoto, Nature photonics 1, (2007) 581.

[15] E. Lim, T. Manaka, R. Tamura, and M. Iwamoto, Jpn. J. Appl. Phys. 45, (2006) 3712.

[16] D. Taguchi, T. Shino, L. Zhang, J. Li, M. Weis, T. Manaka, and M. Iwamoto, Applied Physics Express 4, (2011) 021602.

[17] L. Zhang, D. Taguchi, J. Li, T. Manaka, and M. Iwamoto, J. Appl. Phys. 108, 093707 (2010).

[18] E. Itoh, Y. Highchi, D. Furuhata, and T. Shirotori: Jpn. J. Appl. Phys. 50 (2011) 01BC14.

[19] G. Li, V. Shrotriya, J. Huang, Y. Yao, T. Moriarty, K. Emery, and Y. Yang: Nature Mater. 4 (2005) 864.

[20] W. Cai, X. Gong, and Y. Cao: Sol. Energy Mater. Sol. Cells 94 (2010) 114.

[21] J.C. Wanga, X.C. Ren, S.Q. Shi, C.W. Leung, and P. Chan: Org. Electron. 12 (2011) 880.

[22] X. Chen, D. Taguchi, K. Lee, T. Manaka, and M. Iwamoto: Chem. Phys. Lett. 511 (2011) 491.

[23] X. Chen, D. Taguchi, T. Shino, T. Manaka, and M. Iwamoto: J. Appl. Phys. 110

(2011) 074509.

[24] Y. Kim, S. Cook, S. M. Tuladhar, S. A. Choulis, J. Nelson, J. R. Durrant, D. D. C. Bradley, M. Giles, I. McCulloch, C. Ha, and M. Ree: Nat. Mater. 5 (2006) 197.

[25] C. G. Shuttle, B. O. Regan, A. M. Ballantyne, J. Nelson, D. D. C. Bradley, J. de Mello, J. R. Durrant, Appl. Phys. Lett. 92 (2008) 093311.

[26] A. J. Mozer, G. Dennler, N. S. Sariciftci, M. Westerling, A. Pivrikas, R. O. sterbacka, G. Juska, Phys. Rev. B 72 (2005) 035217.

[27] N. A. Schultz, M. C. Scharber, C. J. Brabec, N. S. Sariciftci, Phys. Rev. B 64, (2001) 245210.

[28] C. Arndt, U. Zhokhavets, G. Bobsch, C. Winder, C. Lungenschmied, N. S. Sariciftci, Thin Solid Films 60, (2004) 451.

[29] A. F. Nogueira, I. Montanari, J. Nelson, J. R. Durrant, C. Winder, N. S. Sariciftci, C. J. Brabec, J. Phys. Chem. B 107, (2003) 1567.

[30] T. Kobayashi, Y. Terada1, T. Nagase, H. Naito, Appl. Phys. Express 4 (2011) 126602.

[31] M. J. Ross and K. R William, Impedance Spectroscopy: Emphasizing Solid Materials and Systems, John Wiley & Sons, New York, 1987.

[32] I. H. Campbell, D. L. Smith, J. P. Ferraris, Appl. Phys. Lett. 71, (1995) 3030.

[33] G. Yu, Y. Cao, C. Zhang, Y. Li, J. Gao, A. J. Heeger, Appl. Phys. Lett. 73, (1998) 111.

[34] J. Lin, M. Weis, D. Taguchi, T. Manaka, M. Iwamoto, Thin Solid Films 518,

(2009) 448.

[35] Q. Wang, J. Moser, M. Grätzel, J. Phys. Chem. B 109, (2005) 14945.

Chapter 3 Visualization of carrier behavior in OSCs

In order to better study the carrier behavior and dielectric performance in OSCs, we need to achieve the real-time observation of the variation of interfacial electric field. The best technique for us is the EFISHG measurements, as we explained in last chapter. However, if you apply a new technique to the study field of OSCs, you need to compare it with some well-established ones. Hence, we firstly carried out the conventional IS measurements on the samples. Actually, the IS measurement method itself has already been widely used for characterizing OSCs, however, the results and analysis we show in this chapter are not conventional because we realized dielectric nature of OSCs and applied Maxwell-Wagner model for analyzing the experimental data, which is a new practice. Both IS and EFISHG measurements confirmed dielectric nature of OSCs. At the meantime, the comparison between EIFSHG measurement and IS measurement also showed the capability and advantages of EFISHG measurement for the study of OSCs.

3.1 Sample fabrication and I-V testing

Figure 3.1 portrays OSCs with an indium zinc oxide (IZO)/donor/C_{60}/blocking layer/Al structure. These OSCs were prepared as follows: IZO-coated glass substrates were UV/ozone treated to be nearly free from organic residuals. The donor layer with the materials of Pentacene and Copper phthalocyanine (CuPc) (d_1) were deposited

onto the UV/ozone treated IZO. After that, the C_{60} layer was deposited on top of (d_2) donor layer. Then, a BCP layer with a thickness of 10 nm was selectively deposited for the triple-layer sample, while the double-layer sample is only consisted by two organic active layers. Finally, Al electrodes with a thickness of 100 nm were deposited onto the top of the sampler, where the working area of the OSCs was A = 3.1 mm^2. The relative dielectric constants of pentacene layer and C_{60} layer at 1 kHz were $\varepsilon_1 = 4.2$ and $\varepsilon_2 = 6.5$, respectively (BCP: 3.2, CuPc: 3.5). All the organic materials were directly purchase from the company without further purification before use. IZO electrode was also used as received without further treatment except for solution cleaning. Organic layers and Al electrode were sequentially deposited in vacuum. The typical vacuum was 10^{-6} Torr during the deposition of the organic materials. Prepared OSCs were sealed with a dry agent to avoid degradation during the I-V, IS and EFISHG measurements.

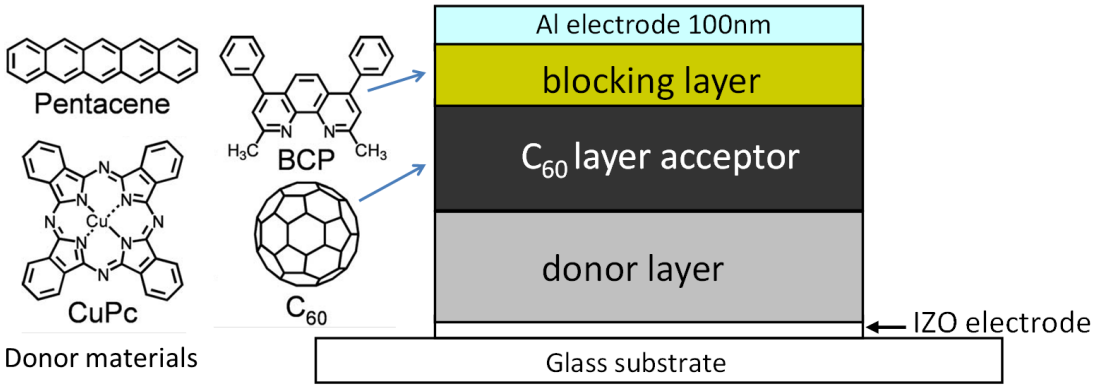

Figure 3.1: Sample structure of OSCs in our research

A red light from a light-emitting diode (wavelength 630 nm, intensity 10 mW/cm^2) was used as a light source to provide illumination pulse (repetition rate 10 Hz, duration 50 ms, switching on and off times within 50 ns) to the OSCs devices. The

pentacene, CuPc and C_{60} layers absorb light at a wavelength of 630 nm and generate excitons inside the layers. The detailed absorption spectral can be found in Figure 3.2(a) and (b). The I-V performance of the two kinds of double-layer sample was also measured. Figure 3.3(a) shows the I-V characteristics of the IZO/pentacene (40nm)/C_{60}(100nm)/Al OSCs under illumination and in dark, where the open-circuit voltage V_{oc} was 0.22 V, the short-circuit current density J_{sc} was -0.09 mA/cm^2 and the fill-factor was 0.26. Figure 3.3(b) is the I-V characteristics of the IZO/copper-phthalocyanine (CuPc) (40nm)/C_{60}(35nm)/Al OSCs and the V_{oc} was 0.325 V, the J_{sc} was -0.963 mA/cm^2 and the fill factor was 0.18. It is important to note that the sample prepared in this chapter is for the physical process study. Hence, the sample structure is not optimized value and the I-V performances also have low quality. The samples with different structures (see Fig. 33(a) and (b)) are prepared for different experiments and the details will introduce in after sections. However, this kind of sample holds rather straightforward physical process and can help us establish some basic picture of carrier behavior and photovoltaic effect.

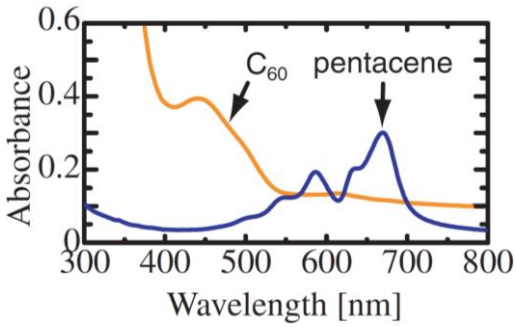

(a)

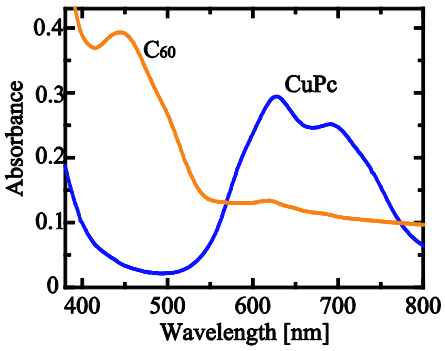

(b)

Figure 3.2: Illumination absorption spectral of (a) pentacene and C_{60} (b) CuPc and C_{60}

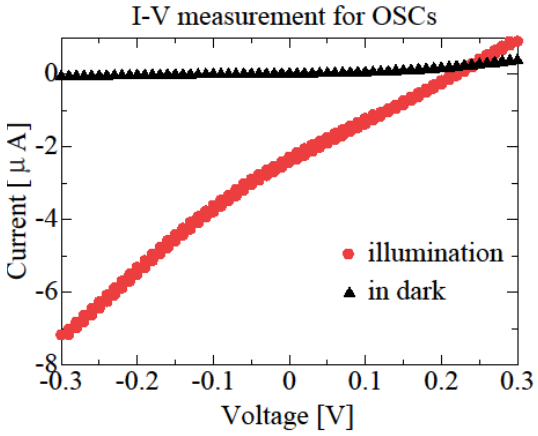

(a)

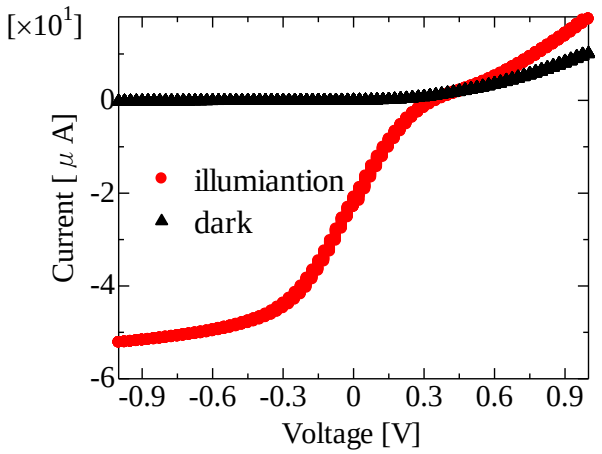

(b)

Figure 3.3: I-V performance of OSCs with (a) pentacene/C_{60} structure (b) CuPc/C_{60} structure

3.2 Analysis of photovoltaic effect based on dielectric model

3.2.1 IS measurements

In this study, OSCs with a pentacene/C_{60} double-layer were investigated using IS measurements, and the results were analyzed based on a Maxwell–Wagner model, assuming that pentacene and C_{60} are considered as dielectric materials. The IS technique was employed in dark and under illumination for studying arrier accumulation and relaxation at the double-layer interface. Finally the contribution of photovoltaic effect was discussed in terms of interfacial Maxwell-Wagner type carrier relaxation.

Impedance spectroscopy (IS) is a small signal analysis and widely used for characterizing device parameters [1]. By applying a small AC signal to devices under

various DC biasing conditions, components of the equivalent circuit of devices are evaluated. This technique has an advantage in that it can distinguish contributions of the interface from the bulk, when the equivalent circuit of device is well-known on the basis of device physics. Consequently it has been used as a tool for characterizing devices over the past several ten years [1-3].

The current-voltage (I–V) characteristics of the IZO/pentacene/C_{60}/Al OSC under illumination and in dark can be found in Fig. 3.3(a) in last section, where the open-circuit voltage is 0.22 V and the short-circuit current density is -0.16 mA/cm^2. The IS measurements were performed with a Solartron 1260 impedance/gain-phase analyzer in the frequency range of 10 Hz -1 MHz in dark and under photo-illumination. The OSCs were short-circuited, and an AC voltage with amplitude of 10 mV was applied in the measurements. The obtained spectra were curve-fitted using the equivalent circuit of Fig. 3.4.

Figures 3.5 (a) and (b) show the results of IS measurements, where $C(\omega)$ and θ = arctan (ωC /G) are plotted. In the $C(\omega)$, there are two relaxations (A and B), due to charging onto electrodes with $\tau_{RC} = R_o C_t$ (B) and the Maxwell-Wagner type interfacial relaxation with $\tau_{MW} = \dfrac{C_1 + C_2}{G_1 + G_2}$ (A), respectively. Figure 3(a) shows $C_t \approx 2.1\,\text{nF}$ at 10^3-10^5 Hz in dark. Curve fitting analysis was employed using the equivalent circuit of Fig. 2(a), and the obtained device parameters were listed in Table 1. Using these device parameters, we estimated the relaxation time as $\tau_{MW} = 3.8\times10^{-3}$ s ($f_{MW} = 41$ Hz) and $\tau_{RC} = 3.4\times10^{-7}$ s (f_{RC}=4.7×10^5 Hz) in dark condition, while $\tau_{MW} = 4.9\times10^{-5}$ s ($f_{MW} = 3200$ Hz) and $\tau_{RC} = 4.5\times10^{-7}$ s (f_{RC}=3.5×10^5 Hz) under illumination.

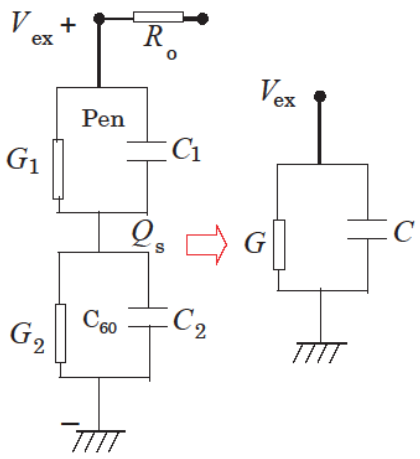

Figure 3.4: Equivalent circuit for IS measurement.

Table 3.1 Fitted parameters for equivalent model based on Maxwell-Wagner effect.

Dark		Illumination	
$1/G_1$	$6.3\times10^{5}\,\Omega$	$1/G_1$	$1.0\times10^{4}\,\Omega$
$1/G_2$	$9.9\times10^{5}\,\Omega$	$1/G_2$	$3.1\times10^{4}\,\Omega$
R_o	160 Ω	R_o	160 Ω
C_1	3.2×10^{-9} F	C_1	4.4×10^{-9} F
C_2	7.0×10^{-9} F	C_2	7.8×10^{-9} F

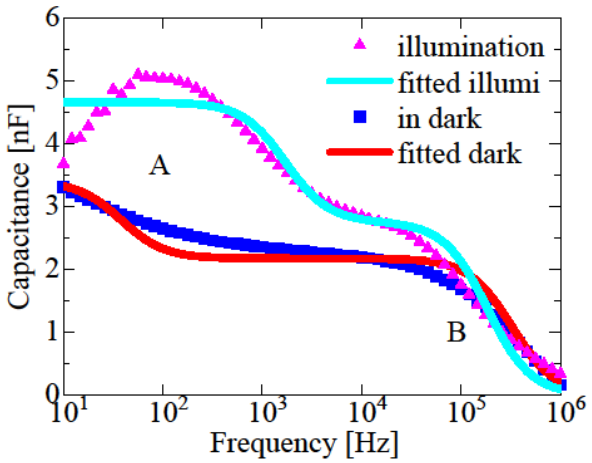

(a)

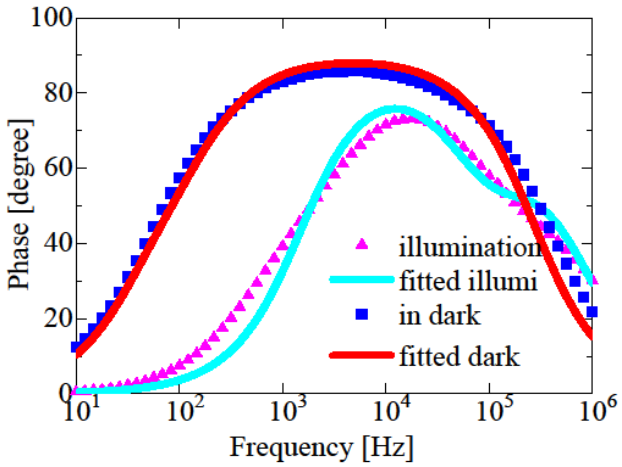

(b)

Figure 3.5: IS results of the (a) IS results with $C(\omega)$ and (b) IS results with phase.

It is instructive to note that the τ_{MW} under illumination is about 70 times shorter than that in dark. The conductance is given as $G = \frac{en\mu S}{L}$, where n is the carrier density, μ is the mobility, S and L are the electrode area and thickness of the material, respectively. Under the illumination, the carrier density in pentacene and C_{60} layers increased due to the photovoltaic effect. Accordingly, G increased by illumination as

that $G_1 = 1.6\times10^{-6}$ S and $G_2 = 1\times10^{-6}$ S in dark, whereas $G_1 = 1\times10^{-4}$ S and $G_2 = 3.2\times10^{-5}$ S under illumination (see Table 1). Since τ_{MW} is given by $\frac{C_1 + C_2}{G_1 + G_2}$, the relaxation of the interface charges was accelerated by illumination, due to the increase of the conductance G_1 and G_2. On the other hand, the series capacitance C_t of the two layers was also increased slightly by the photo illumination, as shown in Fig. 3(a) (also see C_1 and C_2 in Table 1), possibly due to the increase of the effective area of the capacitor caused by the spreading of the charges on the electrode to surrounding. The charge relaxation time on the electrode τ_{RC} also increased under illumination as the C_t was increased. However, these are merely speculation based on the MW model.

The obtained IS results only identified interfacial process related to the conductance changing, and the photovoltaic (PV) effect in the device was not clear. To elucidate the contribution of the PV effect, other experiments that can probe interfacial carrier behaviors are needed. In our previous study [4], by applying EFISHG measurement to double-layer OSCs under short circuit condition, the contribution of the photovoltaic effect was verified by the observation of electric field distribution in the double layer. Taking into account these, we employed here the EFISHG measurement to investigate the photovoltaic effect in the OSC device.

3.2.2 EFISHG measurements

For studying the contribution of photovoltaic effect to the interfacial relaxation observed in the IS spectrum, we employed the EFISHG technique to probe the local electric field change during transient state of the OSCs. In our experiments, EFISHG signal is generated from C_{60} layer due to the coupling of electrons in C_{60} molecules

and electro-magnetic waves of incident laser beam $E(\omega)$ in the presence of electrostatic local electric field $E(0)$ in the C_{60} layer. Note that the square-root of the SHG intensity is in proportion to the electric field $E(0)$ [5, 6]. $E(0)$ is given by E_0+E_s, where E_0 ($=Q_m/\varepsilon_r\varepsilon_0$) is the electric field originated from charges $+Q_m(t)$ on top-Al and $-Q_m(t)$ on bottom-IZO electrodes of the OSCs and E_s is the electric field originated from charges $Q_s(t)$ accumulated on the pentacene/C_{60} interface. Consequently, the EFISHG measurement probes the interfacial carrier behavior of the OSCs.

Figure 3.6 shows the transient EFISHG generated from electrically shorted OSCs by illumination and by succeeding no-illumination. Single relaxation was observed at around 10^{-5} -10^{-4} s during the illumination and the succeeding no-illumination processes, respectively. Under the short circuit condition, the change of electric field E_0 induced in OSCs by electrode charging Q_m with a relaxation time $\tau_{RC} = R_o C_t$ should be zero. Consequently the EFISHG response with a single relaxation shown in Fig. 4 was ascribed to the Maxwell-Wagner type interfacial carrier charging at the pentacene/C_{60} interface [4]. On the other hand, in the IS measurements, small AC signal is applied to the OSCs during the measurement, and this activates the electrode charging process with a relaxation time $\tau_{RC} = R_o C_t$. This is the reason why relaxation B is always observed in Fig. 3(a). The time-constants of the two relaxation processes are estimated by employing a curve-fitting method based on a filtering technique to the transient EFISHG [7-9] and the detailed explanation as well as an calculation example can be found in next section (section 3.2.3). From Fig. 3.6, we obtained the relaxation time of $\tau_{MW} = 3.3\times10^{-5}$ s. This value is nearly the same with the value of

$\tau_{MW} = 4.9 \times 10^{-5}$ s estimated from the IS measurement under illumination (A in Fig. 3.5 (a)). These results suggested that both IS and EFISHG measurements are available for probing the interfacial charging processes in the OSCs.

It is instructive here to note that IS and EFISHG measurements are different in that EFISHG directly probes interfacial charging, while IS measurement is based on an analysis of equivalent circuit which models an interfacial carrier charging process. In order to further clarify the advantage of the use of these two IS and SHG measurements at the same time in terms of the photovoltaic effect, we used these measurements to study interfacial carrier charging of open-circuited OSCs. Figure 3.7 shows the square-root of the SHG intensity generated from the pentacene/C_{60} double-layer OSC in response to the applied square-wave voltage pulse (V_{ex}=0.2 V), close to the V_{oc} of 0.22 V. In dark condition, as shown in Fig. 3.7(a) a two-step relaxation process was observed during the measurements, which represented charging process on electrodes and to the pentacene/C_{60} interface (see section 3.2.1). Here the relaxation was the result of the change of electric field across the C_{60} layer. Meanwhile it was also found from the SHG measurement that the relaxation time τ_{MW} was $\tau_{MW} = 2.6 \times 10^{-4}$ s, which was one order smaller than that in the IS measurement. After charge injection happens with an applied DC voltage $V_{ex,}$ the conductance of the device is given as $G = \frac{\varepsilon_0 \varepsilon_s V_{ex} \mu S}{L^2}$, under assumption that space charge limited current governs the electrical conduction. Here ε_s is the relative dielectric constant. Since the applied voltage signal in the SHG measurement was 20 times larger than the AC signal used in the IS measurement, the relaxation at the

interface is activated significantly due to the increase of the conductance of organic layers during the EFISHG measurement [5]. This activation is also further confirmed by the conductance dependence of the interfacial relaxation process, as discussed in last section. The SHG measurement has also been carried out under illumination in the same way, as shown in Fig. 3.7(b), where only one relaxation process was observed. Comparing with Fig. 3.7(a), the responding time of SHG signal in Fig. 3.7(b) corresponds to the charging process on the electrode. That is, interfacial charge accumulation caused by the Maxwell-Wagner effect was not seen. When the external voltage was close to the open voltage V_{oc}, no current flowed across the device, that is, I_c was nearly zero. Hence, according to Eq. (2.7) the accumulated charge Q_s at the pentacene/C_{60} interface became very small, and related induced electric phenomena were not observed by the EFISHG measurement.

Figure 3.8 shows the results of the IS measurements for the OSCs sample with a DC bias of 0.2 V, where a two-step wise relaxation was observed. Results showed that the electrode and interfacial charging were active in the IS measurement in accordance with the applied AC signal. Meanwhile, for the EFISHG measurement, the electrostatic electric field formed in organic layers in C_{60} layer was probed with time. When the external DC voltage was close to the V_{oc} (=0.22 V), almost no current flowed through the circuit. Accordingly, the MW type interfacial charging was negligible, and this resulted in no change in the EFISHG signal by the interface carrier charging (see Fig. 3.7(b)). That is, the EFISHG evidently shows that the photovoltaic effect significantly gives an effect on the carrier interfacial relaxation of the OSCs devices. As mentioned above, both IS and EFISHG measurements are available for probing interfacial phenomena, but there is a difference between them in

the detection of interfacial carrier behaviors. Therefore, for evaluating the interfacial relaxation of the OSCs in terms of photovoltaic effect, the SHG technique coupled with the IS measurement offers a clear physics picture in comparison with the sole IS measurement.

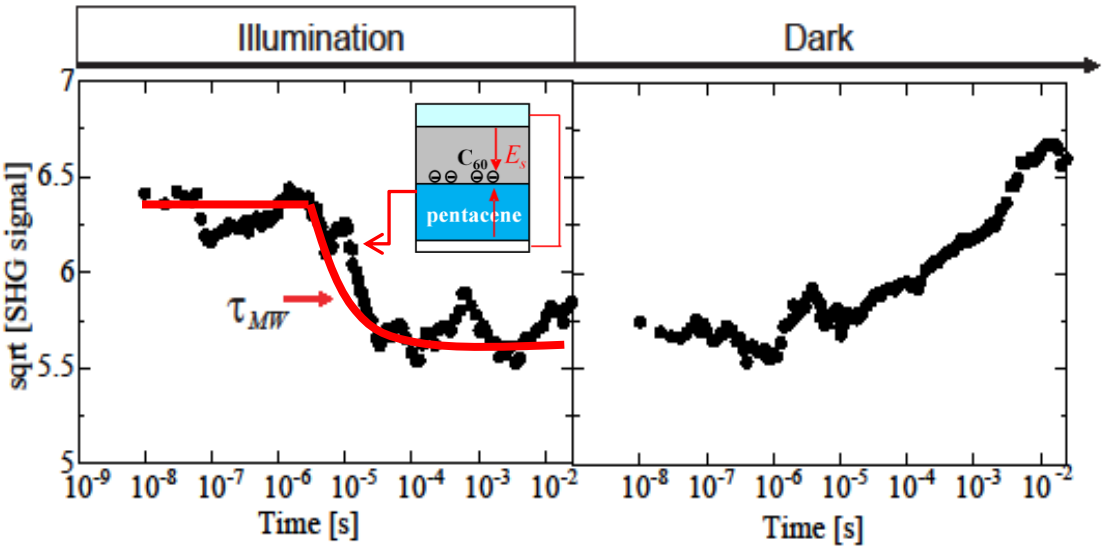

Figure 3.6: EFISHG measurement under short cirtcuit condition

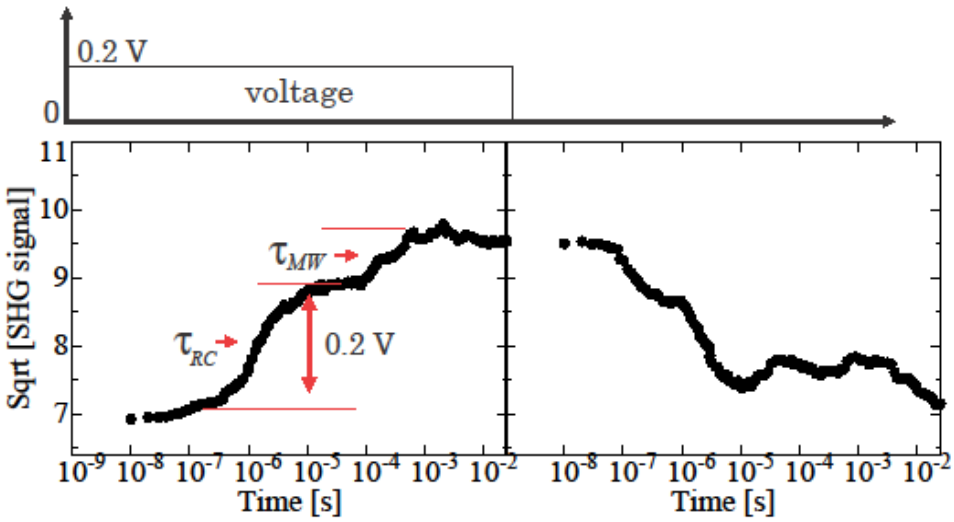

(a)

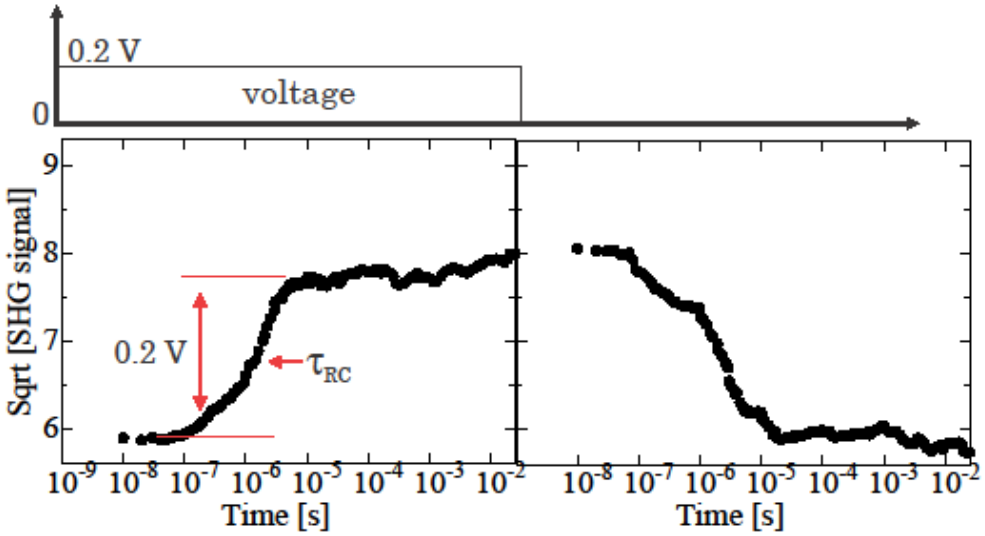

(b)

Figure 3.7: EFISHG measuremnts under square-wave voltage application (V_{ex}~V_{oc}). (a) SHG measurement in dark, and (b) SHG measurement under illumination.

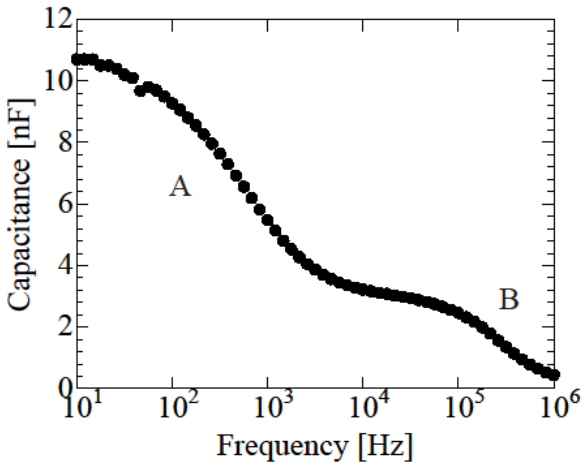

Figure 3.8: IS measurement under illumination with DC bias at 0.2 V.

Finally, based on the Maxwell–Wagner model, the interfacial carrier relaxations of OSCs with a pentacene/C_{60} double-layer have been studied in terms of photovoltaic effect under both dark and illuminated conditions. IS combined with EFISHG

measurements revealed that the photo-illumination gives directly an effect on the interfacial charges relaxation from two aspects. Firstly the increasing of carrier density caused by the illumination consequently enhances the relaxation process of the interface. Meanwhile, due to the photovoltaic effect, interfacial relaxation process is not observed when the external voltage V_{ex} approaches V_{oc}. The analysis based on Maxwell-Wagner model well accounts for the changing of the relaxation processes. Finally we discussed that EFISHG measurement coupled with IS measurement provides a clear physics picture of interfacial phenomena related to the photovoltaic effect in OSCs.

3.2.3 Analysis of carrier lifetime

In last section, we found that the SHG measurement is also available to study photovoltaic effect of OSCs. Since the SHG signal directly reflects carrier behavior, analysis of the signal response gives information on carrier lifetime. In this part, by using the SHG measurement, we directly probed carrier behavior, i.e., carrier generation and decay processes, in double-layer IZO/CuPc(60nm)/C_{60}(40nm)/Al OSCs. Results showed that negative excess charges accumulated at the CuPc/C_{60} interface under photoillumination, whereas the accumulated charges decayed in a two-step process in dark. We analyzed the experimental data quantitatively, and showed that 24% of the accumulated negative charges decayed with a lifetime $\tau_1=5.3\times10^{-5}$ s, and the other 76% of the charges decayed with a lifetime $\tau_2=6.2\times10^{-2}$ s. We conclude that the SHG measurement is a direct way for investigating carrier lifetime in OSCs.

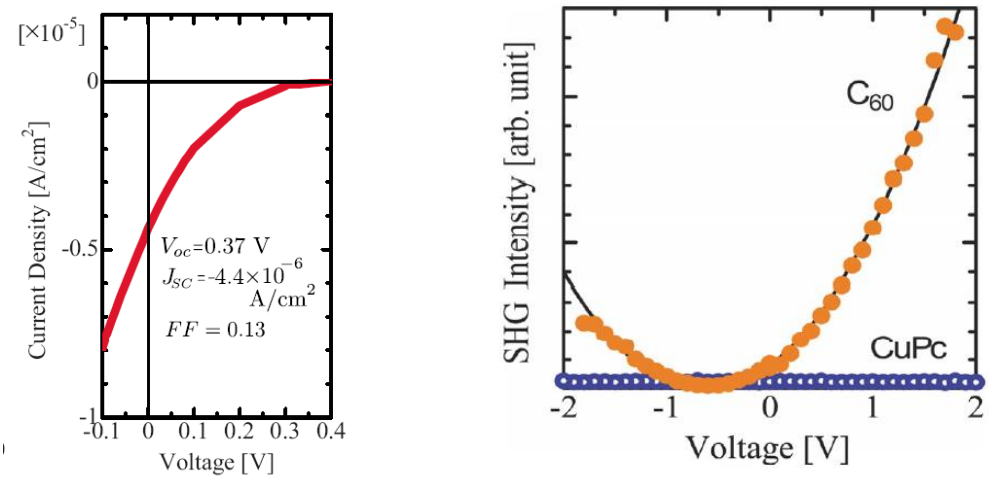

Figure 3.9: (a) I-V performance of double layer OSCs (b) SHG intensity changing of signal layer CuPc and C_{60} [17]

Figure 3.9(a) shows the I-V characteristics of the CuPc(60nm)/C_{60}(40nm) OSC where the cell parameters were obtained as open-circuit voltage V_{oc}=0.37 V, short-circuit current density J_{sc}=−4.4×10^{-6} A/cm^2, and fill-factor FF=0.13. (This I-V performance is different from the I-V results in section 3.1) Under photoillumination, excitons created in the CuPc and C_{60} layers diffused to the CuPc/C_{60} interface to generate free holes and electrons. Then the generated holes (electrons) were conveyed across CuPc (C_{60}) layer to the IZO (Al) electrode. Consistently, the negative photocurrent (J_{sc}<0) flowed through the external circuit. Figure 3.9(b) shows the SHG intensity generated in the CuPc and C_{60} single-layer devices under step-voltage application. The SHG signal of the C_{60} single layer device was a quadratic function of the applied voltage. The average electric field E (0)= V/d (d: layer thickness) is applied to the organic layer, and the square dependence on the E (0) in the Fig. 39.(b) suggested that the observed SHG was induced through the EFISHG process expressed in Eq. (2.17). On the other hand, CuPc showed negligibly small SHG response. These

results support that we can selectively probe the electric field in C_{60} layer of the double-layer CuPc/C_{60} OSC. Figure 3.10(a) shows the SHG intensity of the OSC in response to the photoillumination, where we plotted the square root of the SHG intensity that is directly proportional to the charges Q_s. The SHG intensity increased under photoillumination, while the SHG intensity decreased in dark accordingly. Excess charges Q_s at the interface is a source of a space charge field E (s) and additionally formed electric field in the C_{60} layer, and it was probed in the SHG measurement. In order to determine the direction of the electric field E (s), we also carried out the SHG measurements under voltage application to the OSC devices. The SHG intensity increased under negative voltage application in a way similar to the SHG response under photoillumination, whereas the SHG intensity decreased under positive voltage application. These results suggested that negative excess charges accumulated at the CuPc/C_{60} interface under photoillumination and formed negative electric field ($E_s < 0$) in the C_{60} layer.

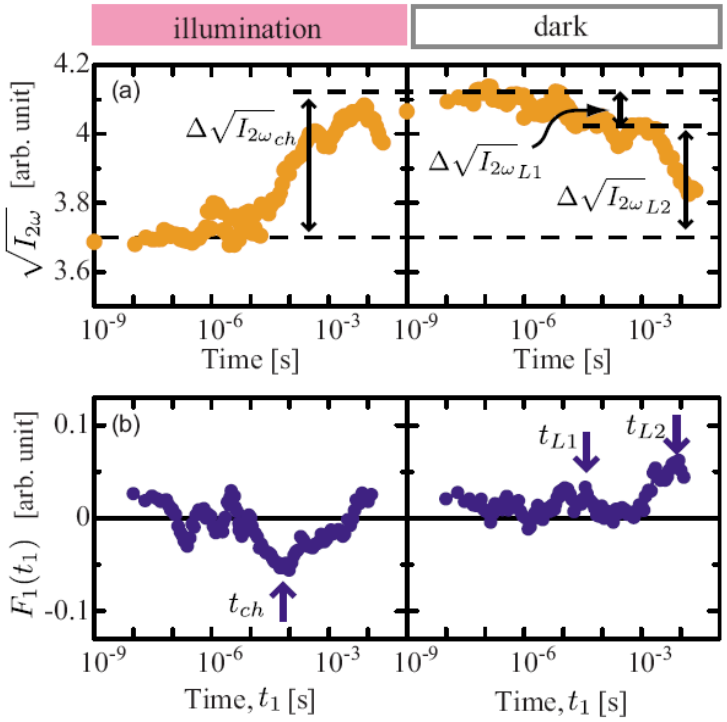

Figure 3.10: (a) square root of SHG response from the CuPc/C_{60} OSC to the Photoillumination (50 ms illumination followed by 50 ms break). (b) The first-order filtering function $F_1(t_1)$ of the SHG response. [17]

The SHG signal response directly catches charge accumulating and decaying processes at the CuPc/C_{60} interface. Hence, analysis of the SHG transient provides a direct way to obtain a carrier lifetime at the donor-acceptor interface of the OSC. For the analysis, we employed a filtering technique that can well reproduce relaxation process in solids. [7, 8] The first-order filtering function defined as $F_1(t_1)=s(t_1)-s(2t_1)$ was used in the analysis, where s(t) is a signal response. The filtering function gives peaks at times that correspond to time-constants of the signal response, and this is an effective way to determine time-constants of a signal response. For example, the filtering function of a single relaxation process $s(t)=s_0+s_1\exp(-t/\tau)$ (s_0 and s_1:

constants and τ: relaxation time) gives one peak at a time $t_1=\tau \ln 2$ with its peak height of $s_1/4$. In the SHG measurement, the square root of the SHG intensity $\sqrt{I_{2\omega}}$ is the signal response s(t). Figure 3.10(b) shows the filtering function $F_1(t_1)$ of the SHG response. Under the photoillumination, the SHG intensity fluctuated in the region $<10^{-6}$ s due to an unstable carrier generation process. As the result, the filtering function $F_1(t_1)$ changed up and down while the average of $F_1(t_1)$ was zero in this region. After that, the SHG intensity increased and saturated. Correspondingly, the first-order filtering function $F_1(t_1)$ showed a negative peak at a time $t_{ch}=9.7\times10^{-5}$ s, and indicated that the excess charges accumulated at a rate of $\tau_{ch}(=t_{ch}/\ln 2)=1.4\times10^{-4}$ s. The peak height at t_{ch} was 5.6×10^{-2} and it was smaller than that expected for a single relaxation process $s_1/4(=\Delta\sqrt{I_{2\omega ch}}/4)=0.11$, where $\Delta\sqrt{I_{2\omega ch}}/4$ is the change of $\sqrt{I_{2\omega}}$ under photoillumination as displayed in Fig. 3.10(a). This result suggested that the charge accumulated in a manner as represented by a stretched exponential function.[16] On the other hand, the filtering function of the charge decay process showed two positive peaks at times $t_{L1}=3.7\times10^{-5}$ s and $t_{L2}=4.3\times10^{-2}$ s, as indicated by arrows in Fig. 3.10(b). The heights of the two peaks were 3.3×10^{-2} $(\sim\Delta\sqrt{I_{2\omega L1}}/4=2.5\times10^{-2})$ at the time t_{L1} and 6.2×10^{-2} $(\sim\Delta\sqrt{I_{2\omega L2}}/4=0.8\times10^{-2})$ at the time t_{L2}, and suggested that the two decay processes were single relaxation process. In the SHG measurement, the square root of the SHG intensity is in proportion to the charge density accumulated at the interface. Thus, the ratio $(\Delta\sqrt{I_{2\omega L1}})/(\Delta\sqrt{I_{2\omega L1}}+\Delta\sqrt{I_{2\omega L2}})=0.24$ represents a ratio of charges that decayed in the first decay process. Similarly, $(\Delta\sqrt{I_{2\omega L2}})/(\Delta\sqrt{I_{2\omega L1}}+\Delta\sqrt{I_{2\omega L2}})=0.76$ is a ratio of the

charges that decayed in the second decay process. That is, the filtering analysis of the SHG response suggested that, (1) in the first decay process, 24% of the accumulated negative charges decayed at a lifetime of $\tau_{L1}(=t_{L1}/\ln 2)=5.3\times10^{-5}$ s. Then, (2) in the second decay process, remaining 76% of the charges decayed at a lifetime of $\tau_{L2(}=t_{L2}/\ln 2)=6.2\times10^{-2}$ s. We conclude that the SHG measurement is useful to study carrier behavior in OSCs and provides a direct way to investigate the carrier lifetime distribution at the two-layer interface of the OSCs.

3.2.4 Effect of photoconductivity changing

In some series-connected OSCs structure, a thin film, composited by the organic material such as CuPc and boron subphthalocyanine (SubPc), was inserted in the OSCs as the internal layer, in order to enhance the reflection and absorption of light [10, 11]. Noteworthy, organic materials, such as CuPc or SubPc, are very sensitive to the illumination [12, 13] and the photoconductivity of these materials may strongly influence the carrier behavior of the OSCs. Hence, further study on carrier transport with taking into account the photoconductivity charging of the organic active layer will be of help to improve the performance of OSCs.

The authors' group has been developing an electric-field-induced optical second-harmonic generation (EFISHG) technique that can directly probe carrier motions in organic field-effect transistors, organic light-emitting diodes and OSCs [14-16]. By applying illumination signal to the OSCs under various external conditions, carrier transits in OSCs were visualized and the mechanism of the electric field generation inside the OCSs was identified [16-18]. In the present study, we prepared IZO/CuPc/C_{60}/Al OSCs and studied the interfacial charging processes of the

OSCs. In order to further clarify the contribution of the photoconductivity changing to the interfacial carrier behavior, we carried out the transient EFISHG experiments and analyzed the results using a Maxwell-Wagner model. We concluded that the change in the conductance induced by illumination caused the converse charging behavior on the CuPc/C_{60} interface.

The current-voltage (I-V) characteristics of this CuPc/C_{60} OSCs were shown in Fig. 3.3(b), where the open-circuit voltage V_{oc} was 0.325 V, the short-circuit current density J_{sc} was -0.963 mA/cm^2 and the fill factor was 0.18. We also tested the sample under the AM1.5 irradiation, and the power conversion efficiency was about 0.6%. In a manner as described in section 3.2, OSCs device with double-layer structure is modeled using a parallel conductor-capacitor (*G*-*C*) circuit, as shown in the Fig. 3.4. Here, a conductor (G_1, G_2) and a capacitor (C_1, C_2) represent the conductance and capacitance value of CuPc and C_{60} layer, respectively. With a DC voltage applied to the OSCs in dark, charge $\pm Q_e$(t) is induced on the top and bottom electrodes with a response time $\tau_{RC} = R_e \frac{C_1 C_2}{C_1 + C_2} \approx 2 \times 10^{-7}\,\mathrm{s}$, where R_e= 160 Ω is the external resistance [18]. This is the electrode charging process. After that electrode charges on the IZO are injected into the pentacene and interfacial charging process happens.

Note that we can trace the interfacial carrier charging process through the local electric field E (0) estimated from the EFISHG signal I_{SHG} [7, 19], using the relation $I_{SHG} \propto |E(0)|^2$. Hence, the generated EFISHG offers us the information about the carrier behaviors in OSCs.

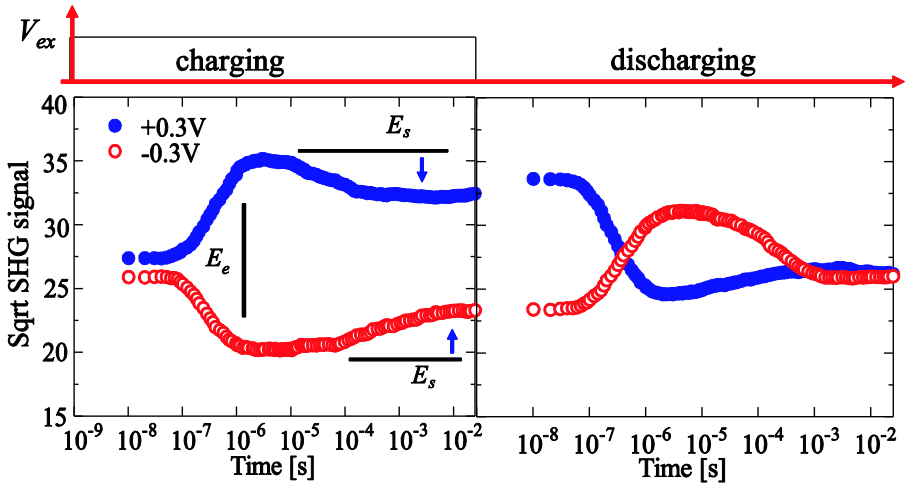

Figure 3.11: EFISHG measurement with voltage pulse in dark.

Figure 3.11 shows the EFISHG generated from the IZO/CuPc/C_{60}/Al OSCs in response to the AC square-wave voltage pulse (10 Hz) in dark, where the amplitude of the DC applied voltage V_{ex} was +0.3V or -0.3V. The voltage signal was applied on the IZO electrode with Al electrode grounded. Two relaxation processes were identified during the EFISHG measurement, corresponding to the electrode charging (E_e) and the interfacial charging (E_s) [18]. The first relaxation process was observed just after applying AC square-wave voltage pulse, due to the electrode charging, which resulted in the E_e across the whole sample. Here, we found that positive electric field (from IZO to Al) led to the increase of the EFISHG signal, while the negative electric field (from Al to IZO) resulted in the decrease of the EFISHG signal. After the electrode charging, the interfacial charging process followed. For V_{ex} = 0.3 V, the SHG signal was decreased, suggesting that the C_{60} layer was relaxed and electrons accumulated at the CuPc/C_{60} interfaces. Accordingly the two electric fields, E_e and E_s, were successively formed in the C_{60} layer along with electrode charging and interfacial charging and their electric field directions inside the C_{60} layer were opposite with each

other. Similarly, for V_{ex} = -0.3 V, EFISHG signal decreased firstly and then increased, indicating that holes accumulated at the CuPc/C_{60} interfaces. Both experiments proved that C_{60} layer relaxed faster than CuPc layer and thus $\tau_{C60} < \tau_{CuPc}$ in dark condition. Noteworthy that applying positive pulse (V_{ex}=-0.3 V) lead to the increase of the SHG signal. This result indicated that the background electric field E_b of the triple-layer sample was pointing in the direction from IZO electrode to the Al electrode. This background is just possibly generated by the local internal field, such as interfacial dipole, deep traps or Fermi-level difference between two organic materials. The detailed physical reason of the creation of this background electric field is out of scope of this study, but we should note that the experimental results were well explained by assuming the presence of this background electric field E_b. Meanwhile, the time-constants of the charging processes were evaluated by using a curve-fitting method based on a filtering technique [7, 20]. In the analysis, the first-order filtering function was defined as $F_1(t_1)= s(t_1)-s(2t_1)$, where $s(t)$ is an square-root of EFISHG intensity. The filtering function gives peaks at times that correspond to time-constants of the signal response $s(t)$, and it can effectively determine time-constants of a signal response [21]. In other words, the presence of the three relaxation time constants, corresponding to electrode charging and two kinds of interfacial charging, was verified by employing the filtering method. Accordingly, the relaxation time of interfacial charging was $\tau_{s1} \approx 6.4\times10^{-5}$s for V_{ex} = 0.3 V, while the relaxation time of interfacial charging was $\tau_{s2} \approx 1.6\times10^{-3}$s for V_{ex} = -0.3 V. It is important to note that the application of positive voltage (0.3V) assisted holes to smoothly inject from the IZO to the CuPc layer and resulted in the acceleration of

interfacial relaxation. The relaxation times obtained from filtering method were in good agreement with the I-V performance of the OSCs.

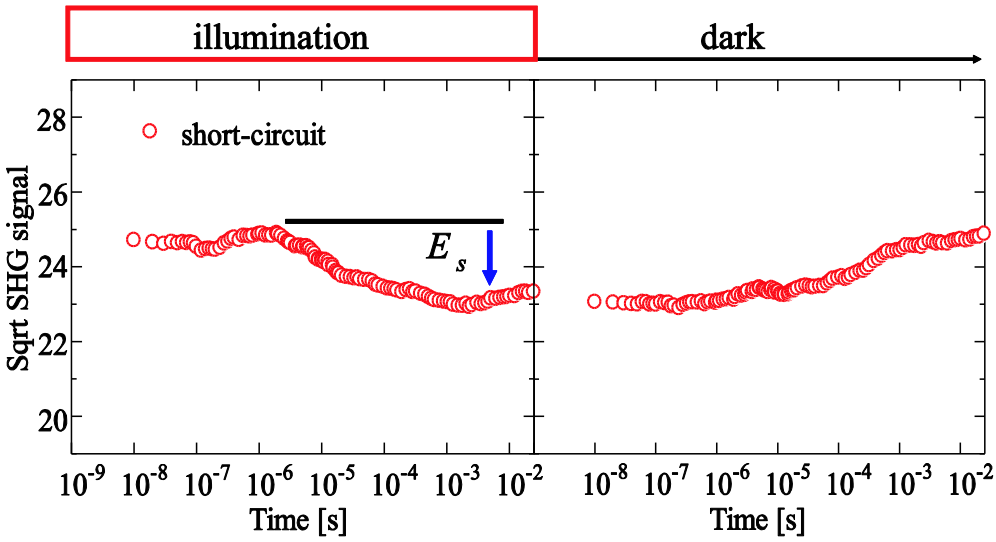

Figure 3.12: EFISHG measurement with illumination pulse under short-circuited condition.

Figure 3.12 shows the transient EFISHG generated from electrically shorted OSCs by illumination and by succeeding no-illumination, where the OSCs was in short-circuited condition. Single relaxation process was observed at around 10^{-5} —10^{-3} s during the illumination and the succeeding no-illumination processes, respectively. Under the short circuit condition, the change of electric field E_e induced in OSCs by electrode charging Q_e should be zero. Consequently the EFISHG response with a single relaxation shown in Fig. 3 was ascribed to the Maxwell-Wagner type interfacial carrier charging (E_s) at the CuPc/C_{60} interface. Knowing that the photocurrent flows in the direction from Al electrode to IZO electrode inside the OSCs, which is the same as the case of V_{ex}=-0.3V in dark. As can be seen in Fig. 2, the induced the interfacial charging process under the external voltage of -0.3V led to

the increase of the EFISHG signal, indicating the holes accumulation on the CuPc/C_{60} interface. However, as shown in Fig. 3, the EFISHG signal decreased under the applied illumination pulse though the direction of conduction current is the same. These results indicated that electrons (Q_s) accumulated on the CuPc/C_{60} interface under illumination. According to the Maxwell-Wagner effect, Q_s in the steady states is given as: $Q_s(\infty) = I_c \Delta\tau = I_c(\tau_2 - \tau_1)$ (see eq. (2.17)). Consequently, the relaxation time difference between two adjacent organic layers governs the polarity of the accumulated charges at the interface. With taking into account the conduction current flowing from the Al electrode to the IZO electrode inside the OSCs, the holes (electrons) accumulation at the CuPc/C60 interface suggested that the charge relaxation of the C_{60} (CuPc) layer is faster. Hence, the applied illumination can change the polarity of the accumulated charges on the CuPc/C_{60} interface and therefore under illumination $\tau_{C60} > \tau_{CuPc}$. It is important to note that this photo-induced switching of the interfacial charge polarity is so far only observed with this CuPc/C_{60} OSCs. Nevertheless the study of the interaction between photoconductivity and the photo-induced carrier behavior can be applied to many other photosensitive organic devices. The reason of these converse carrier behavior can be attributed to the photo-induced conductivity changing. The conductivities ($\sigma_1$andσ_2) of the active layers, CuPc and C_{60}, were considered to be increased after applying the illumination [22-24]. However, the CuPc layer is more sensitive to the illumination and thus the conductivity of the CuPc layer is changed more significant than that of C_{60} layer under illumination. Note that the light source we used in experiment is red illumination (wavelength 639nm), which decided that excitons are mainly generated

inside the CuPc layer (see Fig. 1(b)). The photo-induced conductivity changing of the CuPc layer can strongly enhance the relaxation of the carriers. Thus relaxation time of the CuPc layer is increased lager than C_{60} and finally led to this converse interfacial charging process comparing with dark condition. On the other hand, it is also possible that other type of illumination may result in the less significant contribution of the photoconductivity to the interfacial charging processes as reported in the paper [10, 11]. Usually, it is believed that the contribution of photoconductivity is the cause of the thickness dependent of the OSCs devices. Nevertheless, the interfacial charging process is also influenced by the photoconductivity of the two different layers. As proved by our previous papers [25, 26], the existence of charge accumulation on the interfaces deteriorates the performance of OSCs. Hence, we suggested two methods available for suppressing the interfacial charging inside the OSCs, in order to improving the performance of the OSCs. This study suggested that it is possible to switch the polarity of the accumulated charges by considering the photoconductivity changing of the organic layer. It also offers us a possible way to further reduce the interfacial charge accumulation and achieve a better internal condition for the OSCs. It is also important to note that the charge relaxation highly depending on the material properties of the organic layer and therefore different fabrication processes may also change the speed of the relaxation. In our experiment, we did not use any blocking layers or internal layers to protect the organic active layer. Due to the oxidation or the existence of deep traps, the relaxation of the C_{60} may sometime slower than CuPc layer in dark condition. However, under illumination we can always confirm that $\tau_{C60} > \tau_{CuPc}$.

3.3 Summary

In this chapter, the direct observation of interfacial carrier behavior inside OSCs was achieved by using IS and EFISHG measurement. Firstly, interfacial carrier relaxation in pentacene/C_{60} double layer OSCs has been analyzed in terms of photovoltaic effect under both dark and illuminated conditions. The IS measurements showed that the interfacial carrier relaxation time was diminished 70 times under photo illumination, due to the increase of carrier density caused by the photovoltaic effect. The equivalent circuit analysis using a Maxwell-Wagner effect model well accounted for the IS results. On the other hand, the EFISHG measurements directly probed the interfacial carrier behaviors caused by the photovoltaic effect. The results showed the suppression of the Maxwell-Wagner type carrier relaxation in OSCs by applying a voltage corresponding to the open circuit voltage V_{oc}. The results also proved that OSCs can be modeled as Maxwell-Wagner elements, which is a typical model based on dielectric physics. After that, EFISHG measurement was employed for studying interfacial processes in CuPc/C_{60} OSCs. Results suggested that interfacial charging process happened on the CuPc/C_{60} interface and the applied illumination can change the polarity of the accumulated charges on the double-layer interface while the direction of conduction current is the same. The Maxwell–Wagner model analysis revealed that the photo conductance change is responsible for these converse behaviors with and without illumination.

Results obtained here confirmed the dielectric performance of OSCs and thus will be helpful for understanding basic carrier behavior related to photovoltaic effect. The comparison between IS and EFISHG measurements also proved the capability of

EFISHG for evaluating the carrier behavior inside OSCs sample. Hence, EFISHG can be an effective method for study the mechanism of OSCs. EFISHG measurement coupled with IS measurement provides a clear physics picture of interfacial phenomena related to the photovoltaic effect in OSCs.

Bibliography of Chapter 3

[1] M. J. Ross and K. R William, *Impedance Spectroscopy: Emphasizing Solid Materials and Systems*, John Wiley & Sons, New York, 1987.

[2] J. Lin, M. Weis, D. Taguchi, T. Manaka, and M. Iwamoto, Thin Solid Films 518, (2009) 448.

[3] Q. Wang, J. Moser, and M. Grätzel, J. Phys. Chem. B 109, (2005) 14945.

[4] D. Taguchi, T. Shino, L. Zhang, J. Li, M. Weis, T. Manaka, and M. Iwamoto, Applied Physics Express 4, (2011) 021602.

[5] L. Zhang, D. Taguchi, J. Li, T. Manaka, and M. Iwamoto, Appl. Phys. Lett. 98, (2011) 092109.

[6] E. Lim, T. Manaka, R. Tamura, and M. Iwamoto, Jpn. J. Appl. Phys. 45, (2006) 3712.

[7] C. R. Crowel and S. Alipanahi, Solid-State Electron 24, (1981) 25.

[8] I. Thurzo, D. Pogány, and K. Gmucová, Solid-State Electron 35, (1992) 1737.

[9] D. Taguchi, T. Shino, X. Chen, L. Zhang, J. Li, M. Weis, T. Manaka, and M. Iwamoto, Appl. Phys. Lett. 98, (2011) 133507.

[10] K. Cnops, B.P. Rand, D. Cheyns, P. Heremans, Appl. Phys. Lett. 101 (2012) 143301.

[11] C. Zhang, S. W. Tong, C. Jiang, E. T. Kang, D. S. H. Chan, C. Zhu, Appl. Phys. Lett. 93, (2008) 043307.

[12] M. Wang, H. Chen, S. Yang, J. Photochem. Photobiol. A: Chem. 88 (1995) 183.

[13] X. Mo, H. Chen, Y. Wang, M. Shi, M. Wang, J. Phys. Chem. B 109 (2005) 7659.

[14] K. Bazaka, M. Jacob, D. Taguchi, T. Manaka, and M. Iwamoto, Chem. Phys. Lett. 503 (2011) 105.

[15] L. Zhang, D. Taguchi, J. Li, T. Manaka, and M. Iwamoto, J. Appl. Phys. 108 (2010) 093707.

[16] D. Taguchi, T. Shino, L. Zhang, J. Li, M. Weis, T. Manaka, and M. Iwamoto, Appl. Phys. Express 4 (2011) 021602.

[17] D. Taguchi, T. Shino, X. Chen, L. Zhang, J. Li, M. Weis, T. Manaka, and M. Iwamoto, Appl. Phys. Lett. 98 (2011) 133507.

[18] X. Chen, D. Taguchi, K. Lee, T. Manaka, and M. Iwamoto, Chem. Phys. Lett. 511 (2011) 491

[19] Y. R. Shen: *Principle of Nonlinear Optics*, (Wiley, New York, 1984) chapter 2.

[20] I. Thurzo, D. Pogány, and K. Gmucová, Solid-State Electron. 35 (1992) 1737.

[21] M. Weis, T. Manaka, and M. Iwamoto, J. Appl. Phys. 105 (2009) 024505.

[22] R. PETRITZ, Phys. Rev. 104 (1956) 1508.

[23] C. Lee, G. Yu, D. Moses, K. Pakbaz, C. Zhang, N. Sariciftci, A. J. Heeger, F. Wudl, Phys. Rev. B 48 (1993) 15425.

[24] J. Takada, H. Awaji, M. Koshioka, A. Nakajima, W. A. Nevin, Appl. Phys. Lett. 61 (1992) 2184.

[25] X. Chen, D. Taguchi, T. Manaka, M. Iwamoto, Org. Electron. 14 (2013) 320.

[26] X. Chen, D. Taguchi, T. Manaka, M. Iwamoto, J. Appl. Phys. 111 (2012) 113711.

Chapter 4 Analysis of electrode and interfacial charging

In last chapter, we already proved the capability of EFISHG measurement to visualize the carrier behavior in OSCs. Hence, in this chapter, we will establish our physical understanding about interfacial carrier processes based on Maxwell-Wagner model and EFISHG observation. We also further demonstrate the application of I-V, IS and EFISHG for analyzing the carrier injection and transport properties in OSCs. We focused on two interfacial charging processes, electrode charging and interfacial charging. OSCs built up their internal electric field trough these two charging processes. According we studied the detailed variation of these charging processes under various external conditions.

$0<Vex<Voc$ Studied by external resistance

The electrode charging and the interfacial charging generated electric fields with opposite direction across the C_{60} layer.

$Vex<0$ Studied by applied external biases

Interaction between Vex and electrode charging happened, charge neutralization happened on the electrodes, which induced another electrode charging process.

$0<Vex$ Studied by applied external biases

Only interfacial charging happened and it is corresponding to current changing.

4.1 OSCs with external resistance

4.1.1 Explanation of the experiment

Application of double-layer structure to the OSCs simplifies the carrier-path as well as the energy structure, and allows us to understand OSCs in terms of interface carrier charging due to the Maxwell–Wagner effect [1-5]. Noteworthy that besides the MW type interfacial carrier charging, electrode charging that provides the external electric field makes a significant contribution to carrier behavior in OSCs, owing to the dielectric nature of organic materials. Consequently we need a technique that is capable of detecting carrier motion as well as electric field in OSCs for getting the whole picture of the carrier behavior of the OSCs. The second-harmonic generation technique has been proved to be useful for determining the electric fields occurring at the interfaces of both organic and inorganic materials [11,12]. In previous section, we have shown that optical EFISHG measurement was available for probing the effect of Maxwell-Wagner type interface charging of pentacene/C_{60} OSCs under short circuit condition. This result motivated us to apply the EFISHG technique for further analyzing the two charging processes in OSCs, i.e., electrode charging and interface charging. In this section, by making use of EFISHG experiments on OSCs connected to various external resistances R_e, we analyzed the two charging processes, and showed that the two charging processes exhibited opposite tendency due to the photovoltaic (PV) effect of OSCs, whereas the response time of the two processes had very similar changing tendency. The results also showed the insufficiency of the model based on semiconductor physics for studying the interfacial behavior of the OSCs, while Maxwell-Wagner model analysis is more suitable.

Double-layer OSCs with an indium zinc oxide (IZO)/pentacene/C_{60}/Al structure were prepared as portrayed in Fig. 4.1(a). The pentacene layer with a thickness of 40 nm (d_1) and C_{60} layer with a thickness of 100 nm (d_2) were successively deposited onto the UV/ozone treated IZO surface as the organic active layer. The working area of the OSCs was A = 3.1 mm^2. The relative dielectric constants of the pentacene layer and the C_{60} layer at 1 kHz were $\varepsilon_1 = 4.2$ and $\varepsilon_2 = 6.5$, respectively. A red light from a light-emitting diode (wavelength 630 nm, intensity 1 mW/cm^2) was used as a light source to provide illumination pulse Fig. 4.1(b) shows the I-V characteristics of the OSC under red illumination and in dark, where the open-circuit voltage V_{oc} was 0.22 V, the short-circuit current density J_{sc} was -0.09 mA/cm^2 and the fill-factor was 0.26.

In order to study the PV effect on carrier behavior in OSCs, we measured the EFISHG at various I-V conditions by connecting various external resistances R_e to the OSCs in series, where transient EFISHGs were recorded. Hence, the external resistances R_e were 10, 25, 47, 100 and 180 kΩ, and these resistances resulted in the external voltages of 0.010, 0.050, 0.075, 0.100 and 0.150 V under illumination, which make the OSCs to exhibit the corresponding I-V characteristics shown in Fig. 4.1(b). The external resistance can keep the OSCs working at certain condition. It is like to connect two I-V characteristic together, as shown in Fig. 4.1(c). The I-V performance of the single resistance is a straight line with the slope I/V=R_e. The crossing point of two I-V curve is the I-V condition that exhibited by the OSCs connected to resistance and the value of the R_e can be directly obtained from the ratio of current and voltage value of OSCs at that crossing point. Hence, by using the external resistance, we can selectively maintain the different I-V condition for OSCs, which can be helpful for

characterizing the variation of the charging processes and thus for establishing a clear physical picture for OSCs.

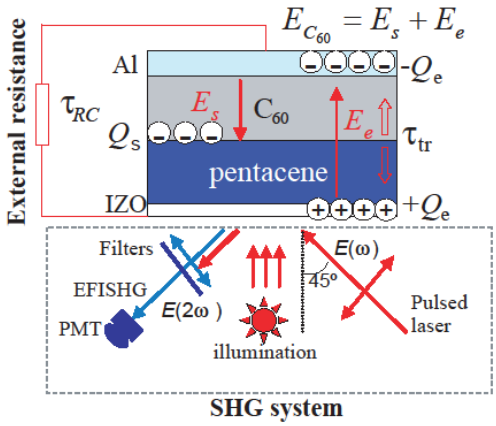

(a) Sample structure and experimental arrangement.

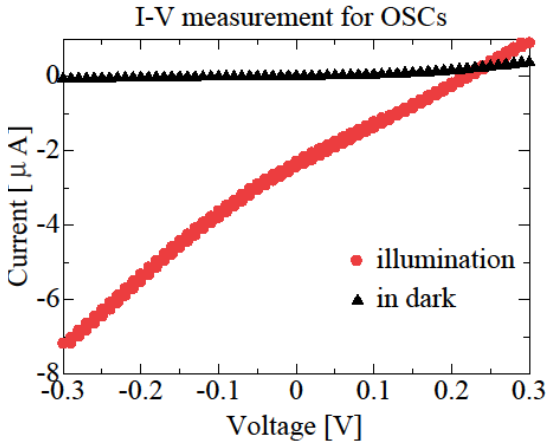

(b) I-V characteristics of the sample.

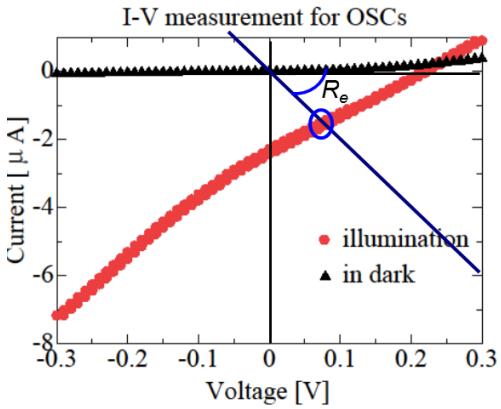

(c) OCSs with external resistance

Figure 4.1: Expreiment set up and I-V results (a) Sample structure and experimental arrangement, and (b) I-V characteristics of the sample. (c) OCSs with external resistance

4.1.2 Interfacial charging and internal electric field

Figures 4.2(a) and (b) show the square-root of the SHG intensity generated from the double-layer IZO/pentacene/C_{60}/Al device in response to the red illumination pulse (10 Hz). Under the illumination, the SHG intensity increased and then saturated, whereas the SHG intensity decayed and returned to the initial intensity in dark. Here, the SHG measurements were carried out with various external resistances R_e, on gradually changing from open circuit condition ($R_e = \infty$) to short circuit condition (R_e =0). We also carried out additional SHG experiment by applying AC square-wave voltage to determine the electric direction and the magnitude through the SHG intensity [6, 7]. The results were shown in the inset of Fig. 4.2(b). Using the linear relationship between the change of EFISHG intensity and applied voltage [8], the electric field was rescaled on the right hand side y-axis of Fig. 2. From Figs. 4.2(a) and (b) we found that the SHG signal under the illumination increased in the open circuit condition ($R_e = \infty$), while it decreased in the short circuit condition (R_e =0),

suggesting that the directions of the electric field formed across C_{60} layer are opposite with each other under these two conditions. As described in section 2.2, OSC device is modeled using a paralleled conductor-capacitor (*G*-*C*) circuit, assuming that the dielectric nature dominate the double layer properties, and charge Q_s accumulated at the pentacene/C_{60} interface is calculated (see section 2.2):

$$Q_s(t) = Q_s(\infty)[1-\exp(-\frac{t}{\tau_{MW}})] \quad (2.7)$$

with the MW type relaxation time $\tau_{MW} = \frac{C_1 + C_2}{G_1 + G_2}$ and $Q_s(\infty) = I_c(\frac{C_2}{G_2} - \frac{C_1}{G_1})$, where I_c is the steady-state's conducting current flowing across the OSCs. It is instructive to note that OSC devices generate photo currents due to the PV effect, and their equivalent circuits usually contain a current source. In our analysis, the conducting current I_c stands for the generated steady-state current across the device due to the PV effect. That is, the contribution of the PV current source is taken into account in Eq. (4.1), by using the MW type model. Noteworthy that the EFISHG measurement in this study corresponds to small signal analysis. The applied illumination pulse is the signal for triggering the OSCs sample, like the small AC signal used in the impedance spectroscopy measurement. In this situation, OSCs can be treated as the simple double layer system with an electrical excitation, which is suitable for the Maxwell-Wagner model application. Therefore, the current source is omitted from an equivalent circuit. For the open circuit condition, the current I_c is nearly zero and thus the $Q_s(t) \approx 0$, suggesting that the charging $\pm Q_e(t)$ on the two electrodes results in the change of the SHG signal under the illumination ($E(0) = E_e \propto Q_e(t)$), where $Q_e(\infty) = \frac{V_{ex}}{A}\frac{C_1 C_2}{C_1 + C_2}$,

(V_{ex}: external voltage). After the saturation of SHG intensity, the electric field across the C_{60} layer is 1.3×10^6 V/m and it is very close to the external electric field induced by the external voltage corresponding to V_{oc} ($E_s = \frac{V_{oc}}{d_2}\frac{C_1}{C_1+C_2} = 1.32\times10^6$ V/m), which proved no charge accumulated on the interface in a manner expected from the MW model. It is instructive here to note that conventional electrical measurements such as I-V measurements cannot directly provide information on the electric field distribution of the double layer system, while the EFISHG measurements directly probe the electric field and we used this result in the above analysis. On the other hand, under short circuit condition, electrode charging is negligible, because of $V_{ex} \approx 0$. The observed relaxation of the SHG intensity was due to the charging at the pentacene/C_{60} interface caused by the flowing of short circuit current, where the SHG signal changed in negative direction under illumination, suggesting electrons were accumulated at the interface [6]. The polarity of accumulated charges is governed by the time constants difference of the two facing organic layers. Material properties, such as dielectric constant and conductivity, will change due to degradation, and results in different SHG performance, which explains the different polarity of the SHG signal changing we reported in the reference [7]. In the present study, we repeated the SHG experiments using many samples, and found that most of the samples showed decrease of the SHG intensity under short circuit condition within the limits of our experimental atmosphere. Noteworthy that for the photovoltaic model based on semiconductor physics [9, 10], the internal electric field of OSCs under open circuit condition is governed by the depletion layer of so-called PN junction. The electric field of depletion layer would be offset by the V_{oc} under illumination, and can

be a source of SHG signal. Meanwhile, under the short circuit condition the changing of the band energy structure caused by the illumination is negligible, and this does not lead to the change of SHG signal. However, our results were different from this situation, due to the MW type charging at the pentacene/C_{60} interface.

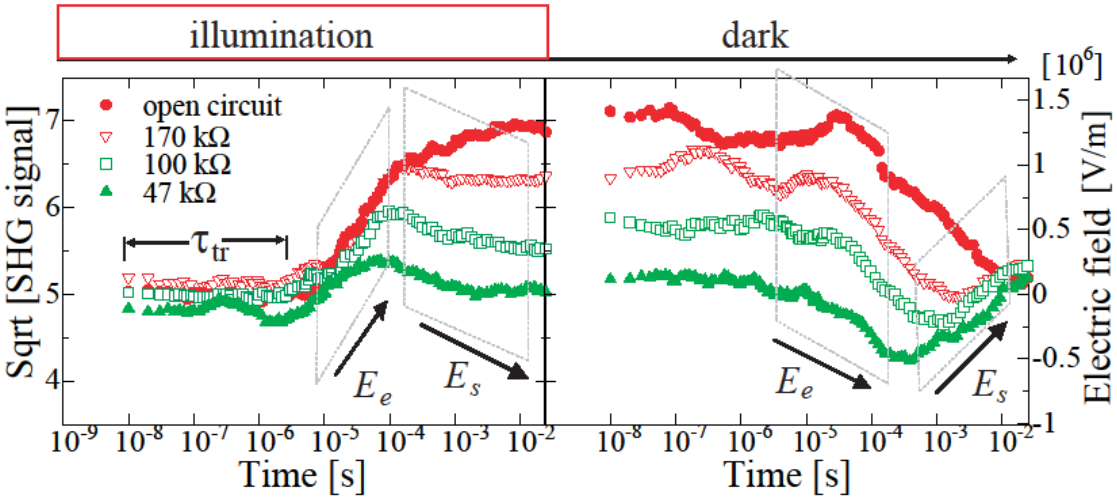

(a) R_e from open circuit to 47 kΩ.

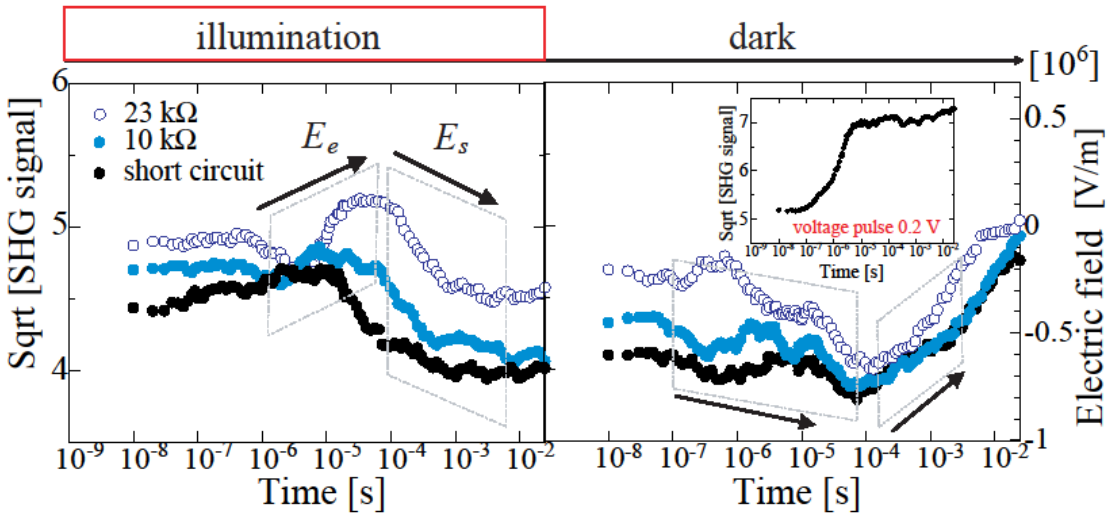

(b) R_e from 25 kΩ to short circuit.

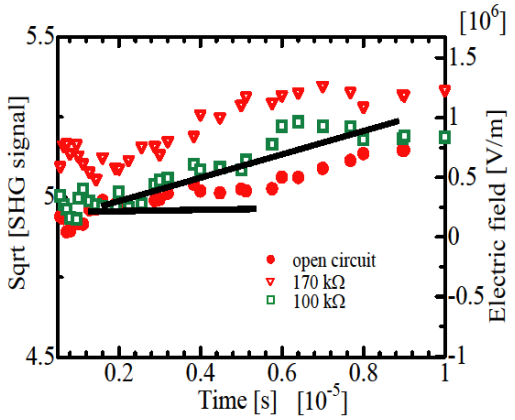

(c) SHG results with different external resistance in linear scale.

Figure 4.2: SHG measurement with different external resistance (a) R_e from open circuit to 47 kΩ, and (b) R_e from25 kΩto short circuit. (c) SHG results with different external resistance in linear scale.

For the experiments with external resistance connected to OSCs, both of the two charging processes are activated and the electric field in the OSCs changes accordingly. Note that the two charging processes provide the electric fields with opposite directions in the C_{60} layer. As the result, under the illumination, the SHG intensity increases at the beginning, and then decreases (see Figs. 4.2(a) and (b)). After stopping the illumination, two discharging processes were also observed in Figs. 4.2(a) and (b), where the two discharging processes showed a similar sequence with the charging processes. In order to clarify the initial rise of the SHG generation of Fig. 4.2(a), this figure is enlarged and plotted as Fig. 4.2(c) in linear scale. Here, we calculated the charge density provided by the charging processes on the two electrodes and at the interface ($Q_e = \varepsilon_2 \varepsilon_0 E_e$, $Q_s = E_s d_2 (\frac{\varepsilon_1 \varepsilon_0}{d_1} + \frac{\varepsilon_2 \varepsilon_0}{d_2})$). The results

were shown in Fig. 4.3(a). With the increase of R_e, Q_e on the two electrodes increased, while the Q_s at the interface decreased. The Q_e on the electrodes is proportional to the external voltage V_{ex}, while the Q_s at the pentacene/C_{60} interface changes in proportion to the current I_c. For the illuminated OSCs in the external voltage region from 0 to V_{oc}, the increase of the V_{ex} led to the decrease of the magnitude of I_c, due to the PV effect. Accordingly the two charging processes inside the device would exhibit the opposite changing tendency. Note that, when the R_e was around 47 kΩ, E_e=E_s with Q_e=0.62Q_s, and the EFISHG signal returned to initial state at t = 0.01 s after the illumination, as shown in Fig. 4.2(a). Figure 4.2 also indicated that the residual of the SHG signal gradually increased from the open-circuit condition to the short-circuit condition. This residual was possibly due to the presence of deep traps at the pentacene/C_{60} interface, and the decrease of the SHG signal indicated that the trapped charges were electrons. Since the conducting current of the OSCs gradually increased from open-circuit condition to short-circuit condition, the trapping would be activated correspondingly, as seen in Fig. 4.2. The presence of traps slows down the charging processes, but this effect will be eliminated by prolong the period time of the illumination pulse.

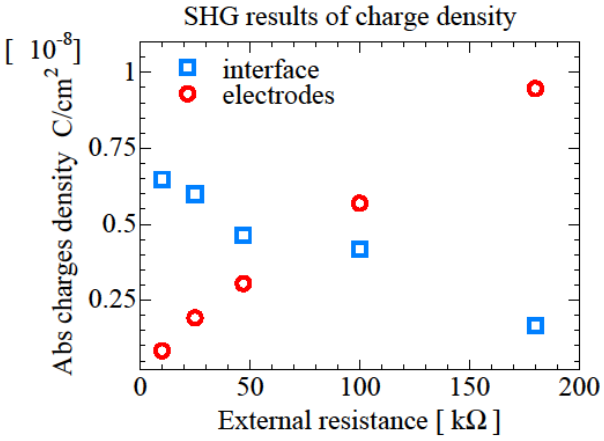

(a) Charge density of two charging processes.

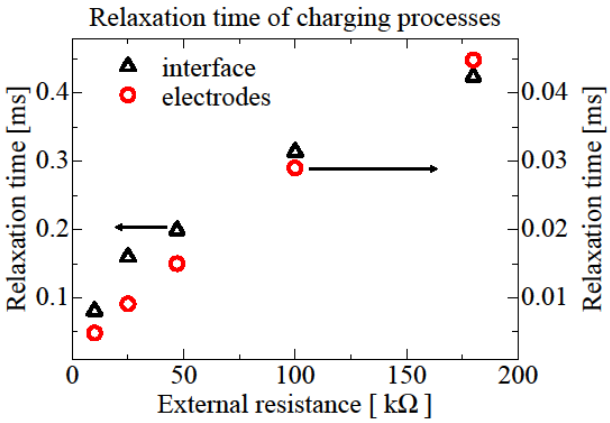

(b) Relaxation time of two charging processes.

Figure 4.3: Charge density and relaxation time changing with external resistance (a) Charge density of two charging processes, and (b) Relaxation time of two processes.

By using a curve-fitting method based on a filtering technique described in section 3.2.3 [11, 12], the time-constants of the two charging processes were evaluated, and the results were plotted in Fig. 4.3(b), where the relaxation times of the both processes increased with increase of the external resistance. Here, the source of the electrode charging is the charges generated at the pentacene/C_{60} interface due to the PV effect, unlike other organic electronic devices whose charges are supplied by the externally

applied potential with a response time $\tau_{RC} = R_e \frac{C_1 C_2}{C_1 + C_2}$ [2, 13]. Accordingly the relaxation time τ_e of the electrode charging is given as $\tau_e = \tau_{tr} + \int_0^{Q_e} \frac{AdQ}{I(Q)}$ ($\tau_e << \tau_{RC}$), where the τ_{tr} (on the order of 10^{-6}s) is the transit time for charges to research the electrodes, which is estimated from the intercept on the time scale in Fig. 4.2(a) (also see Fig. 4.2(c)), $I(Q)$ is the current value that depends on the Q_e on the electrodes, and it decreases with increase of the Q_e due to PV effect (see the I-V curve in Fig. 4.1(b)). Since the electrode charge density $\pm Q_e$ increases with the increase of the R_e (see Fig. 4.3(a)), the response time τ_e is prolonged accordingly. On the other hand, the response time τ_s of the charging on the pentacene/C_{60} interface is approximately given as $\tau_s = \tau_{RC} + \tau_{MW}$ [6], where τ_{RC} is the response time of the external circuit. The increase of τ_{RC} in accordance with the increase of the R_e accounts for the delay of the relaxation time τ_s shown in the Fig. 4.3(b). As mentioned, the photovoltaic effect observed in the OSCs were well explained by assuming electrode and interface charging made a significant effect on the carrier processes of OSCs.

4.1.3 Discharging processes

In last section, EFISHG technique has been applied to analyzing carrier behaviors in OSCs. By connecting external resistance to the OSCs, carrier transits in OSCs were visualized and nonreversible interface charging and electrode charging processes were identified. Interestingly, the charge density at the interface increased in the discharging process. Noteworthy that such increase of charge carrier density has not been observed for other organic devices, such as OLEDs and OFETs, suggesting that

photovoltaic effects were responsible for this process. In the present section, in order to further clarify this anomalous interfacial recharging process, we further carried the transient EFISHG experiments and analyzed the recharging process using a Maxwell-Wagner model. We concluded that change of conductance induced by illumination caused the anomalous discharging. Finally, we showed that the IS analysis supported this conclusion.

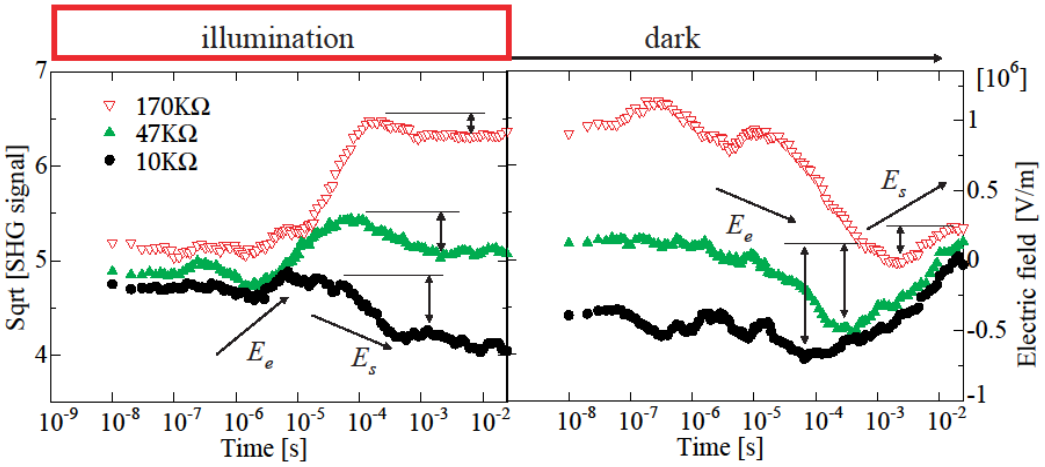

Figure 4.4: EFISHG measurement with external resistance of 10, 47 and 170 KΩ.

Figure 4.4 shows the SHG intensity generated from the double-layer IZO/pentacene/C_{60}/Al device in response to the red illumination pulse (10 Hz). Here, the measurements were carried out with connecting external series resistances R_e= 10, 47 and 170 kΩ, respectively. Upon the illumination the SHG intensity increased and then saturated, whereas it decayed by stopping the illumination. In Fig. 4.4, y-axis represents the electric field, which was estimated using the linear relationship between the EFISHG intensity and applied voltage [7, 14]. The transient SHG signal response under the illumination indicated the presence of two series charging processes, and

the formation of the electric field in the C_{60} layer in opposite directions successively with elapsed time. These were electrodes charging and interfacial charging on the double-layer interface [14]. The response time of the electrode discharging is given as $\tau_e = \tau_{RC} = R_o \frac{C_1 C_2}{C_1 + C_2}$, and it is different from the response time τ'_e in the charging process ($\tau'_e = \tau_{tr} + \int_0^{Q_e} \frac{AdQ}{I(Q)}$, where the τ_{tr} is the transit time for charges to research the electrodes and A = 3.1 mm^2). The experimental discharging response time τ_e obtained using the filtering method (see section 3.2.3) was in good agreement with the response time τ_{RC} of the equivalent circuit, and it was $\tau_e = \tau_{RC} \approx 0.8 \times 10^{-3} s$. As shown in section 2.2, a simple Maxwell-Wagner model can be used for analyzing interfacial processes in double-layer samples. The double layer is modeled using a parallel circuit comprised of conductor (G_1, G_2) and capacitor (C_1, C_2), as also shown in Fig. 4.5(a). According to the Maxwell-Wagner effect, charge Q_s is accumulated with a response time τ_{MW} at the interface between layers 1 and 2. The detailed calculation of the accumulated charges ca be explained by Eq. (2.7). Noteworthy that interfacial charging process and its discharging should be reversible if conductance (G_1 and G_2) and capacitance (C_1 and C_2) are constant. However, our EFISHG experiments showed that the interface discharging process and the charging process were non-reversible, as shown in Fig. 4.4. For R_o= 47 KΩ (V_{ex}= 0.075 V) , the electric field increased about 0.25×10^6 V/m due to the interface charging of Q_s (=0.46×10^{-8} C/cm^2) in the charging process, while in the discharging process the electric field decayed about 0.5 $\times 10^6$ V/m, corresponding to the interface discharging of Q_s (=0.92×10^{-8} C/cm^2). Similar phenomena were also found in the OSCs sample with other R_o (see Fig. 4.4).

This result indicated that the pentacene/C_{60} interface experienced a recharging process during the discharging process. According to the Maxwell-Wagner effect, Q_s at the steady-states is given as $Q_s(\infty) = I_c(\frac{\varepsilon_2}{\sigma_2} - \frac{\varepsilon_1}{\sigma_1})$ (see Eq.(2.7)). Consequently, the conductivity (σ_1 and σ_2) of the active layers, pentacene and C_{60}, was considered to be decreased after stopping the illumination [15-17]. With decrease of the conductivity, the saturated charge density $Q_s(\infty)$ on the interface could be increased, which met the precondition of the interface recharging. Meanwhile, conduction current continuously flowed through the circuit during the electrode discharging process. Eventually, the interface was recharged. Fig. 4.5(b) illustrates the recharging process based on the above mentioned discussion.

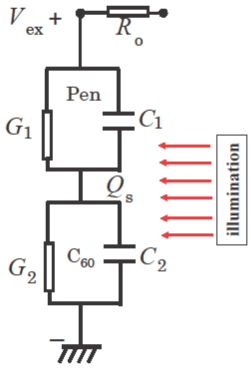

(a)

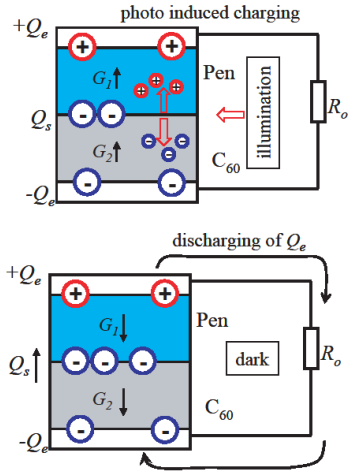

(b)

Figure 4.5: (a) Equivalent circuit for the sample. (b) Simple model for explaining recharging process.

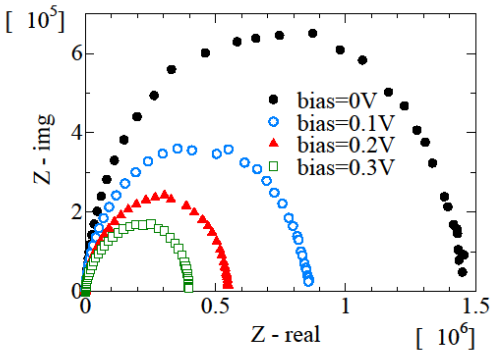

(a)

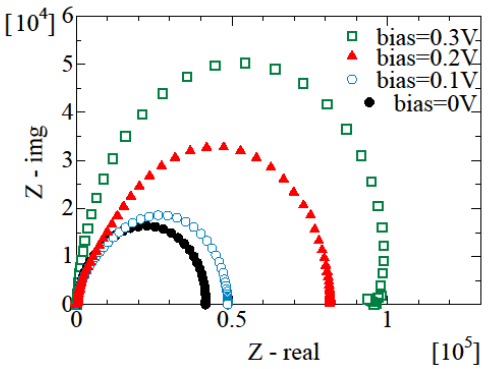

(b)

Figure 4.6: IS measurements of the OSCs with different DC biases (a) In dark condition and (b) Under illumination.

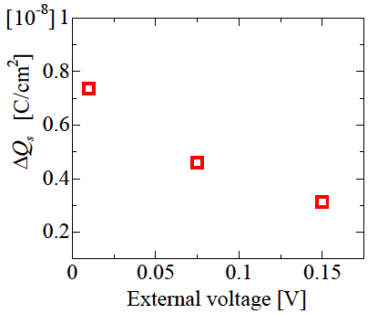

Figure 4.7: The increased charge density ΔQ_s during the interface recharging with different V_{ex}.

In order to verify the contribution of the conductivity change in terms of the recharging, we employed the impedance spectroscopy (IS) technique, and measured the frequency dependence of the impedance of our sample. Figure 4.6 shows the results plotted as the Nyquist plot, where the x- and y-axes represent the real part and imaginary part of impedance, respectively. The single relaxation process of impedance is given as $Z = \frac{G}{G^2+\omega^2C^2} - j\omega\frac{C}{G^2+\omega^2C^2} = X - jY$, where G (=G_1//G_2) and C (=C_1//C_2) are the total conductance and capacitance of the OSCs, respectively. Consequently, the following expression of a Nyquist circle is obtained

$$\left(X-\frac{1}{2G}\right)^2 + Y^2 = \frac{1}{4G^2}, \text{ with } \theta = \arctan\left(\frac{C\,\omega}{G}\right). \qquad (4.1)$$

The diameter of the Nyquist circle is G^{-1}. In dark condition (see Fig. 4.6(a)), the increase of DC bias led to the narrowing of the Nyquist circle, indicating the increase

of conductivity of the organic layer. It is instructive here to note that *G* and *C* in Eq. (4.1) are a.c. conductance and a.c. capacitance, and they are defined as $G(V_0) = \partial G / \partial V\big|_{V=V_0}$ and $C(V_0) = \partial C / \partial V\big|_{V=V_0}$ at $V = V_0$, respectively. With applying the d.c. bias to OSCs, carriers injected into organic active layer and a current flows in a manner as space charge limited current, $I \propto V^2$. That is the current increases nonlinearly with applied voltage. Consequently, the a.c. conductivity of the organic layer increased in proportional to the DC biasing, as shown in Fig. 4.6(a). By contrast, under the illumination, Fig. 4.6(b) indicates that the a.c. conductivity of the organic layer decreases with increase of d.c. bias. This result is supported by the I-V characteristics of Fig. 4.1(b), where the slope defined by $G(V_0) = \partial G / \partial V\big|_{V=V_0}$ under illumination decreases with increase of the d.c. bias. In more details, in the region 0 V~V_{oc}, the increase of the a.c. conductance is suppressed due to the photovoltaic effect, and resulted in the expanding of the Nyquist circle in Fig. 4.6(b). In other words, the d.c. conductance significantly increased by the illumination, but the increase of the a.c. conductance with respect to biasing voltage is limited and decreased in the region 0 < V < V_{oc}. This evidently supported our conclusion on the interface recharging during the discharging process. Furthermore, according to the IS results, the recharging process was supposed to be suppressed by increase of external voltage. Similar phenomena were also found with the EFISHG measurements. Figure 4.7 summarized the increase of the charging density ΔQ_s due to the interface recharging, where the increase of the V_{ex} led to the inhibition of the interface recharging. The SHG results is well supported by the IS measurement.

4.2 OSCs under external biases

In last section 4.1, we applied this technique to study carrier behaviors in OSCs, by connecting an external resistance to the OSCs. The result showed that non-zero electric field was formed in OSCs by the PV potential V_e, but a current flowing through the external resistance decreased this initial electric field, in a manner as $E \propto V_{oc} - I_p R_{ex}$. Here I_p is the photocurrent and R_{ex} is the external resistance. Accordingly, the carrier behavior in the region $0 < V_{ex} < V_{oc}$ (V_{ex}: external voltage) was able to be explored. However, we could not examine the carrier behaviors in the region $V_{ex} < 0$ and $V_{ex} > V_{oc}$. On the one hand, using an external d.c. voltage to the OSCs enables us to examine the carrier behaviors over the entire region of V_{ex}. Note that potential difference across OSCs is constant in the measurement using an external voltage, whereas it varies with a current flowing through OSCs in the measurement using an external resistance. In this study, by connecting an external battery to double-layer IZO/pentacene/C_{60}/Al OSCs, transient carrier behaviors in the OSCs were studied with and without photo-illumination using the EFISHG.

4.2.1 EFISHG measurement by applying pulse voltages in dark

The EFISHG probes the electric field across the C_{60} layer and it reflects carrier behaviors as described in section 4.1.2. The electric field $E(0)$ is sum of the external electric field (E_{ex}), space-charge field (E_s) caused by accumulated charges at the pentacene/C_{60} interface, and PV field (E_{ph}). In the absence of photoillumination, obviously $E_{ph}=0$. Figure 4.8(a) shows the EFISHG response of the double-layer IZO/pentacene/C_{60}/Al device in dark, in response to the AC square-wave voltage

pulse (10 Hz). Here the biasing d.c. voltage V_{ex} was +0.3V or -0.3V, and it was applied on the IZO electrode with reference to the Al electrode. By using a curve-fitting method based on a filtering technique (see section 3.2.3), two carrier relaxation processes (denoted by τ_{RC}, τ_{MW}) were identified from the transient SHG signal, as depicted in Fig. 4.8(a). The $\tau_{RC} = 2\times10^{-7}$ s is the response time for electrode charging through the external circuit, and τ_{MW} is the response time for the Maxwell-Wagner type interfacial charging (see Eq. (2.7)) and $\tau_{MW} = 2.4\times10^{-6}$ s with V_{ex}=0.3 V, while $\tau_{MW} = 3\times10^{-5}$ s with V_{ex}= -0.3 V.

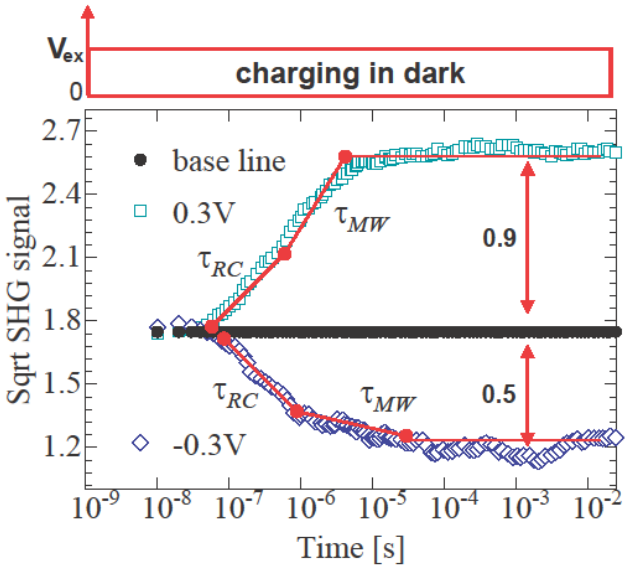

(a)

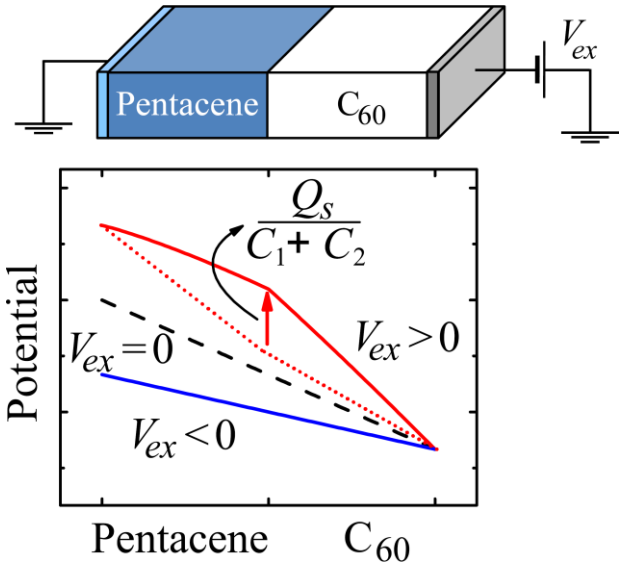

(b)

Figure 4.8: (a) EFISHG measurement with applied voltage pulse in dark condition. Relaxation times τ_{RC} and τ_{MW} stand for the electrode charge and double-layer interface charge relaxations. (b) The sketch of the steady-state potential profiles across the double-layer under external voltage.

Interestingly, the responses of the SHG under +0.3 V and -0.3 V were similar and mirror-symmetric with the base line at V_{ex}=0, but there was a significant difference in the change of the SHG response, where the change under V_{ex} = +0.3 V was bigger than that under V_{ex}=-0.3 V. In more details, the magnitude of applied external field E_{ex} was the same for both positive and negative biasing conditions, i.e., at V_{ex}=±0.3 V, but the MW interface charge field E_s was more significant for the positive biasing voltage, V_{ex}=+0.3 V. Noteworthy that a diode-like dark current flows across the OSCs with a rectification ratio of one order at ±0.3 V, in a manner as depicted in the inset of Fig. 4.8(b). The forward current flows when the OSCs is positively biased to the IZO electrode (Al electrode grounded), suggesting smooth hole injection from the IZO to

pentacene. Owing to the Maxwell-Wagner effect, excess charges are accumulated at the double-layer interface and non-zero space charge electric fields are formed in the OSCs (see Eq.(2.7)). The accumulated charge Q_s at the double-layer interface is governed by the conduction current I_c that flows across the interface, and it is given as $Q_s(\infty) = I_c \Delta\tau$ (see Eq.(2.7)). For the negative biasing V_{ex}< 0, I_c is very small. As a result, accumulated charge at the double-layer interface is negligible and E_s is nearly zero for V_{ex}<0. The difference in the amount of accumulated charges accounts for the difference of the SHG response observed in Fig. 4.8(a) for V_{ex}= +0.3 V and -0.3 V. Suggested potential profiles in the OSC are displayed in Fig. 4.8(b), where accumulated positive charges enhance electric field in the C_{60} layer (V_{ex}>0), whereas accumulated negative charges decrease the electric field, but nearly zero (V_{ex}<0). The suggested potential profiles accounts for the non-symmetric response of Fig. 4.8(a). Note that the SHG enhancement is observed at V_{ex}=0, as can be seen as the base line of Fig. 4.8(a). This is possibly due to an internal electric field (pointing in the direction from IZO to Al electrode), induced by such as work function difference between two electrodes and others. However, the presence of this field does not lose the generality of our discussion.

4.2.2 EFISHG measurement with illumination pulse under d.c. biasing

Figures 4.9(a) and (b) show the SHG generated from the double-layer IZO/pentacene/C_{60}/Al device in response to the red illumination pulse. The EFISHG measurements were carried out at various biasing voltages (V_{ex}), in the region between −0.3 V and 0.3V. As shown in Figs. 4.9(a) and (b), the initial value of the SHG is

dependent on bias voltage, and it corresponds to the saturated value at 10^{-3} s in Fig. 4.8(a). As discussed in our previous paper [14], the photo-induced internal electric field has two origins. One is induced in the direction from the IZO to the Al electrode as a result of PV effect ($E_{ph,e}$). Another one is generated by the accumulated charges Q_s at the double-layer interface due to Maxwell-Wagner effect ($E_{ph,s}$) and its direction is dependent on the polarity of Q_s. As that, a local electric field is given as the sum of the two electric fields, $E_{ph}=E_{ph,e}+E_{ph,s}$.

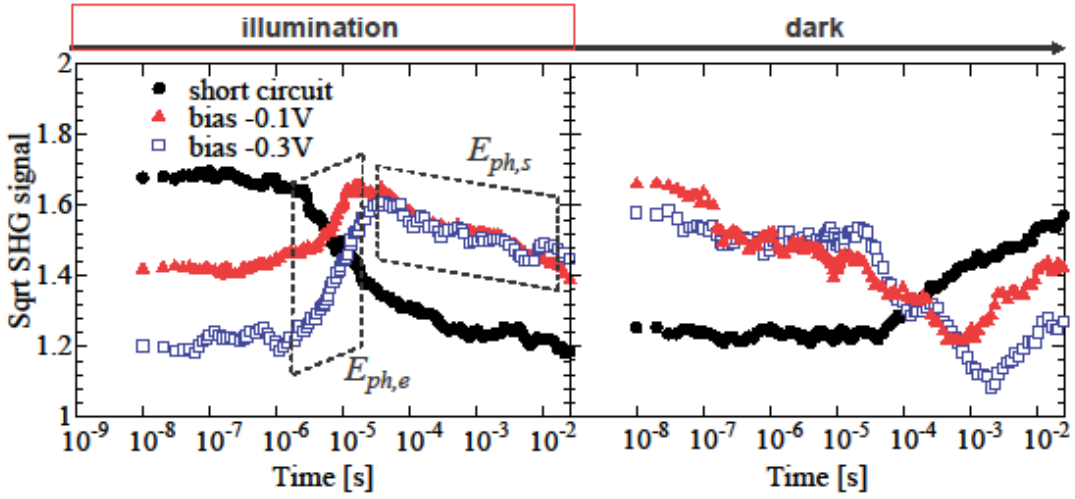

(a)

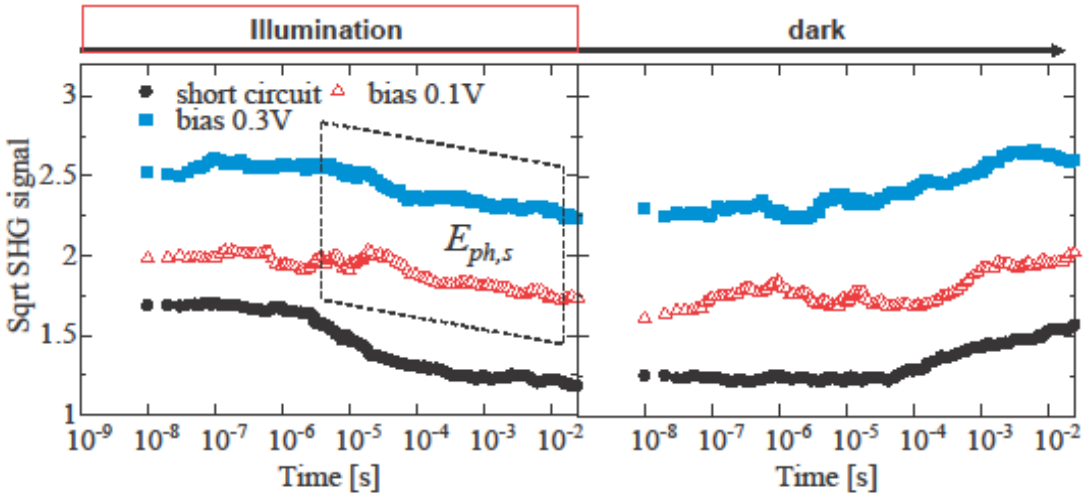

(b)

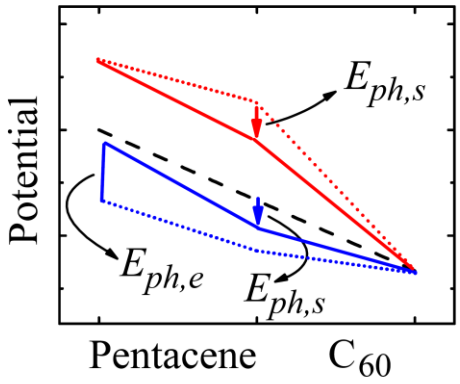

(c)

Figure 4.9: EFISHG results with the different voltage bias (a) from 0 V to -0.3 V and (b) from 0 V to 0.3 V and (c) sketch of potential profiles across double-layer structure under illumination, where dotted line is the potential provided by the bias voltage in dark and solid line is the potential profile under illumination.

Figure 4.9(a) shows the SHG results for $V_{ex} \le 0$. For $V_{ex} = 0$ (short-circuit condition), the SHG decreased with applying illumination, suggesting that PV effect apparently induced a Maxwell-Wagner type interfacial electrons charging [7]. On the other hand,

with V_{ex}= -0.3 V and -0.1 V, upon illumination the EFISHG increased firstly and then decreased, indicating that $E_{ph,e}$ and $E_{ph,s}$ were activated successively and the direction of these two electric fields were opposite to each other. Under illumination photocurrent I_{ph}<0 flowed across the double-layer interface, which resulted in the accumulation of electrons due to Maxwell-Wagner interfacial charging (see Eq. (2.7)). Accordingly, the SHG intensity should be gradually decreased, and indicates that the first relaxation process (the SHG increasing process) was not the Maxwell-Wagner type interfacial charging. On the other hand, the relaxation time less than 10^{-5} s is in agreement with the carrier transit time across the organic film layer [14], suggesting that the first relaxation process was due to the electrode charging caused by the PV effect. In more detail, under the illumination, carriers were created in OSCs due to exciton dissociation at double-layer interfaces, and electrons and holes were transported to the opposite electrodes. Meanwhile, the polarity of the charges conveyed to the electrodes was opposite with the charges on the electrodes induced by the applied V_{ex}. Consequently, recombination occurred on the electrodes. Through this process, the PV field $E_{ph,e}$ compensated the field by applied V_{ex} as observed in Fig. 4.9(a). The $E_{ph,e}$ increased the SHG signal, and finally the SHG reaches the intensity value corresponding to the short-circuit condition in dark. Therefore, $E_{ph,e}$ is generated in the opposite direction with applied V_{ex}, and $E_{ph,e} \approx -E_{ex} = -\frac{C_1}{C_1 + C_2}\frac{V_{ex}}{d_2}$. After photo-induced electrode charging, the second relaxation process follows due to the MW interface charging. This interface charging accumulates electrons at the double-layer interface and establishes an additional electric field $E_{ph,s}$ accordingly. As

a result, the SHG signal decreases in a manner similar to the SHG decaying under the short-circuit condition as shown in Fig. 4.9(a).

Under biasing condition of $0 < V_{ex} < V_{oc}$ and $V_{oc} < V_{ex}$ (V_{ex} =0.1 V and 0.3 V), respectively, the SHG response was measured upon illumination, as shown in Fig. 4.9(b). Interestingly, only one relaxation was observed. It is instructive here to note that the current flowing across the OSCs was proportional to the square of the applied voltage $I \propto V^2$, suggesting the space-charge limited current condition (SCLC) was established in the OSCs, and the electric field distribution through the device was in a manner as $E \propto (x/d)^{1/2}$ [18] from the electrode surface (x=0) and provided a very strong electric field across the C_{60} layer. In this situation, accumulation of the charge Q_e on the IZO electrode is suppressed owing to the smoothly SCLC carrier injection from electrodes by applied voltage. Accordingly the electrode charging due to the PV effect cannot be activated ($E_{ph,e}$=0). As a result, the SHG signal mainly traces the interface charging ($E_{ph,s}$) caused by the flowing photocurrent. As described in section 4.1.2, the interface charging under biasing condition of $0 < V_{ex} < V_{oc}$ causes the decrease of the SHG signal, in a similar manner shown in Fig. 4.9(b). For V_{ex}=0.3 V, the SHG signal slightly decreased with illumination. The relaxation time of the SHG signal corresponded to the Maxwell-Wagner interfacial relaxation, suggesting that the decrease of the SHG signal reflected the change of space charge field $E_{ph,s}$. According to Eq. (2.7), accumulated charge Q_s at the interface is given by $Q_s(\infty) = I_c \Delta\tau$. Note that I_c was nearly the same under illumination and in dark at V_{ex}=0.3 V. Accordingly the change of $\Delta\tau$ due to illumination was a main physical reasoning for the change accumulation Q_s, which led to the decrease of the SHG signal by illumination.

Pentacene and C_{60} are photosensitive materials [15-17], and their carrier relaxation times decrease by illumination. Our impendence measurements showed that the $\Delta\tau$ changes by a factor of 3 due to illumination [15, 16, 19]. Hence, the discharging of the Q_s on the interface can be considered as the generation of the $E_{ph,s}$ to compensate the E_s. Fig. 4.9(c) illustrates the suggested potential profiles. As described above, the carrier behavior in OSCs under photoillumination was probed by the EFISHG measurements, and the carrier behaviors over the entire region of applied d.c. biasing conditions can be discussed with consideration of the dielectric nature of organic double layers in OSCs.

4.3 Summary

In this chapter, EFISHG measurement was applied to investigate electrode charging and interfacial charging happened inside pentacene/C_{60} double-layer OSCs in terms of photovoltaic effect. Making use of OSCs connected to various resistances R_e showed that the two charging processes exhibit opposite changing tendency due to the photovoltaic effect, while the response time of the both two charging processes increase with the increases of R_e. The EFISHG measurements also demonstrated that two charging processes produce electric fields with opposite directions in the C_{60} layer. Moreover, we also studied discharging process on the double-layer interface of OSCs by using the same measurement, and modeled the recharging process at such interface. The charging and discharging processes on the double-layer interface by photo illumination were nonreversible, and a recharging process continued after the

illumination stopped. This discovery was supported by the IS analysis and the analysis of OSCs based on the Maxwell-Wagner model.

On the other hand, by applying external biasing voltage to the OSCs, we carried the EFISHG measurement with photo illumination. Results showed that only organic double-layer interface charging was induced under positive d.c. biasing by photoillumination, while interface and electrode charging were induced under negative d.c. biasing. Hence, we confirmed the OSCs build up its internal electric field due to the PV effect as well as the interfacial charging processes. That is, the carrier behaviors in the OSCs were governed by the dielectric nature of the organic double layer.

Results obtained here further confirmed the dielectric performance dominate the performance of OSCs. By connecting external resistance and external biases to the OSCs, the carrier behavior over the entire region of V_{ex} was examined and a clear physical picture of OSCs based on dielectric physics was established. This physical understand enable us to study the interfacial carrier behavior and its contribution to the OSCs performance. Finally, based on this physical model we will bring out some suggestion for improving the performance of OSCs and this is research purpose of next section.

Bibliography of Chapter 4

[1] L. Zhang, D. Taguchi, J. Li, T. Manaka, M. Iwamoto, J. Appl. Phys. 108 (2010) 093707.

[2] D. Taguchi, L. Zhang, J. Li, M. Weis, T. Manaka, M. Iwamoto, J. Phys. Chem. C 11 (2010) 15136.

[3] M. Weis, T. Manaka, M. Iwamoto, J. Appl. Phys. 105 (2009) 024505.

[4] M. Iwamoto, T. Manaka, M. Weis, D. Taguchi, J. Vac. Sci. Technol. B 28 (2010) C5F12.

[5] J. Lin, M Weis, D. Taguchi, T. Manaka, M. Iwamoto, Thin Solid Films 518 (2009) 448.

[6] D. Taguchi, T. Shino, L. Zhang, J. Li, M. Weis, T. Manaka, M. Iwamoto, Appl. Phys. Express. 4 (2011) 021602.

[7] D. Taguchi, T. Shino, X. Chen, L. Zhang, J. Li, M. Weis, T. Manaka, M. Iwamoto, Appl. Phys. Lett. 98 (2011) 133507.

[8] Y. R. Shen: Principle of Nonlinear Optics, Wiley, New York, 1984.

[9] B. Kayes, H. Atwater, T. Watson, N. Lewis, J. Appl. Phys. 97 (2005) 114302.

[10] Z. Liao, Y. Xu, D. Xu, Adv. Mater. Res. 204 (2011) 1669.

[11] C. R. Crowel, S. Alipanahi, Solid-State Electron. 24 (1981) 25.

[12] I. Thurzo, D. Pogány, K. Gmucová, Solid-State Electron. 35 (1992) 1737.

[13] J. Lin, M Weis, D. Taguchi, T. Manaka, M. Iwamoto, Thin Solid Films 518 (2009) 448.

[14] X. Chen, D. Taguchi, K. Lee, T. Manaka, M. Iwamoto, Chem. Phys. Lett. 511 (2011) 491

[15] R. PETRITZ, Phys. Rev. 104 (1956) 1508.

[16] Y. Wang, Nature 356 (1992) 585.

[17] O. Ostroverkhova, D. Cooke, S. Shcherbyna, R. Egerton, F. Hegmann, Phys. Rev. B 71 (2005) 035204.

[18] M. A. Lampert and P. Mark, Current Injection in Solids (Academic, New York, 1970).

[19] R. Tamura, E. Lim, T. Manaka, M. Iwamoto, J. Appl. Phys. 100 (2006) 114515.

[20] C. R. Crowel and S. Alipanahi, Solid-State Electron 24, (1981) 25.

Chapter 5 Interfacial charging and I-V performance of OSCs

In this chapter, we pay attention to the contribution of Maxwell-Wagner type interfacial charging to the I-V performance of OFETs. EFISHG measurements were performed to estimate the relaxation time and accumulated charge density on the interfaces of OSCs. Here the Maxwell-Wagner model was used to explain all the experimental data. Finally, we proved that the existence of interfacial charging deteriorates the performance of OSCs. The details are showed as follow:

1. The accumulated charges on the interfaces induce a recombination current and consequently the photo current is depleted by this recombination current at the interfaces.

2. The slow attenuation of this recombination current also leads to the deterioration of the fill-factor of OSCs.

3. The accumulated charges require another external voltage V` to assist photo-generated charges from leaving the interface, which decreases the effective Voc.

We also figured out two methods (exciton blocking layer and interfacial charging blocking layer) to suppress the interfacial charging happened inside OSCs and the I-V performance of OSCs was enhanced accordingly.

5.1 Consumption of JSC

In order to improve the efficiency of OSCs, many ideas have been presented. Among them are the development of new organic molecules with appropriate HOMO and LUMO states, the use of blocking layers between electrodes and active layers of OSCs, and so forth [1-3]. These efforts have made a contribution to increase open voltage as well as short-circuit current of OSCs, and thus to improve the efficiency of OSCs [2-6]. However, the detailed study related to the carrier behavior as well as the electrical phenomena induced by the introduction of the blocking layer is still not sufficient. Owing to the dielectric nature of organic materials, accumulated charges at the interface due to the Maxwell-Wagner effect significantly changes the potential distribution in OSCs, and results in the modification of the energetic [7-9]. Therefore, direct probing of the electric field and potential profiles in OSCs will be of help to understand carrier behaviors in OSCs, and thus to improve the device performance.

We have been developing a technique of the electric field induced optical second harmonic generation (EFISHG) measurement that is capable of directly probing carrier motions and electric field distribution in organic devices, e.g., organic field effect transistors, organic electroluminescence devices [10, 11], and organic solar cells [6, 7], and could show the presence of the Maxwell-Wagner effect interface charges at various interfaces. This motivated us to study the contribution of the blocking-layers in OSCs to the interfacial carrier processes by means of the EFISHG measurement. In this section, we prepared IZO/pentacene/C_{60}/Bathocuproine (BCP)/Al OSCs with a blocking BCP layer, and studied the contribution of interfacial charging to J_{SC}. Modeling the prepared OSCs as Maxwell-Wagner effect elements accounted for our

experimental results, and the contribution of blocking layers to OSCs has been clarified. We carried the EFISHG measurement by applying DC pulse voltage to the OSCs in dark, and also by applying illumination pulse to the OSCs under short-circuit condition. In these two measurements, we probed the SHG generated from the C_{60} layer.

5.1.1 Triple-layer OSCs with exciton blocking layer

Figure 5.1(a) portrays OSCs with an indium zinc oxide IZO/pentacene/C_{60}/ BCP/Al structure. These OSCs were prepared as follows: IZO-coated glass substrates were UV/ozone treated to be nearly free from organic residuals. The pentacene layer with a thickness of 40 nm (d_1) and the C_{60} layer with a thickness of 50 nm (d_2) were successively deposited onto the UV/ozone treated IZO. After that, a BCP layer with a thickness of 10 nm was deposited. Finally, Al electrodes with a thickness of 100 nm were deposited onto the surface of C_{60} layer, where the working area of the OSCs was A = 3.1 mm^2. As the reference, OSCs without BCP layer were also prepared.

In the measurement, a red light from a light-emitting diode (wavelength 630 nm, intensity 1 mW/cm^2) was used as a light source to provide illumination pulse (repetition rate 10 Hz, duration 50 ms, switching on and off time within 50 ns) to the OSCs. Note that pentacene and C_{60} layers absorb light at a wavelength of 630 nm [6], and generate excitons inside their layers. Figure 5.1(b) shows the I-V characteristics of the OSCs under illumination and in dark. The introduction of the BCP layer was effective for improving the device performance, in a manner as other researchers pointed out [1-3]. For the OSC sample with no BCP-blocking layer, V_{oc} = 0.24 V, J_{sc} =

-0.23 mA/cm^2, and *FF* = 0.15, whereas for the sample with BCP-blocking layer, V_{oc} = 0.25 V, J_{sc} = -1.33 mA/cm^2, and *FF* = 0.45.

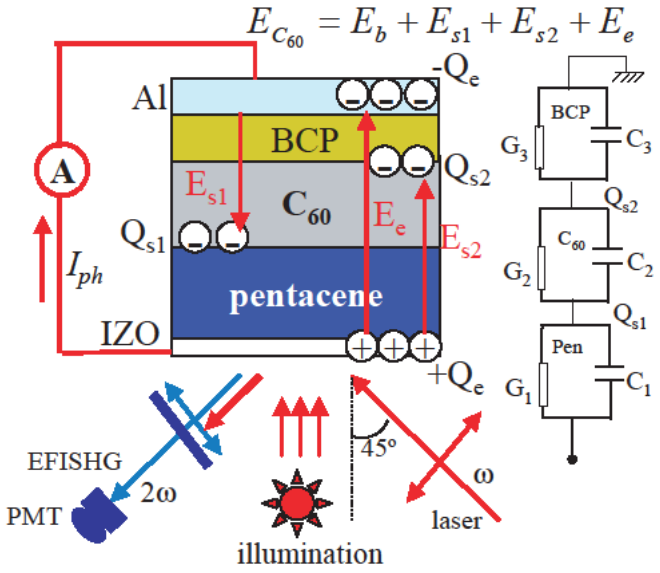

(a)

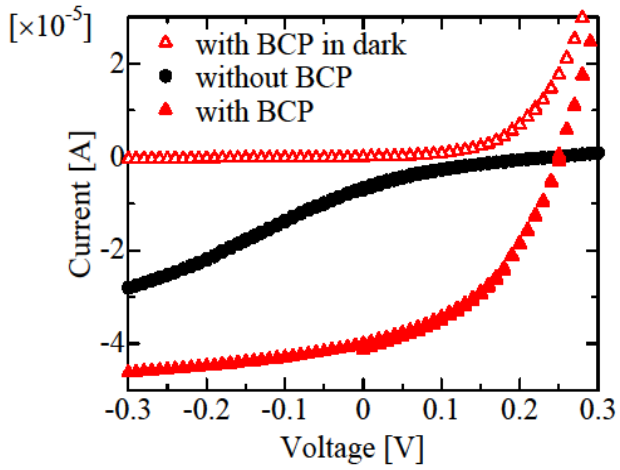

(b)

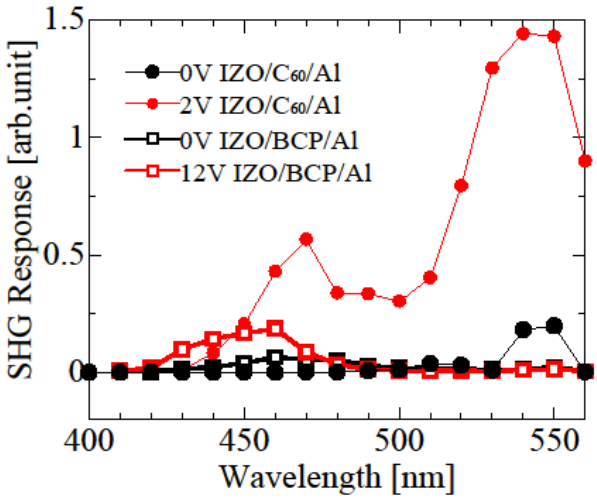

(c)

Figure 5.1: Expreiment set up and I-V results (a) experimental setup for the EFISHG measurement (b) I-V characteristics of the OSCs sample. (c) EFISHG spectra of the IZO/C_{60}/Al and IZO/BCP/Al single-layer devices under shortcircuit condition and voltage application.

Figure 5.1(a) also portrays the arrangement of the SHG measurement for probing the electric field in OSCs. A pulsed laser was used as a probing light (repetition rate 10 Hz, average power 1 mW/cm^2, duration 4 ns), which was generated from an optical parametric oscillator pumped with the third-harmonic light of Q-switched Nd:YAG laser. The delay time of the laser pulse corresponded to the initial time of the illumination pulse. A *p*-polarized pulsed laser beam was focused onto the sample surface at an incident angle of 45º. The SHG light generated from the sample was detected using the photomultiplier tube, and its intensity was recorded with a digital multimeter. The generation of SHG is material dependent and it shows wavelength dependence of incident laser beam. Accordingly, C_{60} layer provides strong SHG signal at a wavelength of $\lambda_{2\omega}$= 500 nm, whereas pentacene shows no SHG response at

this wavelength [6, 9, 12]. Hence, we used a laser beam with a wavelength of λ_ω = 1000 nm, and recorded the generated SHG signal at a wavelength of $\lambda_{2\omega}$ = 500 nm to selectively measure the electric field in C_{60} layer. However, as we used OSCs with a BCP layer, we need to confirm no SHG response from the BCP layer at 500 nm. Figure 5.1(c) shows the SHG spectra of the BCP and the C_{60} single-layer devices, with structures of IZO/BCP(200nm)/Al and IZO/C_{60}(200nm)/Al. Results show that the SHG response from the BCP single layer device at 500 nm is negligibly small at DC biasing voltages of 0 V and 12 V, whereas the SHG response from the C_{60} single layer device is very strong, and clearly dependent on the DC biasing voltages. Therefore the SHG response from our OSCs at 500 nm originates from the C_{60} layer, due to the electric field induced second harmonic generation process, and this SHG response will be of help for investigating the electric phenomena induced in OSCs.

In our EFISHG experiments on the IZO/pentacene/C_{60}/BCP/Al OSCs, by using a laser beam with a wavelength of λ_ω=1000 nm, EFISHG is activated in the C_{60} layer, due to the coupling of electrons in C_{60} molecules and electro-magnetic waves of the incident laser beam E (ω) in the presence of local electrostatic field E (0). Note that the square-root of the generated SHG intensity is in proportion to the electric field E (0) in the C_{60} layer [13]. E (0) is given as $E_b+E_e+E_{s1}+E_{s2}$, where E_b is the background internal electric field established in the devices due to the presence of trapped carriers, work-function difference, etc., E_e is the electric field originated from charges $-Q_e$ (t) on Al and $+Q_e$ (t) on IZO electrodes, E_{s1} is the electric field originated from accumulated charges Q_{s1}(t) at the pentacene/C_{60} interface, and E_{s2} is the electric field originated from accumulated charges Q_{s2}(t) at the C_{60}/BCP interface. Accordingly, we can discuss carrier behaviors in the OSCs by probing the transient EFISHG.

5.1.2 EFISHG measurement by applying pulse voltage in dark

In a manner as described in section 2.2, OSC device with a BCP blocking layer is modeled using a parallel conductor-capacitor (*G*-*C*) circuit, as shown in the Fig. 1(a). With a DC voltage applied to the OSCs in dark, charge $\pm Q_e(t)$ is induced on the top and bottom electrodes with a response time $\tau_{RC} = R_e \frac{C_1 C_3 C_2}{C_1 C_2 + C_1 C_3 + C_2 C_3} \approx 2 \times 10^{-7}\,\mathrm{s}$, where $R_e = 160\Omega$ is the external resistance [7]. This is the electrode charging process. After that electrode charge on the IZO is injected into the pentacene, and charge Q_{s1} is accumulated at the pentacene/C_{60} interface and Q_{s2} at the C_{60}/BCP interface. Here we assumed that the BCP layer is working as a blocking layer. These accumulated charges are given as:

$$Q_{si}(t) = Q_{si}(\infty)[1 - \exp(-\frac{t}{\tau_{MWi}})] \quad (i = 1, 2), \qquad (2.14)$$

with the Maxwell-Wagner (MW) type relaxation times τ_{MWi} ($>> \tau_{RC}$) and $Q_{si}(\infty) = I_c \Delta\tau_i$ (i = 1, 2), where I_c is the steady-state current flowing across the OSCs [21], and $\Delta\tau_i$ (i = 1, 2) is the relaxation time difference between the adjacent materials, i.e., pentacene and C_{60} , and C_{60} and BCP. This is the interfacial charging process. As described in section 2, the EFISHG signal response reflects the electric field E (0) across the C_{60} layer. The electric field E (0) is dependent on the accumulated charges $Q_{si}(t)$ at the pentacene/C_{60} and the C_{60}/BCP interfaces (interfacial charging), and also on the induced charge on the electrode $\pm Q_e$(t) (electrode charging).

Hence, the generated SHG offers us the information about the carrier behaviors in OSCs with a BCP layer. Note that we can trace the interfacial carrier charging process through the local electric field E (0) estimated from the EFISHG signal I_{SHG} [6], using the relation $I_{SHG} \propto |E(0)|^2$.

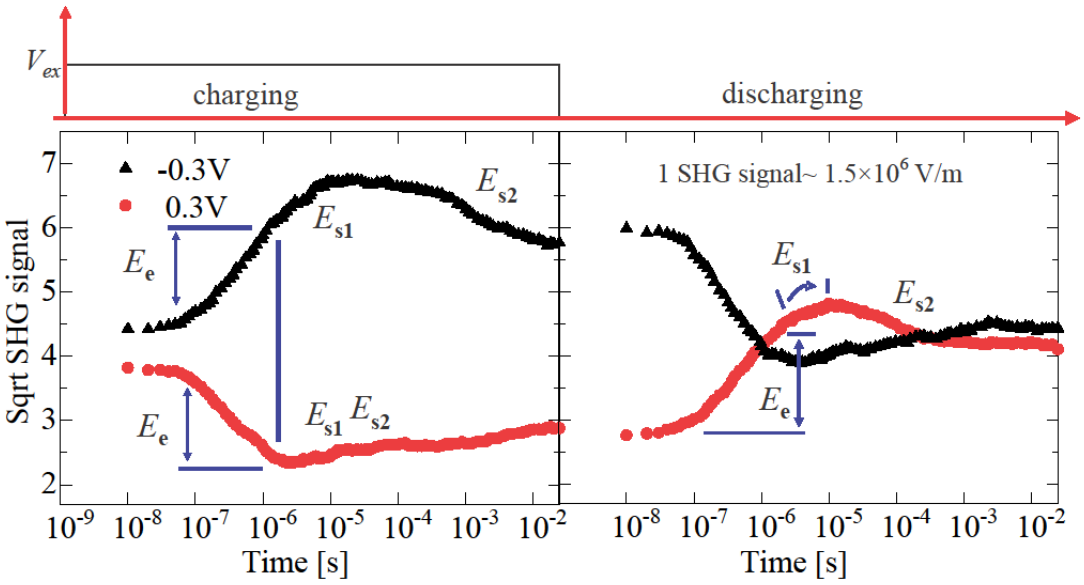

Figure 5.2: EFISHG measurements of the triple-layer OSCs using voltage pulse.

Figure 5.2 shows the EFISHG generated from the IZO/pentacene/C_{60}/BCP/Al OSC in response to the AC square-wave voltage pulse (10 Hz), where the amplitude of the DC applied voltage V_{ex} was +0.3V or -0.3V. Three relaxation processes were identified during the EFISHG measurement, corresponding to the electrode charging (E_e) and two interfacial charging (E_{s1}, E_{s2}). The first relaxation process was observed just after applying AC square-wave voltage pulse, due to the electrode charging, which resulted in the E_e across the Al and ITO electrodes. The established electric field E_e by electrode charging is given as $E_e = \frac{V_{ex}}{d_2}\frac{C_1C_3}{C_1C_2+C_1C_3+C_2C_3} \approx 2.25\times10^6\,\mathrm{V/m}$, and the corresponding EFISHG signal intensity changing is 1.5 within the limit of our

experiment, which means that the increase of the SHG signal beyond this change is related to the interfacial charging process. After the electrode charging, two interfacial charging processes followed [6, 9] ($\tau_{RC} << \tau_{MW}$). For V_{ex} = -0.3 V, firstly the SHG signal was further increased and then decreased, suggesting that the presence of charge accumulation at the two interfaces. Accordingly the two electric fields, E_{s1} and E_{s2}, were successively formed in the C_{60} layer along with interfacial charge accumulation, and their electric field directions inside the C_{60} layer were opposite with each other. Our previous study showed that negative charges (electrons) accumulate at the pentacene/C_{60} interface under V_{ex} =-0.3 V, possibly because the pentacene layer was more conductive than the C_{60} layer [6-9]. With consideration of these, the second and the succeeding third relaxation processes observed after applying AC square-wave voltage pulse were assigned due to the electron accumulation at the pentacene/C_{60} interface and the C_{60}/BCP interface, respectively. The time-constants of the charging processes were evaluated by using a curve-fitting method based on a filtering technique (see section 3.2.3). In the analysis, the first-order filtering function was defined as $F_1(t_1)= s(t_1)-s(2t_1)$, where $s(t)$ is an square-root of EFISHG intensity. The filtering function gives peaks at times that correspond to time-constants of the signal response $s(t)$, and it can effectively determine time-constants of a signal response [8]. In other words, the presence of the three relaxation processes was verified by employing the filtering method. Accordingly, for V_{ex} = -0.3 V, the relaxation time of electrode charging was $\tau_{RC} \approx 2.4\times10^{-7}$s and this value was in good agreement with the response time estimated from the equivalent circuit analysis, $\tau_{RC} \approx 2\times10^{-7}$s . Meanwhile, the

response time of charge accumulation at the pentacene/C_{60} interface and C_{60}/BCP interface were $\tau_{s1} \approx 4.2\times10^{-6}$s and $\tau_{s2} \approx 2\times10^{-3}$s , respectively. Noteworthy that applying negative pulse (V_{ex}=-0.3 V) lead to the increase of the SHG signal, but this result was contradict with our previous experimental results obtained by using OSCs with a structure of IZO/pentacene/C_{60} /Al with no BCP layer [6-9]. This result indicated that the background electric field E_b of the triple-layer sample was pointing in the direction from Al electrode to the IZO electrode. Accordingly, the transport of generated carriers was enhanced and resulted in the increase of the open-circuit voltage (V_{oc}). The detailed physical reason of the creation of this background electric field is out of scope of this study, but we should note that the experimental results were well explained by assuming the presence of this background electric field E_b. It is instructive here to note that for V_{ex}< 0, the high potential barrier of the IZO electrode for electron injection into the pentacene layer suppressed the current to flow across the devices, and slowed down the two interfacial charging processes. Accordingly, we could identify three distinct relaxation processes.

On the other hand, for V_{ex}> 0, the application of positive voltage assisted holes to smoothly inject from the IZO to the pentacene layer and resulted in the acceleration of interfacial relaxation. As shown in the I-V curve of Fig. 5.1(b), the dark current of OSCs exhibits the diode-like behavior with a rectification ratio of nearly two orders at ±0.3 V. As discussed in section 3, the time constants of the two relaxation processes decreased with the increase of the conductivity of the organic layer. Meanwhile, the increase of the conductivity also led to the decrease of $\Delta\tau_{MW}$. Two interfacial charging processes were accelerated and the two time constants (1/α and 1/β) got very close to

each other. Hence, as suggested by eqs. (2.12) and (2.13), the interaction between two charging processes resulted in the suppression of the charge accumulation on the two interfaces. Hence, as seen in Fig. 5.2 with V_{ex} = 0.3 V, only electrode charging process was observed by the EFISHG measurement, and two interfacial charging processes were merged each other completely. Nevertheless, the existence of these two interfacial relaxation processes was identified in the discharging process. That is, under the application of V_{ex} = 0.3 V, holes accumulated on the pentacene/C_{60} and the C_{60}/BCP interfaces very smoothly. Then, in the discharging process, the relaxation of the accumulated charges on the C_{60}/BCP was suppressed owing to the low hole-mobility of the C_{60} layer and the low electric field across the C_{60} layer. As a result, the two interfacial relaxation processes were identified in the discharging process of OSCs (see Fig. 5.2). The experimental results well supported the analysis based on the Maxwell-Wagner model (see section. 2.2). EFISHG measurements with the AC square-wave voltages verified that both holes and electrons can be accumulated on the two interfaces of OSCs and two charging processes depend on each other. Hence, EFISHG measurements with the application of voltage pulses verified that both holes and electrons can be accumulated on the two interfaces of OSCs and the established electric fields E_{s1} and E_{s2} always counteract each other inside the C_{60} layer.

5.1.3 EFISHG measurement with illumination pulse

Figure 5.3 shows the EFISHG generated from the OSC samples with and without a BCP blocking layer. Here the OSCs were activated continuously by an illumination pulse with a frequency of 10 Hz under short-circuit condition. The EFISHG response

records the variation of the photo-induced electric field inside the C_{60} layer, and the local electric fields E (0) are given as $E_b+E_e+E_{s1,d}$ for the OSC without a BCP layer (double-layer sample), and $E_b+E_e+E_{s1}+E_{s2}$ for the OSC with a BCP layer (triple-layer sample), respectively. It is instructive here to note that the directions of the background electric field E_b of these two samples are opposite each other, as mentioned in section 5.1.2. Consequently, electron accumulation at the pentacene/C_{60} interface led to the suppression of the EFISHG response for the double-layer OSC sample without a BCP layer, while it resulted in the enhancement of the EFISHG response for the triple-layer OSC sample with a BCP layer. Accordingly, only one relaxation was observed with the double-layer sample, as shown in Fig. 5.3, The SHG signal decreased significantly, indicating that electrons $Q_{s1,d}$ were accumulated at the pentacene/C_{60} interface with a density of $Q_{s1,d} = E_{s1,d}\frac{d_2}{A}(C_2 + C_1) \approx 1.16\times10^{-8} C/cm^2$ [6, 8]. On the other hand, for the OSC with a BCP layer, firstly the SHG signal slightly increased and then decreased significantly. This result confirmed that two interfacial charging processes dominate the carrier behavior and two electric fields, E_{s1} and $E_{s2,}$ are formed inside the C_{60} layer, with opposite directions. The slight increase of the SHG signal indicated the accumulation of electrons Q_{s1} at the pentacene/C_{60} interface, where $Q_{s1} = E_{s1}\frac{d_2}{A}\frac{C_2C_3 + C_1C_3 + C_2C_1}{C_3} \approx 1.86\times10^{-9} C/cm^2$. Noteworthy that $Q_{s1,d} \approx 7Q_{s1}$, and this relation indicates that the charge accumulation on the pentacene/C_{60} interface has been significantly suppressed by the BCP layer inserted into the OCSs. With the BCP layer served as an exciton blocking layer [1, 2], the generation of the photocarrier would be highly enhanced and this results in the increase of the conductivity of the two organic active layer. Moreover, BCP layer is on top of C_{60}

layer, which means that it can protect the C_{60} layer against the degradation caused by the open-air. Hence, the response time of the SHG changes accordingly with the conductivities of pentacene and C_{60} layers [7, 12], while the accumulation charge density at the interface is governed by the current flowing across the interface, I_c and the relaxation time difference $\Delta\tau$ (see Eq.(2.14)), according to the Maxwell-Wagner effect [7, 9]. As a result, the increase of the conductivity of the organic active layer suppressed the charging process at the pentacene/C_{60} interface. On the other hand, the second relaxation process of the SHG signal for the triple-layer OSC sample (decrease of the SHG signal) was related to the accumulation of electrons Q_{s2} at the C_{60}/BCP interface, where $Q_{s2} = E_{s2}\frac{d_2}{A}\frac{C_2C_3 + C_1C_3 + C_2C_1}{C_1} \approx 2.4\times10^{-8} C/cm^2$. Meanwhile, the time-constants evaluated by using the curve-fitting method [8, 14, 15] were as follows: $\tau_{s1,d}$ = 2×10^{-5} s is the relaxation time of pentacene/C_{60} interface in the double-layer OSC sample, while τ_{s1}=5×10^{-6} s and τ_{s2}=2.3×10^{-4} s are the relaxation times of the pentacene/C_{60} interface and C_{60}/BCP interface in the triple-layer OSC sample. Note that the introduction of a BCP layer with a thickness of around 10 nm has been believed to have no relation with charge accumulation at the BCP interface [2, 5]. However, our EFISHG results evidently showed that accumulated charge density is still significant for the OSC with a 10 nm BCP layer ($Q_{s2} \approx 12Q_{s1}$), as seen in Fig. 5.3. But, the time-constant τ_{s2} is rather large and thus the charge recombination current ($I_{s2} = \frac{Q_{s2}}{\tau_{s2}} \approx 0.1$ mA/cm^2) [5] caused by the Q_{s2} is still very small.

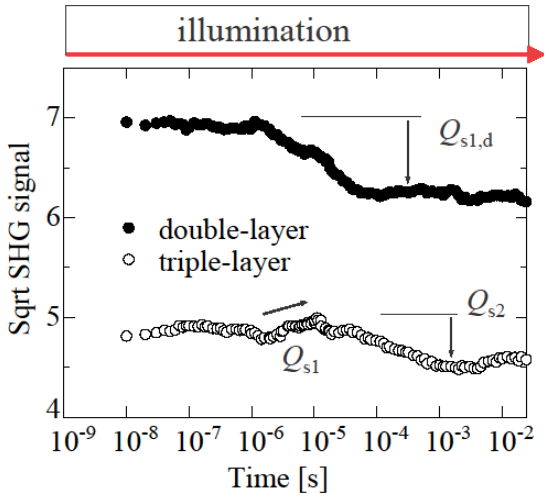

Figure 5.3: EFISHG measurement of both double-layer and triple-layer OSCs under short circuit condition using illumination pulse.

Using an equivalent circuit based on the Maxwell-Wagner model (see Fig. 5.1(a)), we can calculate the short-circuit current in the presence of charge accumulation at the two interfaces. For the double-layer sample, $\frac{dQ_{s1,d}}{dt} = I_{ph} - I_{pe}$, where I_{ph} is photocurrent by holes in pentacene and I_{pe} is photocurrent by electrons in C_{60}. The short-circuit current (I_{sc}) is sum of the recombination current ($I_{s1,d} = \frac{dQ_{s1,d}}{dt}$) and the photo-generated current. Assuming that the pentacene layer is very conductive, the I_{sc} is calculated as $I_{sc} = I_g - I_{s1,d} = I_g - \frac{Q_{s1,d}}{\tau_{s1,d}}$ for the double-layer sample and $I_{sc} = I_g - I_{s1} - I_{s2} = I_g - \frac{Q_{s1}}{\tau_{s1}} - \frac{Q_{s2}}{\tau_{s2}}$ for the triple-layer sample, where $I_g \approx I_{ph}$ is the photogenerated current, $I_{s1,d} = \frac{dQ_{s1,d}}{dt}$, $I_{s1} = \frac{dQ_{s1}}{dt}$, and $I_{s2} = \frac{dQ_{s2}}{dt}$ represent the recombination current caused by the charge accumulation on the pentacene/C_{60} and

C_{60}/BCP interface. Accordingly, $\frac{Q_{s1,d}}{\tau_{s1,d}} = 0.58\,\mathrm{mA/cm^2}$ for the double-layer sample, while $\frac{Q_{s1}}{\tau_{s1}} + \frac{Q_{s2}}{\tau_{s2}} = 0.46\ \mathrm{mA/cm^2}$ for the triple-layer sample. Consequently, $I_{sc} \approx 0.28 I_g$ for the double-layer sample, while $I_{sc} \approx 0.75 I_g$ for the triple-layer sample. This result showed that in the double layer sample 72% of the photogenerated current are depleted by the recombination current of the pentacene/C_{60} interface and this accounts for the low J_{sc} of the double-layer sample, as shown in the Fig. 5.1(b) I-V curve. On the other hand, with the inserted BCP layer, the suppression of the charging process on the pentacene/C_{60} interface enhanced the extraction of the photo generated current into the circuit and thus only 25% of the photogenerated current are depleted in the triple-layer sample, which results in a further improvement of J_{sc}. It should be noted that we repeated the EFISHG experiments using several other samples, and found that all of the samples showed the similar behaviors, although the accumulated charge densities as well as the recombination currents slightly changed. As mentioned above, the EFISHG measurements verified that the inserted BCP layer not only enhances the generation of the photocarriers but also suppresses the depletion of the photo current, which results in further improvement of OSC performance.

The research in this section demonstrated that charge accumulation would occur on every interface of multilayer OSCs. The accumulated charges lead to recombination current, which consume the photo-generated current inside OSCs and significantly degrades the device performance. The charge accumulation is dominated by the conductance of the organic layers in OSCs and thus a blocking layer of BCP can be used to solve this problem. By applying the EFISHG measurements to the

IZO/pentacene/C_{60}/BCP/Al triple-layer OSCs with a BCP blocking layer, we studied the photo-induced carrier behavior with taking into account the dielectric nature of the organic layer. Results showed that the inserted BCP layer leads to the increase of the conductivity of the organic layer, which suppresses the charge accumulation on the pentacene/C_{60} interface and contributes to improve the performance of OSCs. The detailed reason for the increase of conductance is beyond the research in this section. Two possible explanations can be speculated. One is related to exciton blocking. With the BCP layer served as an exciton blocking layer, the generation of the photocarrier would be highly enhanced and this results in the increase of the conductivity of the two organic active layers. The other is about the degradation with open air. BCP layer is on top of C_{60} layer, which means that it can protect the C_{60} layer against the degradation caused by the open-air. With this two effects, the increase of the conductivity can be achieved and the conductance increase of C_{60} layer can be more significant that pentacene layer. Our work showed that the dielectric nature of OSCs dominate the operation of our OSCs and the Maxwell-Wagner type interfacial charging can be an obstacle to the further improvement of OSCs.

5.2 Interfacial charging and Voc

Firstly, we analyze the photo-voltage generation process using an equivalent circuit that stands for the Maxwell-Wagner effect, and discuss the EFISHG transients. Then, we show that excess charge accumulate at the interface in OSCs and electrostatic energy is stored, and this results in the decrease of the open-circuit voltage.

5.2.1 Maxwell-Wagner model analysis of EFISHG transients

Figure 5.4 portrays an equivalent circuit model of the pentacene/C_{60} OSCs as a Maxwell-Wagner effect element. We model the pentacene and the C_{60} layers using parallelly connected conductance (G_1, G_2) and capacitance (C_1, C_2), while photocurrents I_{ph} and I_{pe} flow in pentacene and in C_{60} layer, respectively. Under photoillumination, photocurrents I_{ph} and I_{pe} are generated, while excess charges are accumulated at the pentacene/C_{60} interface owing to imbalance of these photocurrents ($I_{ph} \neq I_{pe}$). Excess charge is a source of a space charge field and forms the fields $E_1=1/d_1 \cdot Q_s/(C_1+C_2)$ in the pentacene layer and $E_2=1/d_2 \cdot Q_s/(C_1+C_2)$ in the C_{60} layer, respectively. The electric fields change in accordance with amount of accumulated charge Q_s, and finally saturate under the condition in that the sum of photocurrent (I_{ph}, I_{pe}) and conduction current (I_{ch}, I_{ce}) in the pentacene and the C_{60} layers are balanced with each other. As a result, in steady state excess charges are present at the interface, $Q_s=0$. We can discuss this situation using a Maxwell-Wagner model. Analyzing the equivalent circuit portrayed in Fig. 5.4 gives accumulated charge $Q_s(t)$ caused by the Maxwell-Wagner effect as we described in section 2.2

$$Q_s(t) = Q_s^{\infty}\left(1 - \exp\left(-\frac{t}{\tau_{MW}}\right)\right) \qquad (2.7)$$

$$\text{with } Q_s^{\infty} = I\left(\frac{C_2}{G_2} - \frac{C_1}{G_1}\right) \text{ and } \tau_{MW} = \frac{C_1 + C_2}{G_1 + G_2}$$

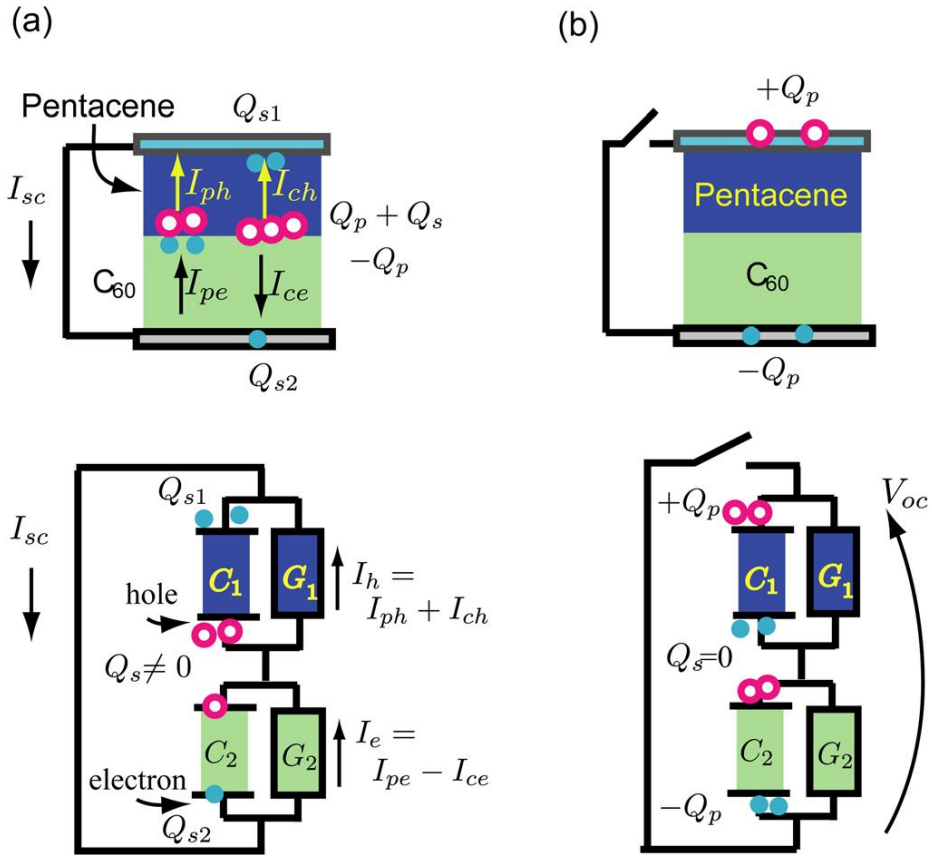

Figure 5.4: Equivalent circuit as a Maxwell-Wagner effect element that models the double-layer OSCs under (a) short-circuit condition, and (b) open-circuit condition. [12]

where I represents a short-circuit current I=-I_{sc}. Equation (2.7) indicates that charges accumulate at two-layer interface wherever the adjacent two layers have different dielectric relaxation time $\tau_1(=C_1/G_1=\varepsilon_1/\sigma_1) \neq \tau_2(=C_2/G_2=\varepsilon_2/\sigma_2)$ (ε_1, ε_2: dielectric constant, σ_1 , σ_2: conductivity). Using the excess charge density $Q_s(=Q_s^{\infty})$ remained in steady state and charging time τ ($=\tau_{MW}$) obtained from the EFISHG results, we calculated conductance G_1 and G_2 of the equivalent circuit by using Eq. (2.7). The results were plotted in Fig. 5.5(a). The conductance of the pentacene (G_1) and C_{60} (G_2) layers were similar, but the conductance of pentacene was a little bit higher ($G_1>G_2$).

Figure 5.5(b) plots the conductance of the OSCs $G=G_1G_2/(G_1+G_2)$ calculated using G_1 and G_2 in Fig. 5(a)

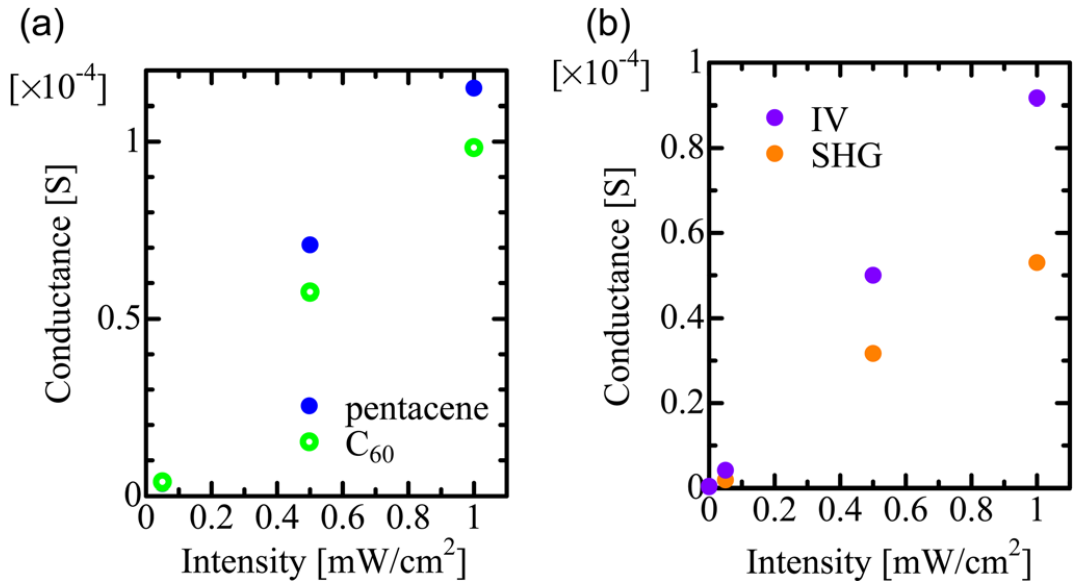

Figure 5.5: (a) Conductance of the pentacene G_1 and C_{60} G_2layers obtained from the EFISHG response. (b) Differential conductance at short-circuit condition obtained from the EFISHG and I-V measurements. [12]

as well as the conductance G (=dI/dV) calculated from the I-V characteristics under short-circuit condition. These plots showed that the conductance evaluated from the two measurements were in good agreement with each other, though the conductance obtained from the EFISHG measurements was about half of that from the I-V measurements. Note that in the EFISHG measurements, we repeatedly illuminated OSCs with 50 ms illumination followed by 50 ms break. This means that transient response reflected the average conductance of $G_0 =(G_d+G)/2\sim G/2$, where conductance were $G_d \sim 10^{-9}$ S in dark and $G \sim 10^{-5}$ S under illumination. Consequently, we conclude that the conductance evaluated using the two measurements were identical and the equivalent circuit model as a Maxwell-Wagner effect element well accounted

for the photo-voltage generation process probed by the EFISHG measurement as well as I-V measurement.

5.2.2 Photovoltaic and Maxwell-Wagner charges

In this part, we will discuss the effect of the Maxwell-Wagner charges on OSC's photovoltaic effect. The open-circuit voltage is given as an energy difference between the HOMO and LUMO levels of the donor and acceptor organic layers. However, actual open-circuit voltage is smaller than this expected value. The contribution of Coulomb interaction energy has been considered to account for the difference, and the estimated open-circuit voltage was corrected as [16, 17]

$$eV_{oc} = E_d - E_a - \frac{e^2}{4\pi\varepsilon_0\varepsilon_r r_{DA}} \quad (5.1)$$

where r_{DA} is the distance between an electron-hole pair of the exciton. Using Eq. (5.1), the open—circuit voltage of the pentacene/C_{60} OSC was estimated as V_{oc} = 0:14 V with $E_d - E_a$ = 0.5 eV, ε_r = 4, and r_{DA} = 1. Here in this estimation we assumed the electron-hole distance was r_{DA} = 1 nm, with taking account that hole located at the center of pentacene molecule (2 nm along molecular long axis) while electron located on the surface of sphere-like C_{60} molecule. However, there is still some deviation from the experimental open-circuit voltage. In addition, the I-V measurements showed that the open-circuit voltage changes with the illumination intensity. That is, it is too early to conclude that Eq. (5.1) represents the photovoltaic voltage of the actual devices. We here consider the effect of interface carrier charging caused by the Maxwell-Wagner effect. As in Eq. (5.1), Coulomb interaction energy contribution is

an important factor of photovoltaic effect in OSCs while the electrostatic energy is localized near excitons. On the other hand, excess charges caused by the Maxwell-Wagner effect store electrostatic energy in the two organic layers macroscopically. The Coulomb interaction energy given by Eq. (5.1) and the Maxwell-Wagner type electrostatic energy are different, but we may consider that the Maxwell-Wagner type electrostatic energy also gives a direct effect on the open-voltage of OSCs. The accumulation of excess charge Q_s at the interface stores electrostatic energy in the bulk of pentacene and C_{60} layers. This electrostatic energy is given by

$$F_s = \frac{Q_s^2}{2(C_1 + C_2)} \quad (5.2)$$

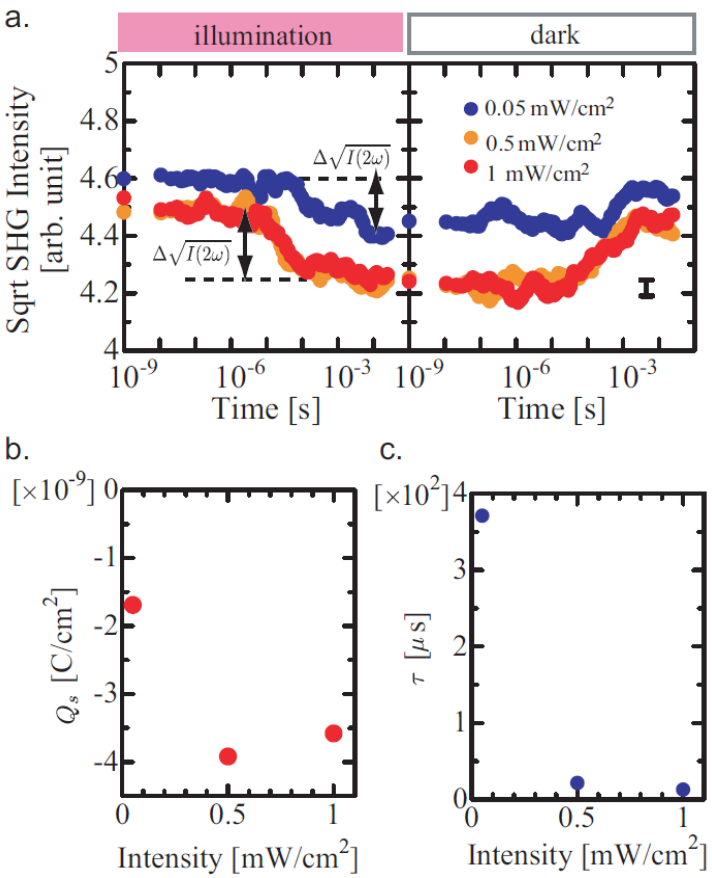

Figure 5.6 (a) EFISHG transient measured with different illumination intensity from 0.05 to 1 mW/cm^2. The square-root of the SHG intensity directly being proportional to the local electric field in C_{60} layer was plotted. The error bar in the figure represents a standard deviation. (b) The excess charge density Q_s remained in steady state, and (c) response time t of the excess charge generation. [12]

The EFISHG results of Fig. 5.6 showed that excess charge Qs was freshly accumulated at the pentacene/C_{60} interface under illumination, evidently suggesting the storage of electrostatic energy given by Eq. (5.2) in C_{60} and pentacene layers. Accordingly, to transfer a hole and an electron from the interface to the IZO and Al electrodes, the energy δF_s is necessary. From Eq. (5.2), δF_s is derived as

$$\delta F_s = e\frac{Q_s}{(C_1 + C_2)}, \text{ assuming } \delta Q_s = e \quad (5.3)$$

This means that the photoillumination activates carriers (holes and electrons) that can separate from the interface to flow across the OSCs double-layer, with an energy of δF_s. On the other hand, when we open-circuit the OSCs, Maxwell-Wagner type charges never accumulate ($Q_s = 0$) at the interface as illustrated in Fig. 4b, because of I = 0. As the result, photo-generated carriers are separated from the interface to the collecting electrodes (IZO and Al) without costing energy $\delta F_s = 0$. In other words, to remove the interface charge Qs, we need the energy given by Eq. (5.4), and this energy directly gives effect on the OSC open voltage. Hence Eq. (5.1) should be modified as

$$eV_{oc} = E_d - E_a - \frac{e^2}{4\pi\varepsilon_0\varepsilon_r r_{DA}} + e\frac{Q_s}{C_1 + C_2} \quad (5.4)$$

where the last term represents the Maxwell-Wagner charge contribution. Using the excess charge density plotted in Fig. 3b. Equation (5.4) gives the open-circuit voltage as V_{oc} = 0.16 V at the illumination intensity of 0.05 mW/cm^2 and V_{oc} = 0.18 V at 1 mW/cm^2. These results account for the illumination intensity dependence of the open-circuit voltage obtained from the I-V measurement, V_{oc} = 0.18 V at 0.05 mW/cm^2 and V_{oc} = 0.26 V at 1 mW/cm^2. Noteworthy that it has been reported that recombination processes as well as energy distribution at the donor-acceptor interface give directly effect on the open-circuit voltage. [18–20] The difference between the calculated V_{oc} and the experimental V_{oc} from the I-V characteristics might be the result of this effect.

5.3 Contribution to fill-factor

Figure 5.7 shows the EFISHG response generated from the pentacene/C_{60}/BCP OSC samples connected to various external resistances R_e. Here the OSCs were activated continuously by illumination pulses with a frequency of 10 Hz, and the external resistances R_e were 0, 1.8 kΩ, 4.7 kΩ and 100 kΩ, corresponding to the external voltage V_{ex} of 0 V, 0.07 V, 0.15 V and 0.24 V under illumination (see section 2). The EFISHG response traces the variation of the photo-induced electric field inside the C_{60} layer, and the local electric fields $E(0)$ is given as E_e+E_{s1}+E_{s2}+ E_b. Accordingly, three relaxation processes were observed in the EFISHG response, as shown in Fig.3. The first relaxation process related to the electrode charging, which induced electric field E_e across the C_{60} layer and $E_e = \frac{V_{ex}}{d_2}\frac{C_1C_3}{C_1C_2+C_1C_3+C_2C_3}$. The increase of the R_e led to the increase of V_{ex}. Accordingly the E_e was also enhanced, as

shown in Fig. 5.7. With the increase of the R_e, the conduction current I_c decreased gradually. Thus, the accumulated charges $Q_{si}(\infty) = I_c \Delta \tau_i$ on the two interfaces decreased. Meanwhile, with the external resistances change from 0 to 100 kΩ, the relaxation time of the circuit increased gradually and the conductivity of the organic layer also decreased due to the suppression of the conduction current, which all led to the delay of the two interfacial charging processes, as marked in Fig. 3 by arrows.

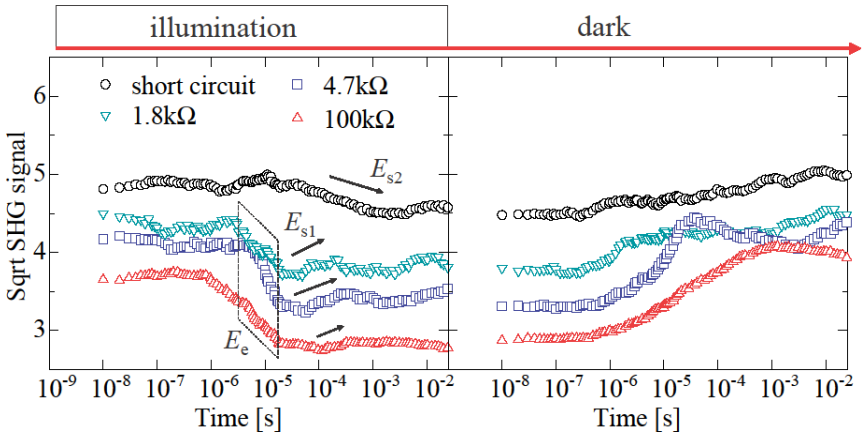

Figure 5.7: EFISHG measurement of triple-layer OSCs connected to various external resistances under illumination pulse.

Based on our previous analysis (see section 5.1), we concluded that the accumulated charges on the interfaces would induce a recombination current $I_{si} = \frac{dQ_{si}}{dt}$ and the photo-generated current is the sum of recombination current ($I_{si} = \frac{dQ_{si}}{dt}$) and short-circuit current (I_{sc}). Therefore, the photogenerated current is depleted by the recombination current of the interfaces and the performance of the OSCs can be improved by suppressing the interfacial charging process. In this study with the similar method, we investigated the contribution of the interfacial charging to

the fill factor (*FF*) of OSCs. The *FF* is given as $FF = \frac{V_m I_m}{V_{oc} I_{sc}}$, where $V_m I_m$ is the maximum value of the power output. In our case it was achieved with the V_{ex}=0.15V. Hence, when the R_e was changed to 4.7 kΩ, the EFISHG results recorded the internal electric field at the V_{ex}=0.15V, as shown in the Fig. 5.7. Meanwhile, for the sample with R_e of 4.7 kΩ, the accumulated charge density on the pentacene/C_{60} and C_{60}/BCP interface can be calculated by checking the changing of the EFISHG signal [11, 12] and $Q_{s1} = E_{s1} d_2 (C_2 C_3 + C_1 C_3 + C_2 C_1)/(AC_3) \approx 1.8 \times 10^{-9} C/cm^2$ $Q_{s2} = E_{s2} d_2 (C_2 C_3 + C_1 C_3 + C_2 C_1)/(AC_1) \approx 1.2 \times 10^{-9} C/cm^2$. The time-constants evaluated by using the curve-fitting and filtering method (see section 3.2.3) were as follows: τ_{s1}=1×10^{-4} s for the pentacene/C_{60} interface and τ_{s2}=9×10^{-4} s for the C_{60}/BCP interface. It is important to note that the time constant obtained from this EFISHG measurement includes the response time (τ_{RC}) of the whole circuit, which is $\tau_{RC} = R_e C_{total}$ ($C_{total} \approx 2.5nF$:total capacitance of three layer together). The τ_{s1} and τ_{s2} is the final value of the time constant after removing the $\tau_{RC.}$ Hence, for the OSCs sample with R_e= 4.7 kΩ, the recombination currents induced by two interfacial charging are calculated as $I_{s1} + I_{s2} = \frac{Q_{s1}}{\tau_{s1}} + \frac{Q_{s2}}{\tau_{s2}} \approx 0.02 mA/cm^2$ and the conduction current of the circuit at that voltage value was $I_c \approx 0.99 mA/cm^2$. This result showed that only 2% of the photogenerated current was depleted due to the recombination current of the two interfaces. On the other hand, for the short-circuit condition, almost 25% of the photogenerated current was consumed by the recombination current of the two interfaces (see section 5.1). Thus, the recombination current induced by two

interfacial charging processes quickly decayed with the increase of the V_{ex} and this may lead to the enhancement of the fill factor.

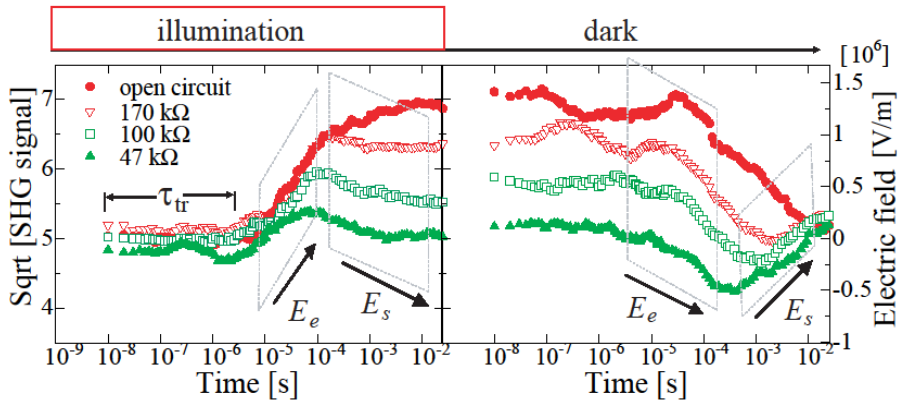

Figure 5.8: SHG measurement with different external resistance R_e from open circuit to 47 kΩ,

Figure 5.8 shows the EFISHG response generated from the double-layer OSC samples (only pentacene/C_{60}) connected to various external resistances R_e. Here, the external resistances R_e were 47 kΩ, 100 kΩ, 170 kΩ and infinite large, corresponding to the external voltage V_{ex} of 0.075 V, 0.1 V, 0.15 V and 0.22 V under illumination. The detailed explanation of this measurement is already introduced in section 4.1. Here, we can apply similar analysis of fill-factor to this double layer experiments. The $V_m I_m$ is achieved with the V_{ex}=0.1V. Hence, when the R_e was changed to 100 kΩ, the EFISHG results at the V_{ex}=0.1 V can be seen in the Fig. 3. Meanwhile, for the sample with R_e of 100 kΩ, the accumulated charge density on the pentacene/C_{60} can be calculated as $Q_s = 0.24 \times 10^{-8} C/cm^2$. The time-constants evaluated by using the curve-fitting and filtering method were as follows: τ_{s1}=0.35×10^{-3} s for the pentacene/C_{60} interface. Hence, for the OSCs sample with R_e= 100 kΩ, the

recombination currents induced by two interfacial charging are calculated as $I_{s1,d} = 8.14\mu A/cm^2$ and the conduction current of the circuit at that voltage value was $I_c = 1.3\mu A/cm^2$. This result showed that 85% of the photogenerated current was depleted due to the recombination current of the two interfaces. For the short-circuit condition, 75% of the photogenerated current was consumed by the recombination current of the two interfaces. Hence, we know that in the double-layer sample the recombination current induced by two interfacial charging processes decayed very slowly with the increase of the V_{ex} and this may lead to the degradation of the fill factor.

5.4 Interfacial charging blocking layer

As shown in our previous parts (section 5.1-3), excess charges are accumulated at the interface of organic active layers due to the Maxwell-Wagner effect, and results in the modification of the potential distribution and the energetic. Meanwhile, it has also been proved that these interfacial charging processes lead to the deterioration of the I-V characteristic of the OSCs [5, 21, 22]. These findings further motivated us to study the effect of inserting additional layer into OSCs by means of EFISHG measurement, which is capable of probing interfacial carrier behaviors. In section 5.1, by introducing a BCP layer as an exciton blocking layer at the interface between C_{60} and Al of IZO/pentacene/C_{60}/Al OSCs, we showed that the interfacial charging process at the pentacnen/C_{60} interface results in the depletion of the photo-generated current. In section 5.2, by using a double-layer OSCs, we analyzed Maxwell-Wagner type interfacial charging and its contribution to the V_{OC}. The results showed that to

transfer a hole and an electron from the interface to the IZO and Al electrodes, the additional energy would be consume to overcome the Maxwell-Wagner type electrostatic energy. Hence, the V_{OC} is decreased by the interfacial charge accumulation. This situation inspired us to study some blocking methods to reduce the interfacial charging accumulations.

In this part, we prepared IZO/pentacene/CuPc/C_{60}/Al OSCs with a Cu-phthalocyanine (CuPc) layer with a thickness of 2, 8, and 18 nm, and studied the contribution of CuPc layer to the interfacial charging under a single red illumination, by using the EFISHG measurement coupled with a single red illumination. Results evidently showed the presence of charge accumulation at the pentacene/CuPc and CuPc/C_{60} interfaces, but the amount of accumulated charges at these two interfaces significantly decreased when the CuPc layer was 8 nm in thickness.

5.4.1 I-V experiments

Figure 5.9(a) portrays an OSC with an indium zinc oxide IZO/pentacene /CuPc/C_{60}/Al structure. The OSCs were prepared as follows: IZO-coated glass substrates were UV/ozone treated to be nearly free from organic residuals. Then the pentacene layer with a thickness of 40 nm (d_1), and the C_{60} layer with a thickness of 50 nm (d_2) were successively deposited onto the UV/ozone treated IZO. Meanwhile, a CuPc layer with a thickness of 2, 8, or 18 nm was deposited between pentacene and C_{60} layers. Finally, Al electrodes with a thickness of 100 nm were deposited on the C_{60} layer, where the working area of the OSCs was A = 3.1 mm^2.

In the measurement, a red light from a light-emitting diode (wavelength 630 nm, intensity 10 mW/cm^2) was used as a light source to provide illumination pulse (repetition rate 10 Hz, duration 50 ms, switching on and off time within 50 ns). It has already been reported that the pentacene/CuPc/C_{60} solar cell with an ultrathin CuPc layer provides a wide spectral band for light absorption and thus the performance of the OSCs [23, 24] is improved. However, as the main purpose of this study was to clarify the carrier behaviors after the introduction of the CuPc interlayer, we only applied the red illumination to the sample. Thus, we can nearly ignore the additional light absorption at other light wavelengths and study the contribution of different carrier behaviors to the I-V performance. Note that both the pentacene and CuPc layers mainly absorb the red light in the wavelength region around 630 nm. Figure 5.9(b) shows the I-V characteristics of the OSCs under red light illumination. For the OSC sample with 18 nm CuPc layer, V_{oc} = 0.39 V, J_{sc} = -0.46 mA/cm^2, and FF = 0.26, for the sample with 8 nm CuPc layer, V_{oc} = 0.43 V, J_{sc} = -0.8 mA/cm^2, and FF = 0.38, whereas for the sample with 2 nm CuPc layer, V_{oc} = 0.28 V, J_{sc} = -0.87 mA/cm^2, and FF = 0.37.

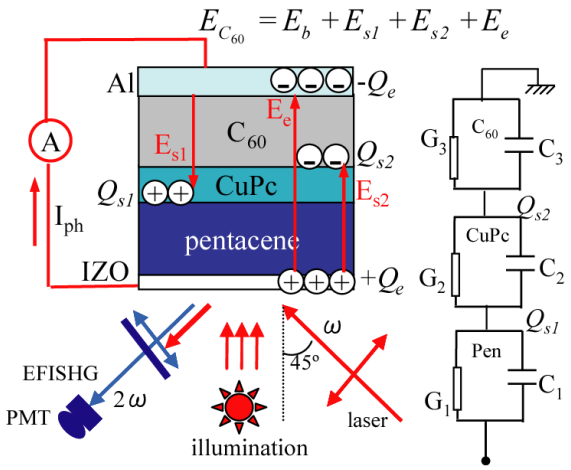

(a)

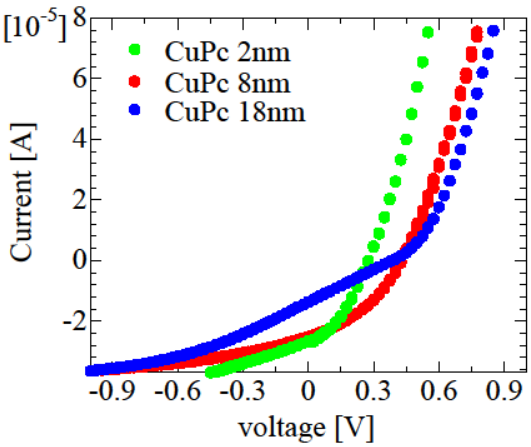

(b)

Figure 5.9: Expreiment set up and I-V results (a) experimental setup for the EFISHG measurement (b) I-V characteristics of the OSCs sample.

5.4.2 Blocking the interfacial charging

In a manner as described in our previous paper [14, 19], OSC device with a CuPc layer is modeled using a parallel conductor-capacitor (*G*-*C*) circuit (in dark), as shown in Fig. 5.9(a). According to the Maxwell-Wagner effect, excess charges Q_{s1} are accumulated at the pentacene/CuPc interface and Q_{s2} at the CuPc/C_{60} interface.

Assuming the CuPc layer is also working as a dielectric layer, upon application of an external voltage to the circuit these accumulated charges Q_{si} (i=1,2) are calculated in Appendix part. Finally, we can get:

$$Q_{si}(t) = Q_{si}(\infty)[1 - \exp(-\frac{t}{\tau_{MWi}})] \quad (i = 1, 2), \qquad (2.17)$$

with the MW type relaxation times τ_{MWi} ($>> \tau_{RC}$) and $Q_{si}(\infty) = I_c \Delta\tau_i$ (i = 1, 2), where I_c is the steady-state current flowing across the OSCs [20], and $\Delta\tau_i$ (i = 1, 2) is the relaxation time difference between the adjacent materials, i.e., pentacene and C_{60}, and CuPc and C_{60}. Under illumination, the conducting current I_c stands for the generated steady-state current across the device due to the PV effect and thus the Maxwell-Wagner model is available for analyzing OSCs [20]. Note that we can trace the interfacial carrier charging process by using the local electric field E (0) estimated from the EFISHG signal I_{SHG} with the relation $I_{SHG} \propto |E(0)|^2$ [22]. It is also necessary to clarify that accumulated charges Q_{si} referred to Maxwell-Wagner type interfacial charging. Note that the trap density cannot be ruled by the time constant difference ($\Delta\tau_i$) of the two adjacent organic active layers. Our previous studies [19-21] have already proved that accumulated charges density is regulated by $Q_{si}(\infty) = I_c \Delta\tau_i$, which indicated that the accumulated charges related to Maxwell-Wagner type interfacial charging.

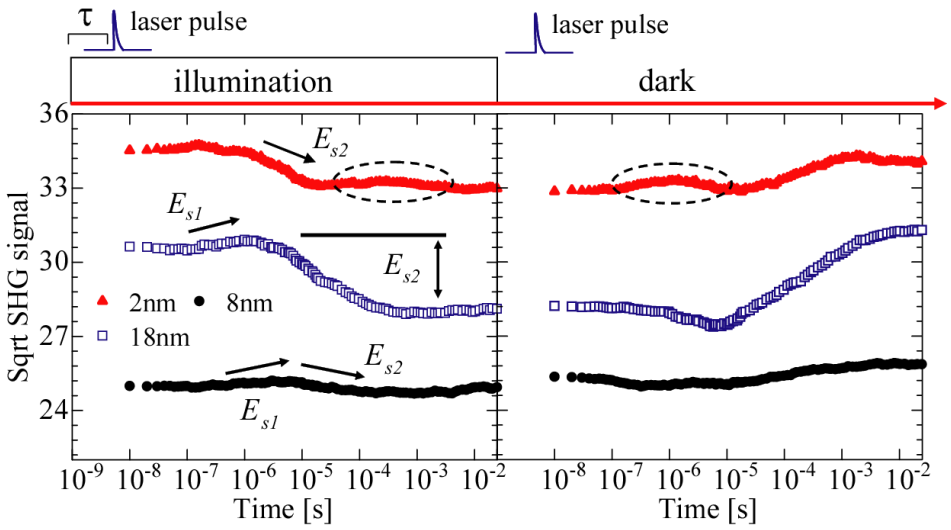

Figure 5.10: EFISHG measurements of the IZO/pentacene/CuPc(x nm)/C_{60}/Al OSCs under short circuit condition (CuPc with the thickness of 2, 8 and 18nm)

Figure 5.10 shows the EFISHG generated from the OSC samples with a CuPc layer, where the thickness of the CuPc layer is 2 nm, 8 nm and 18 nm, respectively. Here the OSCs were activated continuously by a red illumination pulse with a frequency of 10 Hz under short-circuit condition. The EFISHG response records the real-time variation of the photo-induced electric field inside the C_{60} layer, where the local electric field E (0) is given as $E_b+E_{s1}+E_{s2}$ (E_e=0). In Fig. 5.10, for the OSC with a CuPc layer of thickness 18nm and 8nm, firstly the SHG signal slightly increased and then decreased significantly, suggesting that the charge accumulation happened on the two interfaces, and that the induced electric fields (E_{s1} and E_{s2}) across the C_{60} layer were pointing at opposite directions to each other. From the EFISHG experiment under the voltage pulse excitation [12, 14], we confirmed that the decrease (increase) of the SHG signal is due to the accumulation of electrons (holes) on the interface. In

order to get detailed assignation between two interfaces and two interfacial processes, we also prepared double-layer OSCs with the structure of IZO/CuPc(40nm)/C_{60}(50nm)/Al, and measured the photo-induced interfacial charging under short-circuit condition, as shown in Fig. 5.11(a). In Fig. 5.11(a), the significant decrease of the SHG signal was observed and this is due to the accumulation of electrons at the CuPc/C_{60} interface. Note that in Fig. 5.11(a) current flowing in the direction from Al electrode to IZO electrode inside the OSCs. Hence, based on the Maxwell-Wagner model, we conclude $\tau_{\mathrm{CuPc}} < \tau_{\mathrm{C60}}$. Consequently, in Fig. 5.10, the decrease of the SHG signal is ascribed to the electron accumulation (Q_{s2}) on the CuPc/C_{60} interface and the increase of the signal is ascribed to the holes accumulation (Q_{s1}) on the pentacene/CuPc interface. Therefore, relaxation time constants of three different layers have the relationship of $\tau_{\mathrm{CuPc}} < \tau_{\mathrm{pentacene}} < \tau_{\mathrm{C60}}$ and finally two kinds of charges accumulated on the both sides of the CuPc layer. Meanwhile, the relaxation of the pentacene layer is faster than C_{60} layer and thus the accumulation of the Q_{s1} on the pentacene/CuPc interface is always faster than that of Q_{s2} on the CuPc/C_{60} (see Fig. 5.10). Based on the above discussion, the potential profiles in the OSC are suggested as displayed in Fig. 5.11(b). The dotted lines in the figure represents the potential profile across the OSCs under short-circuit condition in dark. By applying the illumination, the photo-induced electric field is generated in the OSCs and the potential profile changes, in a manner as plotted by the solid lines. It is important to note that the surface of Al positively should be charged at short circuit condition due to the lower work function of Al comparing with IZO. However, during the EFISHG measurement, we found that that the background electric field E_b of this triple-layer

sample was pointing in the direction from IZO electrode to the Al electrode. The reason of the presence of this background electric field may be related to the interfacial dipole or the deep traps in the organic active layer. Note that the relaxation of the deep traps usually takes more than 10 second [22, 23] and frequency of the illumination pulse in our experiments is 10Hz, which means that the residual of deep traps can be a source of this background electric field. The detailed physical analysis of the creation of this background electric field is out of scope of this study, but we should note that the experimental results were well explained by assuming the presence of this background electric field E_b.

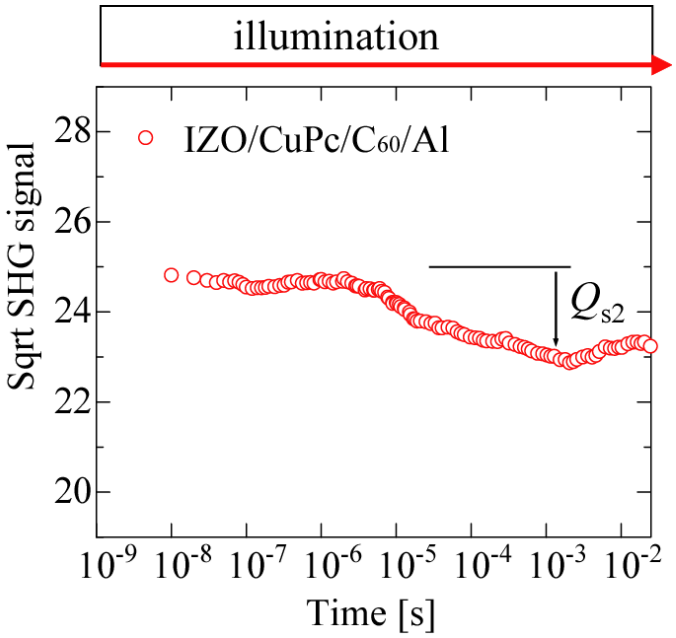

(a)

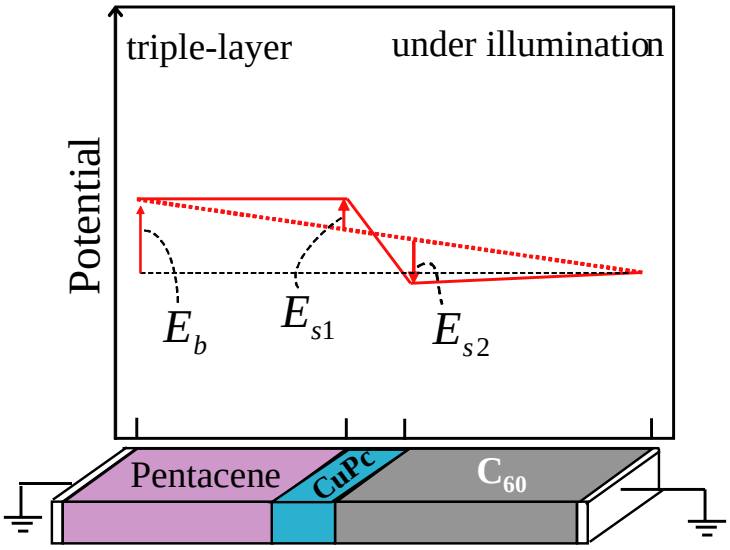

(b)

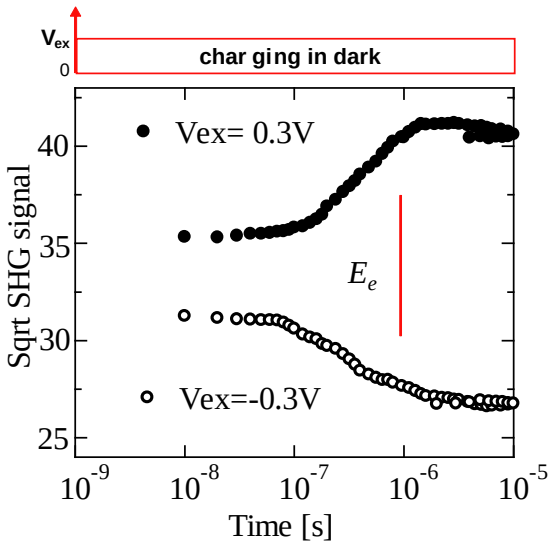

(c)

Figure 5.11: (a)EFISHG measurements of the IZO/CuPc(40nm)/C_{60}(50nm)/Al OSCs under short circuit condition (b)The sketch of potential profiles across triple-layer structure under short-circuits condition with illumination.

In order to clarify the direction of this background electric field E_b in OSCs with the CuPc layer, we carried the EFISHG measurement by applying DC pulse voltages

to the OSCs in dark. Figure 5.11(c) shows the EFISHG generated from the IZO/pentacene/CuPc(18nm)/C_{60}/Al OSC in response to the AC square-wave voltage pulse (10 Hz), where the amplitude of the applied voltage V_{ex} was +0.3V or -0.3V. Three relaxation processes were identified during the EFISHG measurement, corresponding to the electrode charging (E_e) and two interfacial charging (E_{s1}, E_{s2}). The first relaxation process was observed just after applying AC square-wave voltage pulse, due to the electrode charging, which resulted in the E_e across the Al and ITO electrodes. The established electric field E_e by electrode charging is given as $E_e = \frac{V_{ex}}{d_2}\frac{C_1C_3}{C_1C_2 + C_1C_3 + C_2C_3}$. It has been found that forward bias (0.3V) led to the increase of the SHG signal during the electrode charging, while backward bias (-0.3V) resulted in the decrease of the SHG signal. These results proved that the background electric field E_b was pointing in the direction from IZO electrode to the Al electrode.

The induced electric field across the C_{60} layer is calculated as: $E_{s1} = Q_{s1}A(C_1C_2 + C_1C_3 + C_2C_3)/C_2/d_3$ and $E_{s2} = Q_{s2}A(C_1C_2 + C_1C_3 + C_2C_3)/(C_1 + C_2)/d_3$, where d_3 = 50 nm is the thickness of the C_{60} layer (both E_{s1} and E_{s2} are marked with arrows in Fig. 5.10. Note that the variation of EFISHG signal relates to the change of local electric field E (0) in OSCs. As we can see in Fig. 5.10, by changing the thickness of the CuPc layer from 18nm to 8nm, the induced electric field E_{s2} decreased by 80% and E_{s1} was also decreased by about 30%, suggesting that accumulated charge density Q_{s1} and Q_{s2} is significantly reduced. These results proved that interfacial charging processes is significantly suppressed by inserting a CuPc layer with a thickness around 8 nm. Accordingly, the I-V performance of the OSCs was enhanced (see Fig. 5.9(b)). Comparing with the double-layer pentacene/C_{60} OSCs [7, 24], the change of

V_{oc} corresponds to the larger HOMO level of CuPc (5.1 eV) compared with pentacene (5.0 eV). However, the enhancements of V_{oc} and J_{sc} caused by changing the thickness of CuPc layer from 18 nm to 8 nm should be related to the suppression of the interfacial charging processes. Based on our previous research [21], the accumulated charges on the interfaces will induce a recombination current $I_{si} = \frac{dQ_{si}}{dt}$, and the photo-generated current is given as the sum of recombination current ($I_{si} = \frac{dQ_{si}}{dt}$) and short-circuit current (I_{sc}). Consequently, the photogenerated current is depleted by the recombination current at the interfaces. Meanwhile, other group has also proved that the accumulated charges on the interface of the exciton-blocking layer led to the deterioration of the fill-factor of OSCs [25]. Moreover, as reported in our previous study [26], accumulated charges on the donor-acceptor interface restrained the photo-generated charges from leaving the interface, and require another external voltage *V'* to overcome this suppression. Accordingly, the effective V_{oc} is deteriorated by this *V'*. Hence, we concluded that the I-V performance will be improved by suppressing the interfacial charging processes and the I-V results in Fig. 5.9(b)

supported our conclusion.

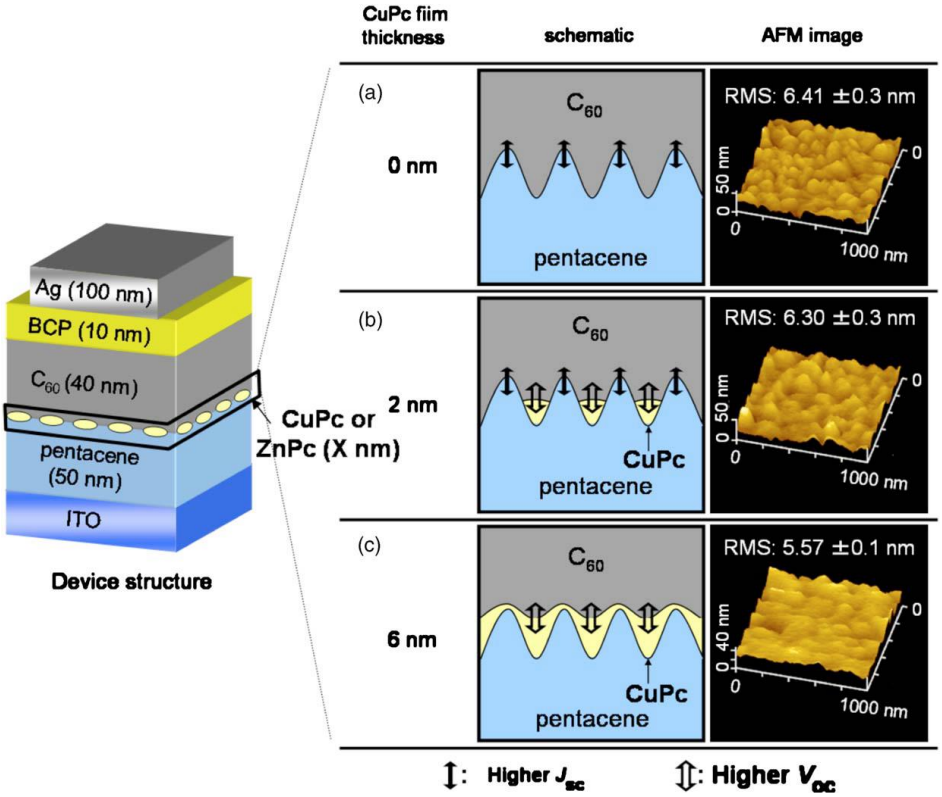

Figure 5.12: AFM images of the surface of (a) pentacene(50nm), (b) CuPc(2nm) /pentacene(50nm) (c) CuPc(6nm)/pentacene(50nm) on ITO substrate. [23]

The suppression of the interfacial charging processes is attributed to the leakage current (I_g) across the CuPc layer, which is caused by the recombination of the accumulated charges on both side of the CuPc layer. The accumulated charges on the both sides of the CuPc layer have different polarities and there would be a strong electric field across the CuPc layer, as seen in Fig. 5.11(b). If the CuPc layer is very thin, the insulating performance of the CuPc layer would be broken and a leakage current I_g is generated by the recombination of the charges from two interfaces. In that case, the effective conduction current around the two interfaces should be $I_{c-eff} = I_c - I_g$ and accordingly the accumulated charge density $Q_{si}(\infty) = I_{c-eff}\Delta\tau_i$.

Thus Q_{si} on the two interfaces should be decreased with the increase of I_g, in proportion to the thickness of CuPc layer. It is also important to note that if we further decrease the thickness of the CuPc layer, the pentacene layer may not be fully covered by CuPc layer, owing to the roughness of the pentacene layer, as has already been pointed out by other groups in their experiments using atomic force microscopy (AFM) observation [23]. The results of AFM observation can be found in Fig. 5.12. With considering this fact, we measured the EFISHG signal from the OSCs with a 2 nm CuPc layer. As shown in Fig. 5.10, the significant interfacial charging was identified again, possibly the charging at the pentacene/C_{60} interface, where the CuPc layer (2 nm) is not coated with the pentacene layer [7, 24]. Meanwhile, during changing process, the changing of the SHG signal was not stable and the turbulence of the signal was observed symmetrically in both charging and discharging processes, as marked in Fig. 5.10. These unstable charging processes suggested that the charge recombination still happened between two interfaces, but was not sufficient for blocking the whole charging process. The lower V_{oc} obtained form the I-V measurement (see Fig. 5.9(b)) also suggested that pentacene/C_{60} interface dominate the photovoltaic effect of the OSCs with 2nm CuPc layer [7, 21]. Hence, we proved that the contribution of the CuPc layer as a charging blocking layer highly depends on the film thickness and the optimized thickness for blocking the interfacial charging processes is around 8 nm. It is noteworthy that the best thickness of the CuPc layer we concluded may be different from the results reported in ref. [23]. This is possibly caused by the red illumination source we used and the lacking of exciton blocking layer. Our study focused on the suppression of the interfacial charging and thus the best thickness of the CuPc layer as a charging blocking layer is around 8 nm. Our

results can be of help to modify the carrier behavior in OSCs and other multilayer organic devices.

5.5 Summary

In order to using our study to improve the performance of the OSCs, we have designed several further experiments with different OSCs samples in this chapter. The results clarified the contribution of the Maxwell-Wagner type interfacial charging to I–V characteristic of OSCs. Firstly, the accumulated charges on the interfaces induce a recombination current and consequently the photo current is depleted by this recombination current at the interfaces. Meanwhile, the slow attenuation of this recombination current also leads to the deterioration of the fill-factor of OSCs. Moreover, the existence of accumulated charges requires another external voltage $V`$ to assist photo-generated charges from leaving the interface, which decreases the effective V_{oc}. Hence, the existence of interfacial charging deteriorates the performance of OSCs. For solving this problem, we suggested two methods to suppress the interfacial charging inside the OSCs. By employing exciton blocking layer of BCP and charging blocking layer of CuPc, interfacial charge accumulation can be strongly decreased and the I-V performance of the OSCs was improved accordingly. Modeling the prepared OSCs as a Maxwell-Wagner effect element accounted for our experimental results.

This chapter is the application research of our theoretical model and evaluation system. In chapter 3 and chapter 4, we analyzed the carrier behavior inside the OSCs with taking into account of dielectric nature and Maxwell-Wagner effect. We focused

on the interfacial charge accumulation processes and how it can change the internal electric field of OSCs. In this chapter, we prove that this Maxwell-Wagner interfacial charging can significantly influence the I-V performance of OSCs. These results not only proved that dielectric nature of organic active dominates the performance of OSCs, but also provided a possible way to further improve the performance of OSCs. The analysis methods and the obtained conclusions can be helpful to the researchers who are doing the performance improvements and new structure development for organic materials. In addition, our EFISHG technique has also been proved to be very useful for the study of organic devices.

Bibliography of Chapter 5

[1] S. Yoo, B. Domercq, B. Kippelen, Appl. Phys. Lett. 85, (2004) 22.

[2] P. Peumans, S. R. Forrest, Appl. Phys. Lett. 79, (2001) 126.

[3] M. Hirade, C. Adachi, Appl. Phys. Lett. 99, (2011) 153302.

[4] E. Itoh, Y. Higuchi, D. Furuhata, T. Shirotori, Jpn. J. Appl. Phys. 50, (2011) 01BC14.

[5] J.C. Wang, X.C. Ren, S.Q. Shi, C.W. Leung, K.L. Chan, Org. Electron 12, (2011) 880.

[6] D. Taguchi, T. Shino, L. Zhang, J. Li, M. Weis, T. Manaka, M. Iwamoto, Appl. Phys. Express. 4, (2011) 021602.

[7] X. Chen, D. Taguchi, T. Shino, T. Manaka, M. Iwamoto, J. Appl. Phys. 110, (2011) 074509.

[8] D. Taguchi, T. Shino, X. Chen, L. Zhang, J. Li, M. Weis, T. Manaka, M. Iwamoto, Appl. Phys. Lett. 98, (2011) 133507.

[9] X. Chen, D. Taguchi, K. Lee, T. Manaka, M. Iwamoto, Chem. Phys. Lett. 511, (2011) 491.

[10] M. Weis, T. Manaka, M. Iwamoto, J. Appl. Phys. 105, (2009) 024505.

[11] D. Taguchi, L. Zhang, J. Li, M. Weis, T. Manaka, and M. Iwamoto, J. Phys. Chem. C 114, (2010) 15136.

[12] D. Taguchi, T. Shino, X. Chen, L. Zhang, J. Li, M. Weis, T. Manaka, M. Iwamoto, J. Appl. Phys. 110, (2011) 103717.

[13] Y. R. Shen: Principle of Nonlinear Optics, Weily, New York, 1984.

[14] C. R. Crowel, S. Alipanahi, Solid-State Electron. 24, (1981) 25.

[15] I. Thurzo, D. Pogány, K. Gmucová, Solid-State Electron. 35, (1992) 1737.

[16] M. Pagliaro, G. Palmisano, R. Ciriminna, Flexible Solar Cells; Wiley-VCH: Weinheim, 2008.

[17] B. P. Rand, J. Genoe, P. Heremans, J. Poortmans, Prog. Photovolt. 15, (2007) 659

[18] B. P. Rand, D. P. Burk, S. R. Forrest, Phys. Rev. B, 75, (2007) 115327/1.

[19] K. Vandewal, K. Tvingstedt, A. Gadisa, O. Inganas, J. V. Manca, Nature Mat. 8, (2009) 904.

[20] G. Garcia-Belmonte, J. Bisquert, Appl. Phys. Lett. 96, (2010) 113301.

[21] X. Chen, D. Taguchi, T. Manaka, M. Iwamoto, J. Appl. Phys. 111 (2012) 113711.

[22] C. Zhang, S. W. Tong, C. Jiang, E. T. Kang, D. S. H. Chan, C. Zhu, Appl. Phys. Lett. 93, (2008) 043307.

[23] Y. Kinoshita, T. Hasobe, H. Murata, Appl. Phys. Lett. 91 (2007) 083518.

[24] X. Chen, D. Taguchi, K. Lee, T. Manaka, M. Iwamoto, Chem. Phys. Lett. 511 (2011) 491.

[25] K. Lee, M. Weis, D. Taguchi, T. Manaka, M. Iwamoto, Chem. Phys. Lett. 551 (2012) 105

[26]J. Wang, X. Ren, S. Shi, C. Leung, P. Chan, Org. Electron. 12 (2011) 880.

Chapter 6 General conclusions and prospects

6.1 General Conclusions

The work described in this thesis which aimed to clarify the carrier behavior of OSCs and thus to improve the performance of OSCs based on theoretical analysis and characterization. In the following, we first summarize each chapter and then proceed to the general conclusions.

In chapter 1, in order to clarify the purpose for the study of carrier behavior of OSCs, I summarized the backgrounds of organic electronics and discussed the current progress in the field of OSCs. I also explained the challenge of the study of OSCs and the importance of carrier behavior to OSCs. Meanwhile, the detailed characteristic of OSCs was also introduced with the consideration of the influence from the carrier behavior.

In chapter 2, firstly, we discussed the dielectric nature of the OSCs and proposed several proof to illustrate the difference between OSCs and common inorganic solar cell. Hence, in order to investigate the dielectric nature of OSCs, we need to apply the Maxwell-Wagner effect element to study the carrier behavior of OSCs. Hence, the interfacial carrier relaxations of OSCs with both double-layer and triple-layer have been analyzed by using this model. On the other hand, we have also summarized the

evaluation technique of OSCs, including simple I-V measurement, IS method and EFISHG measurement. The importance of each measuring methods to study the OSCs were well explained. Finally, optical EFISHG measurement, which enables us directly probe electric field generated in the semiconductor layer, was chosen as the core technique to study the carrier behavior and photovoltaic effect in the OSCs.

In chapter 3, the visualization of interfacial carrier behavior inside OSCs was realized by using IS and EFISHG measurement. Knowing that apply a new technique like EFISHG measurement to the study of OSCs require the conformation from some well-known technique. Hence, the observation of the Maxwell-Wagner type interfacial charging from IS measurement can verify the results from EFISHG measurement. At the meantime, the EFISHG measurement can offer the direct observation of the internal electric field, including relaxation time constant as well as electric field intensity. Results confirmed the dielectric performance of OSCs and also proved that charge accumulation would happen on the double-layer interface. EFISHG measurement coupled with IS measurement provides a clear physics picture of interfacial phenomena related to the photovoltaic effect in OSCs.

In chapter 4, EFISHG measurement was applied to the OSCs sample under various external conditions, including external resistances and external voltage biases. We investigated electrode charging and interfacial charging happened over the entire region of V_{ex} inside pentacene/C_{60} double-layer OSCs in terms of photovoltaic effect. We confirmed the OSCs build up its internal electric field due to the PV effect as well as the interfacial charging processes. That is, the carrier behaviors in the OSCs were governed by the dielectric nature of the organic double layer. Meanwhile, a clear

physical picture of OSCs based on dielectric physics was established, which enable us to study the interfacial carrier behavior and its contribution to the OSCs performance.

In chapter 5, we have done several further experiments with different OSCs samples to study the contribution of interfacial charging to the I-V performance of OSCs. Firstly, the experiments with OSCs using BCP as exciton blocking layer showed that the accumulated charges on the interfaces induce a recombination current and consequently the photo current is depleted by this recombination current at the interfaces. Secondly, the slow attenuation of this recombination current also leads to the deterioration of the fill-factor of OSCs. Third, by using simple double-layer OSCs sample, we found that due to the accumulated charges, photo-generated charges require another external voltage $V`$ to leave the interface, which decreases the effective V_{oc}. Hence, the existence of interfacial charging deteriorates the performance of OSCs. We also suggested two methods to suppress the interfacial charging inside the OSCs. By employing exciton blocking layer of BCP and charging blocking layer of CuPc, interfacial charge accumulation can be strongly decreased and the I-V performance of the OSCs was improved accordingly. Modeling the prepared OSCs as a Maxwell-Wagner effect element accounted for our experimental results.

Finally, there are several conclusions can be considered as the new points of this thesis:

- We proved that dielectric nature dominated the performance of the OSCs and Maxwell-Wagner model can be an effective method to study the carrier behavior in OSCs.

- EFISHG measurement is very powerful technique for the study of the OSCs and the characterization method we designed in this thesis can be helpful to the study of further improvement of OSCs.
- A clear physical picture about the carrier behavior as well as interfacial charging of OSCs have been established on bias of dielectric physics
- Maxwell-Wagner type Interfacial charging can degrade the I-V performance
- Exciton blocking layer and charging blocking layer can suppress the interfacial charging and thus to improve the performance of OSCs

6.2 Prospects

Recently OSCs has received significant attention all over the world, because it can be a potential low-cost alternative to conventional inorganic ones. However, the. Due to very low charge carrier mobility in organic materials, the dielectric performances of organic materials were very significant and thus analysis of OSCs also need to take account of the dielectric nature of organic active layer. Therefore, the EFISHG technique coupled with dielectric physical model provides a clear understanding of interfacial carrier phenomena related to the photovoltaic effect in OSCs. In our previous study, by modeling multilayer OSCs sample as Maxwell-Wagner elements, we clarified the contribution of the interfacial charge accumulation to I–V characteristic of OSCs. It has been found that the existence of interfacial charging deteriorates the performance of OSCs. For solving this problem, we suggested two methods (exciton blocking layer of BCP and charging blocking layer of CuPc) to suppress the interfacial charging inside the OSCs and thus to

improve I-V performance of the OSCs. These results not only proved that dielectric nature of organic active dominates the performance of OSCs, but also provided a possible way to further improve the performance of OSCs.

However, our previous researches are only based on the multilayer OSCs with distinctive interfaces and rather simple structures. Owing to the limitation of the previous SHG system, we cannot distinguish the carrier processes happened inside more complicated organic films, such as blended heterojunction case or OSCs with some surface treatments. The investigation on the carrier processes happened inside the blended bulk-heterojunction layer is very important not only for the further improvement of OSCs, but also for the basic research in surface and interface science. At the meantime, the application of nanostructured plasmonic materials for photovoltaic devices can also be a good research topic for us. The metal subwavelength-sized structures exhibit surface plasmon resonance at specific incident light wavelength and this effect can be applied to enhance OSCs due to additional exciton dissociation or free-charge generation. These applications are limited by the creation of fine and inexpensive plasmonic structure on the solar cell. In my previous research, I have participated in some work concerning with the deposition of metal nanoparticle using Langmuir-Blodgett technique. Hence, I can apply this technique to the deposition of plasmonic nanoparticles onto the photovoltaic devices and investigate the electrical and optical properties by using our SHG technique.

The proposed future research plan is to study the interfacial properties and carrier behavior in OSCs with complicated structure and other optimized treatment. The main content of my proposed research are consisting of three parts:

1. Design new experimental methods for direct observing carrier relaxation inside bulk-heterojunction OSCs based on SHG technique. Study the carrier behavior inside bulk-heterojunction OSCs, including current path across the blended film, carrier relaxation and accumulation inside the blended layer, trapping mechanism and so on. Investigate the quenching behavior happened on the interface between blended film and metal electrodes by using SHG technique and also study the contribution of blocking layer taking into account of dielectric performance of the organic layer. Study the probable influence of evaporation speed and composition ratio of blended film on the carrier relaxation and transport.
2. Participate in a developing project for an improved laser system based on the same working principle of SHG technique. This laser system is possible to have a detecting resolution of twenty or thirty nanometers, which allow us to study the electric field variation along thickness direction and to establish the 3-dimensional observation of the OSCs. Based on the particularity of this technique, design several experiments for further confirming the carrier behavior happened in OSCs. Study the exciton dissociation processes by focusing the laser signal on the donor-acceptor interface.
3. Deposit metal plasmonic nanoparticles onto the interfaces of OSCs through different techniques, such as Langmuir-Blodgett technique or direct evaporation or other surface techniques. Induce additional exciton dissociation or free-charge generation in OSCs by using plasmonic nanostructures and thus enhance the

performance of OSCs. Try to summary the differences and merits between different deposition techniques. Apply SHG technique and Maxwell-Wagner model to the study of OSCs with plasmonic nanostructures. Investigate electrical and optical properties of the interface with plasmonic nanoparticles and clarify the carrier behavior related to performance enhancement caused by plasmonic nanostructures

These developments and applications will be very helpful to not only understand physical image of OSCs, but also to clarify some critical issue for other organic devices. The possible results will be very helpful to understand of the mechanism of photovoltaic effect happened in OSCs with complicated structures, eventually helpful for improving the application of the OSCs in real industrial field.

Acknowledgements

I would like to extend my sincere thanks to the following people for their help and support during my Ph. D study. These people have helped me professionally and personally in every field of my life in Japan.

First of all, a big gratitude to my supervisor and my respectful teacher, Professor Mitsumasa Iwamoto who always guided me and inspired me when I faced difficulties in research and in many related fields. Without his guidance, suggestions and encouragement, my research and study cannot be accomplished smoothly. At the beginning of my study, I am not so good at writing academic thesis and professor always checked my paper over and over again. Finally, I learned a lot of things from his wealth of knowledge and serious spirit. I truly hope we can have further collaboration in coming future.

I would like to acknowledge to Dr. Takaaki Manaka and Dr. Taguchi Dai, who have always guided me especially regarding the SHG measurements. Many thanks for their continuous encouragement and guidance during my studies. They are the co-authors in most of my published papers and it was a great learning experience to collaborate with them.

I would like to acknowledge Prof. Mitsumasa Iwamoto (again), Prof. Makoto Konagai, Prof. Akira Yamada, Prof. Shigeki Nakagawa, Prof. Takamichi Nakamoto, Prof. Kazuhiro Kudo, and Dr. Takaaki Manaka (again) for their kindness and patience to review the thesis and participate in the thesis presentation as examiners.

Many thanks to Dr. Martin Weis, who is the first guide of mine in this lab. His knowledge and experience make me very easy to get into the research field of organic electronics. A great thanks to other lab members, including Dr. Lee Kean Chuan, who accompanied me during meal time, Dr. Wei Ouyang and Dr. Jun Li, who came from the same university as I did, Dr. Le Zhang and Mr. Xuepeng Mo, who are good partners during the experiment. All of them are good friends of mine, but none of them is still here. Thus, I need to thank Miss Xiaojin Cui, without whom I would be very lonely during my last six months in lab.

Finally, I would like to thank my dear parents, who are always supporting me in my research and decision.

List of Publications

(1) 発表した論文

[1] **Xiangyu Chen**, Dai Taguchi, Takaaki Manaka, Mitsumasa Iwamoto, “Study of blocking effect of Cu-phthalocyanine layer in Zinc Oxide /pentacene/CuPc/C60/Al organic solar cells by Electric field-induced Optical Second Harmonic Generation measurement”, Organic Electronics 14, 320 (2013).

[2] **Xiangyu Chen**, Dai Taguchi, Keanchuan Lee, Takaaki Manaka, Mitsumasa Iwamoto, “Analysis of interfacial charging process in pentacene/C60/BCP triple-layer organic solar cells using a Maxwell-Wagner model”, Japanese Journal of Applied Physics Accepted (2013).

[3] **Xiangyu Chen**, Dai Taguchi, Takaaki Manaka, Mitsumasa Iwamoto, “Interfacial Charging of CuPc/C60 Double-layer Organic Solar Cells Induced by Photoillumination: Effect of Photoconductivity change”, Thin Solid films Accepted (2013).

[4] **Xiangyu Chen**, Dai Taguchi, Takaaki Manaka, Mitsumasa Iwamoto, “Investigation of interfacial charging process of pentacene/C60/BCP triple-layer organic solar cell”, IEICE TRANS ELECTRON 96, 3 (2013).

[5] **Xiangyu Chen**, Dai Taguchi, Takaaki Manaka, Mitsumasa Iwamoto, “Analyzing photo-induced interfacial charging in IZO/pentacene/C60/bathocuproine/Al organic solar cells by electric-field-induced optical second-harmonic generation measurement”, Journal of Appilied Physics 111, 113711 (2012).

[6] **Xiangyu Chen**, Dai Taguchi, Keanchuan Lee, Takaaki Manaka, Mitsumasa Iwamoto, “Analysis of Anomalous Discharging Processes in Pentacene/C_{60} Double-Layer Organic Solar Cell”, Japanese Journal of Applied Physics 51, 02BK01 (2012).

[7] **Xiangyu Chen**, Dai Taguchi, Martin Weis1, Takaaki Manaka, Mitsumasa Iwamoto, “Analyzing Photo Induced Internal Electric Field in Pentacene/C_{60} Double-Layer Organic Solar Cells under Various External Voltages by Electric-Field-Induced Optical Second Harmonic Generation Measurement”, Japanese Journal of Applied Physics 51, 041605 (2012).

[8] **Xiangyu Chen**, Dai Taguchi, Keanchuan Lee, Takaaki Manaka, Mitsumasa Iwamoto, “Analyzing interfacial carrier charging in pentacene/C_{60} double-layer organic solar cells by optical electric field induced second-harmonic generation measurement”, Chemical Physics Letters 511, 491 (2011)

[9] **Xiangyu Chen**, Dai Taguchi, Tatsunori Shino, Takaaki Manaka, Mitsumasa Iwamoto, “Analysis of interface carrier accumulation and relaxation in pentacene/C_{60} double-layer organic solar cell by impedance spectroscopy and electric-field-induced optical second harmonic generation”, Journal of Applied Physics 110, 074509 (2011).

[10] **Xiangyu Chen**, Wei Ou-Yang, Martin Weis, Takaaki Manaka, Mitsumasa Iwamoto,“Reduction of hysteresis in organic field-effect transistor by ferroelectric gate dielectric”, Japanese Journal of Applied Physics 49，021601 (2010).

[11] Dai Taguchi, **Xiangyu Chen**, Takaaki Manaka, Mitsumasa Iwamoto, “Analyzing Open-voltage of Double-Layer Organic Solar Cells Using Optical Electric-Field-Induced Second-Harmonic Generation Measurement”, MRS Proceedings,mrsf11-1390-h09-33 (2012).

[12] Wei Ou-Yang, **Xiangyu Chen** , Martin Weis, et al,“Tuning of Threshold Voltage in Organic Field-Effect Transistor by Dipole Monolayer”，Japanese Journal of Applied Physics, 49，04DK04 (2010)

[13] Xiangcheng Chu, **Xiangyu Chen**, Longtu Li, "Disk-pivot structure micro piezoelectric actuator with bimorph", Optics and Precision Engineering， Vol.16, No.12. 2008

[14] Xiangcheng Chu, **Xiangyu Chen**, Long Ma, Longtu Li, “A miniature high-speed piezoelectric motor with a disk-pivot structure”, International Journal of Physics.B , Vol. 24, p 2404, (2010).

[15] Xiangcheng Chu, **Xiangyu Chen**, Long Ma, Longtu Li, “A miniature disk-pivot piezoelectric motor with double rotors”, 全国压电和声波理论及器件技术研讨会 , 2009.

[16] Keanchuan Lee, Martin Weis, **Xiangyu Chen**, at el, “Impact of Illumination on Charge Injection and Accumulation in Organic Transistor in Presence of Plasmonic Nanoparticles”, Japanese Journal of Applied Physics accepted (2013).

[17] Keanchuan Lee, Martin Weis, **Xiangyu Chen**, at el, “Impact of the interfacial traps on the charge accumulation in organic transistors”, Journal of Experimental Nanoscience accepted (2013).

[18] Keanchuan Lee, Martin Weis, **Xiangyu Chen**, Dai Taguchi, Takaaki Manaka, Mitsumasa Iwamoto, “Metal nanoparticles in organic field-effect transistor: transition from charge trapping to conduction mechanism”, Thin Solid Films, *under review* (2013).

[19] Dai Taguchi, Ryota Sumiyoshi, **Xiangyu Chen**, Takaaki Manaka, Mitsumasa Iwamoto, “Study of Interface Layer Effect in Organic Solar Cells by

Electric-Field-Induced Optical Second-Harmonic Generation Measurement", Thin Solid Films, *under review* (2013).

[20] Dai Taguchi, Tatsunori Shino, **Xiangyu Chen**, Le Zhang, et al, "Analyzing carrier lifetime of double-layer organic solar cells by using optical electric-field-induced second-harmonic generation measurement", Applied Physics Letters 98, 133507 (2011).

[21] Dai Taguchi, Tatsunori Shino, **Xiangyu Chen**, Le Zhang, et al, "Analyzing photovoltaic effect of double-layer organic solar cells as a Maxwell-Wagner effect system by optical electric-field-induced second-harmonic generation measurement", Journal of Applied Physics, 110, 103717 (2011).

[22] Dai Taguchi, Tatsunori Shino, **Xiangyu Chen**, Le Zhang, et al, "Determination of Lifetime of Double-Layer CuPc/C_{60} Organic Solar Cells by Optical Electric-Field-Induced Second-Harmonic Generation Measurement", Physics Procedia, 14, 167 (2011).

[23] Wei Ou-Yang, Martin Weis, **Xiangyu Chen,** et al, "Study of phase transition of two-dimensional ferroelectric copolymer P(VDF-TrFE) Langmuir monolayer by Maxwell displacement current and Brewster angle microscopy", Journal of Chemical Physics, 131, 104702 (2009)

[24] Wei Ou-Yang, Martin Weis, Dai Taguchi, **Xiangyu Chen**, Takaaki Manaka, Mitsumasa Iwamoto, "Modeling of threshold voltage in pentacene organic field-effect transistors", Journal of Applied Physics, 107, 12 (2010)

[25] **陈翔宇**，褚祥诚，李龙土,"压电陶瓷直线驱动器的设计与实验研究"，稀有金属材料与工程 , Vol.38, Suppl.2. 2009.

[26] **陈翔宇**，张松，李枢等，"一种锯齿波驱动的压电电机", 压电与声光, Vol.30, No.2. 2008

Invention patent

[1] 采用双足驱动的直线压电电机 (Applicating number：200810114 964.3)

[2] 一种压电电机 (ZL 2006 1 0012004.7)

(2) 国際会議における発表

[1] **Xiangyu Chen**, Dai Taguchi, Takaaki Manaka, Mitsumasa Iwamoto, "Interfacial Charging of CuPc/C60 Double-layer Organic Solar Cells Induced by Photoillumination: Effect of Photoconductivity change", 10th International Conference on Nano-Molecular Electronics (ICNME 2012), poster presentation (The Awaji Yumebutai International Conference Center , Hyogo, Japan/ 12-14, Dec, 2010).

[2] **Xiangyu Chen,** Dai Taguchi, Keanchuan Lee, Takaaki Manaka, Mitsumasa Iwamoto, “Analysis of interfacial charging process in pentacene/C60/BCP triple-layer organic solar cells using a Maxwell-Wagner model", 2012 International Conference on Solid State Devices and Materials (SSDM 2012), oral presentation. (Kyoto, Japan, 2012/09)

[3] **Xiangyu Chen**, Dai Taguchi, Keanchuan Lee, Takaaki Manaka, Mitsumasa Iwamoto, “Analysis of Anomalous Discharging Processes in Pentacene/C60 Double-Layer Organic Solar Cell", 2011 International Conference on Solid State Devices and Materials (SSDM 2011), oral presentation. (Nagoya, Japan, 2011/09)

[4] **Xiangyu Chen**, Dai Taguchi, Takaaki Manaka, Mitsumasa Iwamoto, “Analyzing interfacial carrier charging in pentacene/C60 double-layer organic solar cells by optical electric field induced second-harmonic generation measurement ", 2011 Tsinghua Univ.-Tokyo Tech.-Jingdezhen Ceramic Inst. Joint Symposium on Advanced Materials, poster presentation. (Jingdezhen Ceramic Institute, P. R. China, 2011/11)

[5] **Xiangyu Chen,** Dai Taguchi, Takaaki Manaka, Mitsumasa Iwamoto, “Investigation of interfacial charging process of pentacene/C60/BCP triple-layer organic solar cells", The 7th International Symposium on Organic Molecular Electronics (ISOME2012), oral presentation. (Chiba,Japan, 2012/06)

[6] **Xiangyu Chen,** Dai Taguchi, Takaaki Manaka, Mitsumasa Iwamoto, Fabrication and Analysis of Organic Field Effect Transistor with P(VDF-TrFE) LB films", Tokyo Tech - Asia Materials Week, oral presentation. (Tokyo & Fuji - Yoshida, Japan, 2010/11)

[7] Keanchuan Lee, Martin Weis, **Xiangyu Chen**, Dai Taguchi, Takaaki Manaka, Mitsumasa Iwamoto. “Metal nanoparticles in organic field-effect transistor: transition from charge trapping to conduction mechanism”, 10th International Conference on Nano-Molecular Electronics (ICNME2012), poster presentation (The Awaji Yumebutai International Conference Center , Hyogo, Japan/ 12-14, Dec, 2012)

[8] Keanchuan Lee, Martin Weis, **Xiangyu Chen**, Dai Taguchi, Takaaki Manaka, Mitsumasa Iwamoto. “Impact of the interfacial traps on the charge accumulation in organic transistors”, 2012 International Conference on Enabling Science and Nanotechnology (ESciNano), Oral presentation (Persada Johor International Convention Centre、Johor Bahru, Malaysia/ 5-7 Jan 2012）

[9] Dai Taguchi, Ryota Sumiyoshi, **Xiangyu Chen**, Takaaki Manaka, Mitsumasa Iwamoto, “Study of Interface Layer Effect in Organic Solar Cells by Electric-Field-Induced Optical Second-Harmonic Generation Measurement”, 2012 International Conference on Enabling Science and Nanotechnology (ESciNano), Oral presentation, 10th International Conference on Nano-Molecular Electronics (ICNME2012), poster presentation (The Awaji Yumebutai International Conference Center , Hyogo, Japan/ 12-14, Dec, 2012)

[10] Keanchuan Lee, Martin Weis, **Xiangyu Chen**, Dai Taguchi, Takaaki Manaka,

Mitsumasa Iwamoto. “Effects of silver nanoparticles organic envelope on pentacene organic field-effect transistors”, 2011 International conference on solid state devices and materials (SSDM2011), Oral presentation (Aichi Industry & Labor Center (WINC AICHI), Nagoya, Japan/ Sep 28-30, 2011)

(3) 国内学会・シンポジウム等における発表

[1] **Xiangyu Chen**, Dai Taguchi, Takaaki Manaka, Mitsumasa Iwamoto, “Analyzing interfacial carrier charging in pentacene/C60 double-layer organic solar cells by optical electric field induced second-harmonic generation measurement ", The 72th Autumn Meeting of the Japan Society of Applied Physics, Oral presentation. (Yamagata, Japan, 2011/09)

[2] **Xiangyu Chen**, Dai Taguchi, Takaaki Manaka, Mitsumasa Iwamoto, “Analyzing photo-induced internal electric field in pentacene/C60 double-layer organic solar cells by electric-field-induced optical second-harmonic generation measurement", The 59th Spring Meeting of the Japan Society of Applied Physics, Oral presentation. (Tokyo, Japan, 2011/03)

[3] **Xiangyu Chen**, Dai Taguchi, Takaaki Manaka, Mitsumasa Iwamoto, “Analyzing photo-induced internal electric field in pentacene/CuPc/C60 triple-layer organic solar cells by electric-field-induced optical second-harmonic generation measurement", The 73th Autumn Meeting of the Japan Society of Applied Physics, Poster presentation. (Matsuyama, Japan, 2012/09)

[4] **Xiangyu Chen**, Dai Taguchi, Takaaki Manaka, Mitsumasa Iwamoto, “Analyzing photo-induced internal electric field in triple-layer organic solar cells by electric-field-induced optical second-harmonic generation measurement", The 60th Spring Meeting of the Japan Society of Applied Physics, poster presentation. (Kanagawa, Japan, 2013/03)